LBL--32660

DE93 002561

The Fabrication and Performance of $YBa_2Cu_3O_{7-x}$ SQUID Magnetometers

John Joseph Kingston
Ph.D. Thesis

Department of Physics
University of California

and

Materials Sciences Division
Lawrence Berkeley Laboratory
University of California
Berkeley, CA 94720

July 1992

This work was supported in part by the California Competitive Technology Program and by the Director, Office of Energy Research, Office of Basic Energy Sciences, Materials Sciences Division, of the U.S. Department of Energy under Contract No. DE-AC03-76SF00098.

The Fabrication and Performance of $YBa_2Cu_3O_{7-x}$ SQUID Magnetometers

by

John Joseph Kingston

The Fabrication and Performance of $YBa_2Cu_3O_{7-x}$ SQUID Magnetometers

by

John Joseph Kingston

ABSTRACT

A thin-film planar dc Superconducting QUantum Interference Device (SQUID) is a very sensitive detector of changes in magnetic field, but noise considerations require that it have a small pick-up area , and consequently a relatively poor intrinsic sensitivity to magnetic fields. To enhance the SQUID's field sensitivity, one invariably couples it to a flux transformer, a closed superconducting circuit consisting of a pickup loop, to which a signal is applied, connected in series to an input coil, which is inductively coupled to the SQUID.

To fabricate an optimal flux transformer, one whose input coil has multiple turns, one must use more than one superconducting thin-film layer, each of which is patterned into narrow strips or wires. In some places, it is necessary that wires from different layers cross, yet remain electrically isolated, to form crossovers, while in other places there must be superconducting contact between wires from different layers. Together, the superconducting wire, the superconducting - superconducting contact and the superconducting crossover constitute a superconducting interconnect or multilayer wiring technology that is an essential part of a complete superconducting microelectronics technology.

We discuss the development of an interconnect technology involving the high transition temperature (T_c) superconductor $YBa_2Cu_3O_{7-x}$ (YBCO). Because of the overiding need for epitaxial growth of YBCO thin films, there are strict limitations placed on the materials available for use in the insulating layer that separates the YBCO films in multilayer structures, and on the deposition and patterning techniques used to fabricate

them. We discuss the use of pulsed laser deposition in conjunction with patterning by shadow masks and later by photolithography to produce interconnects, multiturn input coils, and flux transformers.

We also discuss the performance of SQUID magnetometers, in which a flux transformer fabricated on one substrate is coupled to a SQUID fabricated on another. Our first magnetometers were hybrids - high T_c transformers coupled to low T_c SQUIDs, while later ones had both high T_c transformers and SQUIDs and could operate immersed in liquid nitrogen. We report on a magnetometer with a magnetic field sensitivity at 1Hz of about $2pTHz^{-1/2}$ at 77K, that was successfully used to perform magnetocardiograms on human subjects.

Dedication

I dedicate this dissertation to my father who would have been overjoyed to read it, had he lived.

Acknowledgements

I wish to express my appreciation to all those who helped to make this thesis possible. All of my work involved collaborations with others, and I am appreciative of all their assistance. For that reason, the pronoun "we" is used throughout this dissertation.

First of all, I want to express my appreciation to my major collaborators. I thank my advisor John Clarke for his support and guidance and for choosing me to work on his high T_c microelectronics research project. It allowed me to work on a well-funded and high-profile project. Fred Wellstood's ideas and insights were instrumental in helping us to achieve the many successes we shared. It was truly a pleasurable and rewarding experience to have worked with him. Philippe Lerch guided me through my early years as a graduate student and tirelessly assisted me in developing experimental skills. I am also indebted to Andy Miklich for his careful and painstaking measurements. Fortunately for me, his skills complemented mine. I thank Rasmus Kromann for his help in overcoming the many fabrication issues that confronted us. Mark Ferrari, Lise Sagdahl, Yukinori Saito, and Gene Dantsker provided many indispensible measurements. Mats Gustafson instructed us in the art of etching silicon wafers that were used as shadow masks. Nancy Missert provided many helpful suggestions and aided in the interpretation of x-ray diffraction results. We also received help from Diddier Robbes, Roberto Leone, and Bill Link in the initial stages of the project.

We are grateful to Professor Roger Falcone and Harald Hamster for use of their excimer laser deposition system and technical assistance during the early stages of this project prior to the construction of our own laser deposition system.

Mohammed Tidjani and Professor Ronald Gronsky provided TEM images that prooved indispensible.

Eugen Raicu, Guochun Liang, and Professor Theodore Van Duzer expedited the

production of a set of photolithographic masks.

We are very appreciative of all the help and assistance that we have received from many different employees at Conductus Inc. In particular we would like to acknowledge many useful discussions, suggestions, and assistance from Nate Newman, Kookrin Char, Mark Colclough, Luke Lee, Scot Sachtjen, Greg Zaharchuk, Roger Barton, and John Rowell. It was Nate's idea to use Si wafers as shadow masks for better line definition.

From Stanford, we received helpful suggestions and assistance from Professor Mac Beasley, Dave Fork, Peter Rosenthal, and Joe Virrel.

We thank L. Bourne, A. Cardona, and J. Sun from Superconducting Technologies Inc. for the use of one of their high T_c SQUIDs.

Our MgO substrates were expertly polished by Rodney Post.

Dr. D. Crum advised us about magnetocardiograms.

We would also like to thank Andy Brocato, Al Daft, Marco Ambrosini, and Tom Pederson for their considerable assistance in designing and building our laser deposition system.

We depended heavily upon the use of the Micolab in the Department of Electrical Engineering and Computer Science at the University of California. There we received expert assistance from many members of the very capable staff. They included Katalin Voros, Bob Hamilton, Dave Hebert, Debra Hebert, Marilyn Kushner, and Phil Guillory.

We thank Rudy Wenk for the use of his x-ray diffractometers.

I am grateful for the help and friendship of several staff mambers of the Department of Physics. They include Ivo Micheli, Lynne Pelosi, Toni Granger, Abram Hardin, and LeVern Garner. They helped to make my time here more enjoyable.

This work was supported by the California Competitive Technology Program and by the Director, Office of Energy Research, Office of Basic Energy Sciences, Materials Sciences Division of the U.S. Department of Energy under contract number DE-AC03-76SF00098.

I would also like to acknowledge support from a Department of Education Fellowship.

Most importantly however, I thank my wife for patiently enduring a long and trying process. She willingly sacrificed her own needs for mine, and for that I will be forever indebted.

Table of Contents

Chapter 1

Introduction

1.1 Overview:

The discovery of materials with superconducting transition temperatures (T_c) higher than the boiling point of liquid nitrogen[1-3] has aroused considerable interest in practical applications. One such area involves thin-film superconducting microelectronic circuits which operate at 77K Although the development of such a microelectronic technology has been challenged by some of the physical characteristics of the high-T_c materials, very substantial progress has been made.

There was much progress in the quality of high T_c superconducting thin films, especially of $YBa_2Cu_3O_{7-x}$ (YBCO), soon after the discovery of the high T_c materials in 1987. By the summer of 1988, epitaxial thin films of YBCO were being deposited *in situ*, by laser deposition[4]. The films had high critical currents (J_c) and high transition temperatures.

There were also reports by many groups working on weak link and grain boundary junctions[5], that would play the same role as conventional tunnel junctions in low T_c superconducting microelectronics. What was lacking, however, were any reports of interconnects or multilayer wiring, which are an essential component of superconducting microelectronics.

Having been involved in low T_c SQUID (Superconducting QUantum Interference Device) magnetometers for years, it was quite natural for our group to continue its interests in such devices when high T_c materials became available. Low T_c SQUIDs are the most sensitive detectors of magnetic flux, but their need to be cooled by liquid

helium can prove quite cumbersome. High T_c SQUIDs, operating in liquid nitrogen, could have increased applications in such fields as biomagnetism and geophysics, given sufficient sensitivity.

In order to increase their effective pick-up area and thereby enhance their magnetic field sensitivity, SQUIDs are coupled to flux transformers. We recognized that the need for a flux transformer is even more pressing for thin-film high-T_c SQUIDs[6] operated at 77K, where noise considerations require the inductance and hence the pickup area to be smaller than for low-T_c SQUIDs. This motivated us to pursue our research on crossovers and superconductor - superconductor contacts, the key circuit components needed for both interconnects and flux transformers.

We describe the investigation and development of superconducting microelectronic interconnect technologies based on $YBa_2Cu_3O_{7-x}$ (YBCO) and their application to flux transformers. We have used this technology to produce sensitive SQUID magnetometers which operate at 77K and above.

1.2 Superconducting Microelectronics

Almost all thin-film superconducting circuits of technological interest are constructed from just a few fundamental components. Fig. 1.1 shows the superconducting wire, the normal metal wire, the superconducting-superconducting contact, the superconducting-normal metal contact, the superconducting crossover, and the normal metal crossover. The Josephson junction or superconducting weak-link, which can take on many different configurations, is not pictured.

(1) wires

Superconducting or normal metal thin films are patterned into strips.

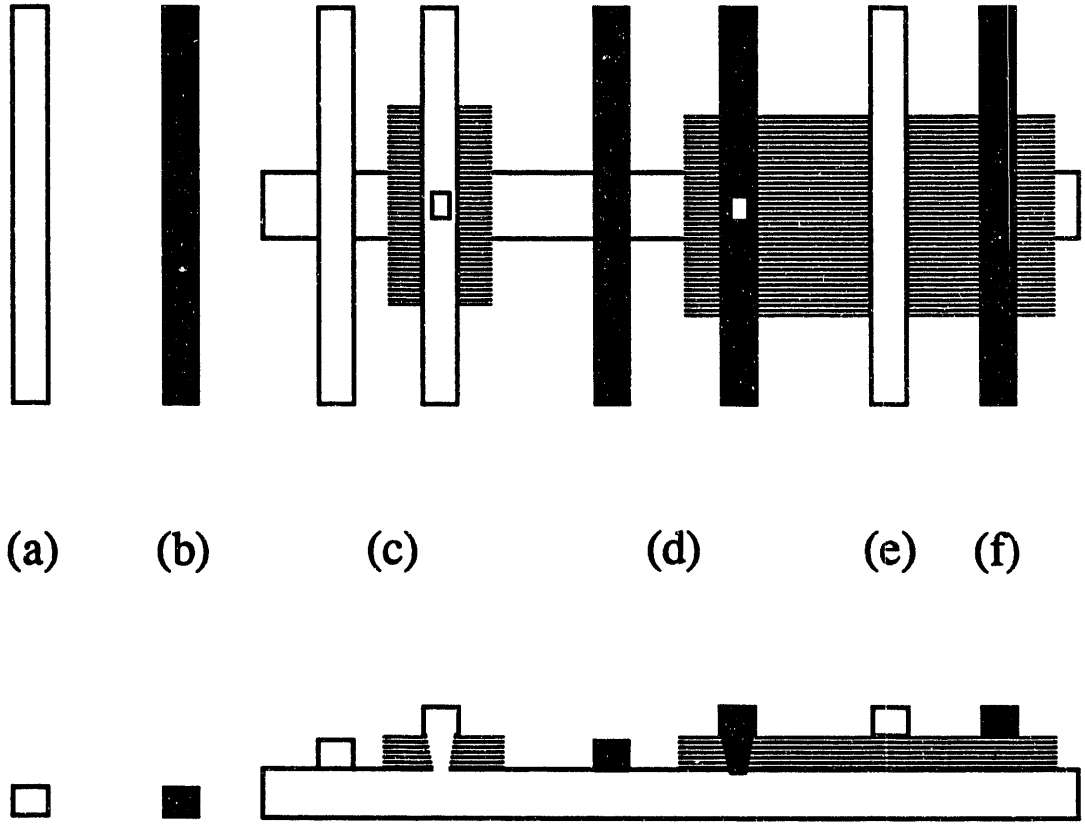

Fig. 1.1 Schematic of superconducting microelectronic circuit components: (a) superconducting (sc) wire, (b) normal metal (nm) wire, (c) sc - sc contact and sc - sc window contact, (d) nm - sc contact and nm - sc window contact, (e) sc - sc crossover, (f) nm - sc crossover.

(2) superconductor - superconductor contacts

Thin film wires from two different superconducting films make superconducting contact to each other. In the window contact, the conducting films make contact through a hole patterned into an insulating film, that otherwise islolates them physically and electrically.

(3) superconductor - normal metal contacts

Metal films are deposited onto the superconducting wires and patterned to form electrical contacts. In the window contact, the conducting films make contact through a hole patterned into an insulating film, that otherwise isolates them physically and electrically.

(4) crossovers

Conducting wires from two different conducting films are physically separated by an intervening insulating film. This allows the wires to cross yet remain electrically isolated.

(5) Josephson Junctions

In low T_c microelectronics, the usual configuration has two superconducting layers separated by a thin insulating tunnel barrier. In high T_c microelctronics, grain boundaries can provide the weak link.

In order to construct an active superconducting device, it is necessary to include one or more superconducting weak links or junctions. While an individual junction is a

two terminal device, three terminal devices with power gain are essential for many kinds of circuits. These can be constructed from weak links by connecting two in parallel, as in the dc SQUID. In this configuration, the critical current is an extremely sensitive function of applied magnetic field, which can be generated by supplying current to a small thin-film coil which is placed next to the junctions.

Thin-film superconducting wires are used for conveying electrical signals with low loss. This loss is smaller at lower frequencies, and vanishes at zero frequency. Thin-film normal metal wires are used to construct resistors or dissipative elements. The superconducting-superconducting contact is used for connecting one superconducting layer to another. When using photolithographic patterning, it is customary to fabricate window contacts or vias. The superconducting-normal metal contact is needed to connect superconducting wires to normal wires. Crossovers become necessary when several components must be interconnected and the connecting lines must not electrically short together. Ordinary passive circuit components such as resistors, inductors, capacitors, and transmission lines can be formed from combinations of superconducting wires, normal wires, contacts, and crossovers.

Together, the superconducting wire, the superconducting-superconducting contact and the superconducting crossover constitute a superconducting interconnect or multi-layer wiring technology. Interconnect technologies are of interest for a number of reasons. First, a superconducting interconnect technology is an essential part of a complete superconducting microelectronic technology. Second, an interconnect technology by itself can be used in a variety of applications: constructing entirely passive circuits, connecting together normal circuit elements with low loss transmission lines, or distributing power to a circuit. Finally, many of the materials and processing problems faced in developing a complete microelectronics technology can be addressed in this simpler system.

1.3 SQUIDs

The dc Superconducting QUantum Interference Device (SQUID) can be a very sensitive detector of changes in magnetic flux, and is widely used as a sensor of magnetic field or magnetic field gradient.[7] Only a brief description of a dc SQUID and ideas pertinent to the design of an optimum high T_c SQUID will be provided here.

A dc SQUID consists of two junctions connected in parallel on a superconducting loop of inductance L as in Fig. 1.2(a). If the junctions are hysteretic, they must be resistively shunted to remove this hysteresis. Fig. 1.2(b) shows that the critical current of the SQUID is modulated by magnetic flux Φ threading the SQUID loop, with maximum critical current occuring when $\Phi = n\Phi_0$ and minimum critical current occuring when $\Phi = (n+1/2)\Phi_0$, where n is an integer and Φ_0 is the flux quantum. If the SQUID is current biased at a value exceeding its critical current, $2I_c$, the voltage across the SQUID oscillates with period Φ_0 as Φ is increased, as shown in Fig. 1.2(c). The SQUID is generally operated on a steep part of the V - Φ curve, in a feedback circuit as a null detector of magnetic flux.

To optimize the design of a SQUID, there are certain conditions that must be met. The first places an upper bound on the inductance of the SQUID. By equipartition of energy, the flux noise energy equals kT/2:

$$\langle\Phi_N^2\rangle/2L = kT/2 \qquad (1.3.1)$$

where k is the Boltzman constant and T is the temperature.

In order that the noise not overpower the signal, we must have that:

$$kT/2 << \Phi_0^2/4L. \qquad (1.3.2)$$

Thus at 77K we require that:

$$L << 940\text{pH}. \qquad (1.3.3)$$

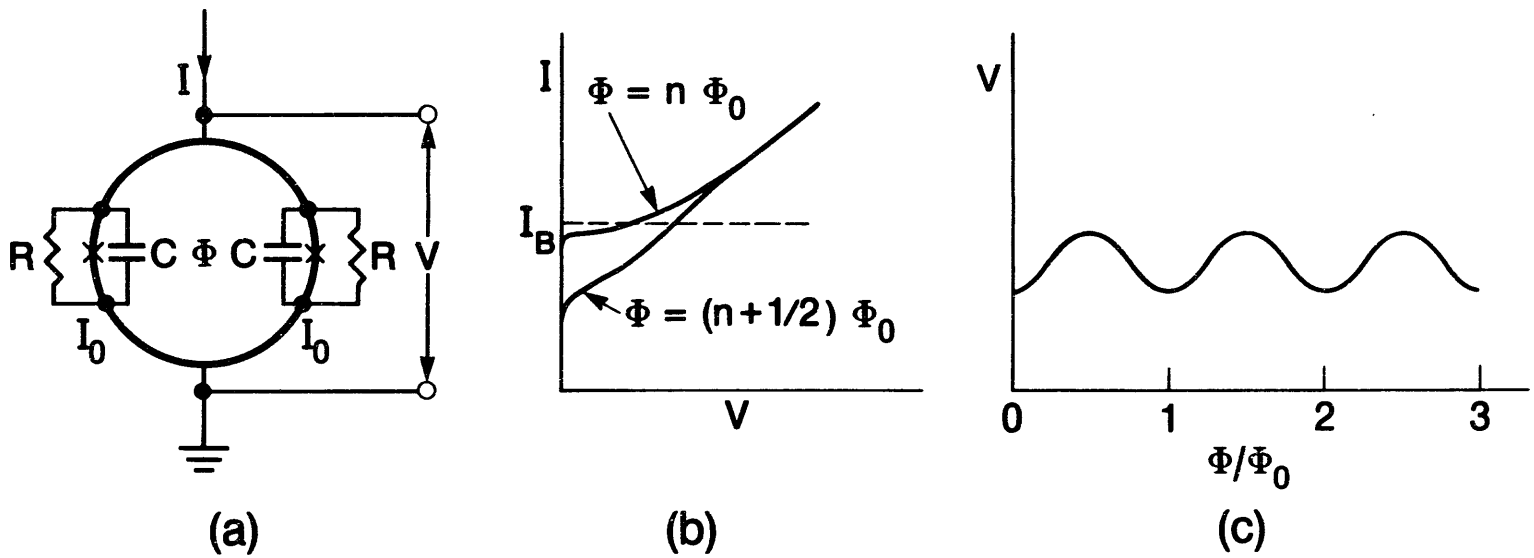

Fig 1.2 (a) The dc SQUID; (b) I-V characteristics; (c) V vs. Φ/Φo at constant bias current I_B.

The second condition places a lower bound on the critical current of each junction. In order to have phase coherence across the junctions, the coupling energy, $I_0\Phi_0/2\pi$, must be much larger than kT:

$$I_c\Phi_0/2\pi >> kT. \tag{1.3.4}$$

Thus at 77K we require that:

$$I_c >> 3.3\ \mu A. \tag{1.3.5}$$

Finally, the noise energy is minimized when the screening parameter, β

$$\beta = 2LI_c/\Phi_0 = 1, \tag{1.3.6}$$

which we can rewrite as:

$$LI_c = \Phi_0/2 \approx 10^{-15}\ Wb. \tag{1.3.7}$$

All three conditions can be met with:

$$I \approx 10\mu A \tag{1.3.8}$$

$$L \approx 100pH. \tag{1.3.9}$$

To achieve a satisfactory value of L, one must make the SQUID washer smaller for high T_c SQUIDs than for low T_c SQUIDs. Thus, the effective pick-up area of high T_c SQUIDs is smaller, and although the flux sensitivity remains high, the magnetic field sensitivity is reduced and the need for a flux transformer is increased.

1.4 Flux Transformers

Because most thin-film planar SQUIDs have small pickup areas, their intrinsic sensitivity to magnetic field is relatively poor, and one almost invariably couples SQUIDs to a superconducting flux transformer[8] to achieve the desired field sensitivity. A flux transformer is a closed superconducting circuit consisting of a pickup loop, to which the signal is applied, in series with a multiturn input coil, which is inductively coupled to the SQUID.

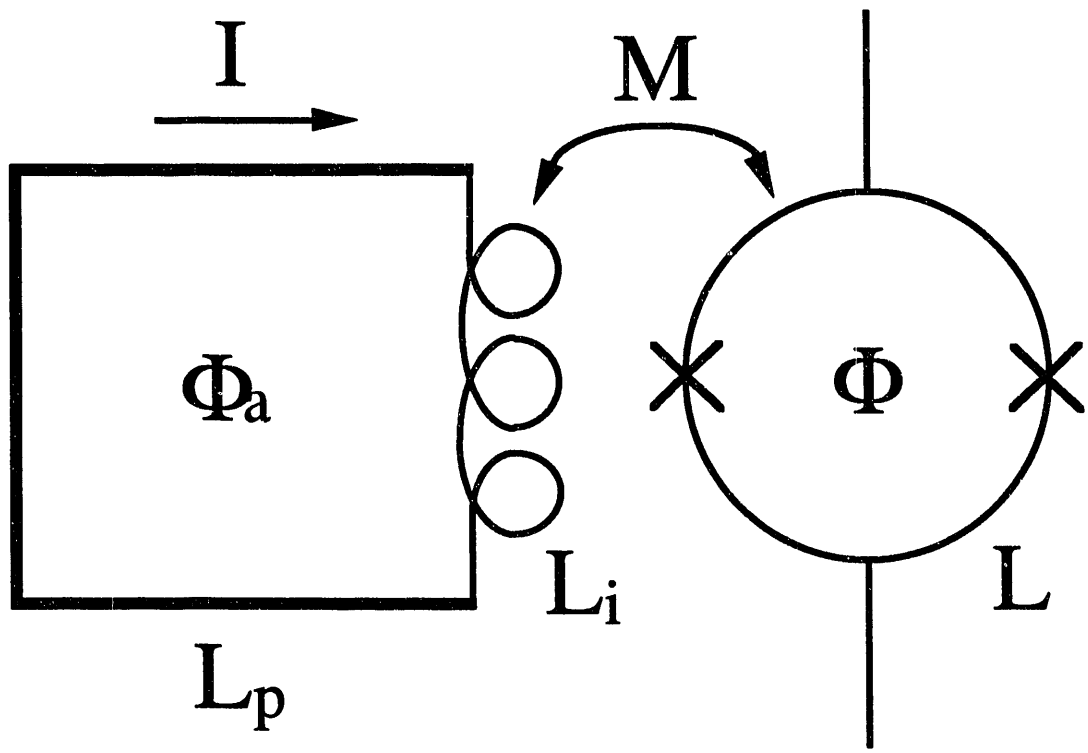

Fig. 1.3 Schematic showing flux transformer coupled to a dc SQUID. The transformer has pickup coil inductance L_p and input coil inductance L_i. A flux Φ_a is applied and induces a screening current I. With mutual inductance M, a flux Φ is coupled to the SQUID with inductance L.

Consider a flux transformer with pick-up coil inductance L_p and input coil inductance L_i, that is coupled to a SQUID as shown in Fig. 1.3. A flux Φ_a is applied to the flux transformer that induces a current I to flow through it. Since a superconducting loop conserves flux,we must have:

$$\Phi_a = I(L_p + L_i). \tag{1.4.1}$$

The flux transformer couples a flux, Φ, to the SQUID,

$$\Phi = MI, \tag{1.4.2}$$

where M is the mutual inductance between the flux transformer and the SQUID. By defining a coupling constant α such that,

$$M = \alpha(LL_i)^{1/2} \tag{1.4.3}$$

we can express Φ as

$$\Phi = BA_p\alpha(LL_i)^{1/2}/(L_p + L_i), \tag{1.4.4}$$

since we can write

$$\Phi_a = BA_p \tag{1.4.5}$$

where A_p is the area of the pick-up coil. For a given A_p and L_p, Φ is maximized when the transformer is well coupled

$$\alpha = 1 \tag{1.4.6}$$

and the inductances are matched.

$$L_i = L_p. \tag{1.4.7}$$

In order to match inductances, the input coil must be multiturn, since its area is much smaller than the area of the pick-up coil. This necessitates the use of at least two superconducting layers. One must be able to fabricate interconnects to construct such a flux transformer.

If the inductances are matched, we can write:

$$\Phi = BA_p\alpha(L/2L_p)^{1/2}. \tag{1.4.8}$$

The design of an optimum flux transformer involves a few simple considerations:

(i) The magnetic field response increases as the area of the pickup coil increases.

(ii) The pickup coil should have the smallest possible inductance, L_p, for its area.

(iii) The input coil should have approximately the same overall size and shape as the SQUID in order to be efficiently coupled to it.

We note that if one is to obtain substantial gain in magnetic field response, the area of the pickup loop should be much greater than that of the SQUID.

We can define the gain of the flux transformer as the ratio of the flux coupled to the SQUID with and without the flux transformer. The flux the bare SQUID sees is,

$$\Phi_{S_o} = \eta AB \tag{1.4.9}$$

where η is the flux focusing factor of the SQUID washer and A is the area of the center hole. So the gain is:

$$G = \Phi/\Phi_{S_o} = \alpha(A_p/2\eta A)(L/L_p)^{1/2}. \tag{1.4.10}$$

Using the values L_p = 20n, α = 0.6, L = 100pH, A_p = 100 mm^2, A = 0.002 mm^2, η = 6, which are typical for high T_c SQUIDs and flux transformers,we obtain:

$$G \approx 175. \tag{1.4.11}$$

It is clear that flux transformers can enhance the field sensitivity of high T_c SQUIDs quitedramatically.

References

1. M. K. Wu *et. al., Phys. Rev. Lett.* **58**, 908 (1987)

2. H. Maeda, Y. Tanaka, M. Fukutomi, and T. Asano, *Jpn. J. Appl. Phys. Lett.* **27**, L209 (1988)

3. Z. Z. Sheng and A. M. Hermann, *Nature* **332**, 55 (1988)

4. S. Witanachchi, H. S. Kwok, X. W. Wang, and D. T. Shaw, *Appl. Phys. Lett.* **53**, 234, (1988); A. Inam, M. S. Hegde, X. D. Wu, T. Venkatesan, P. England, P. F. Miceli, E. W. Chase, C. C. Chang, J. M. Tarascon, and J. B. Wachtman, *Appl. Phys. Lett.* **53**, 908, (1988); J. Frohlingsdorf, W. Zander, and B. Stritzker, *Solid State Communications* **67**, 965, (1988); B. Roas, L. Schultz, and G. Endres, *Appl. Phys. Lett.* **53**, 1557, (1988); G. Koren, E. Polturak, B. Fisher, D. Cohen, and G. Kimel, *Appl. Phys. Lett.* **53**, 2330, (1988); R. K. Singh, J. Narayan, A. K. Singh, and J. Krishnaswamy, *Appl. Phys. Lett.* **54**, 2271, (1989).

5. For example: John Moreland, L. F. Goodrich, J. W. Ekin, T. E. Capobianco, A. F. Clark, A. I. Braginski, and A. J. Panson, *Appl. Phys Lett.* **51**, 540 (1987); G. C. Hilton, E. B. Harris, D. J. Van Harlingen, *Appl. Phys Lett.* **53**, 1107 (1988)

6. For example: R. H. Koch, C. P. Umbach, G. J. Clark, P. Chaudhari, and R. B. Laibowitz, *Appl. Phys. Lett.* **51**, 200 (1987); B. Häuser, M. Diegel, and H. Rogalla, *Appl. Phys. Lett.* **52**, 844 (1988); H. Nakane, Y. Tarutani, T. Nishino, H. Yamada, and U. Kawabe, *Jap. J. Appl. Phys.* **26**, L1925 (1987); R. H. Koch, W. J. Gallagher, B. Bumble, and W. Y. Lee, *Appl. Phys. Lett.* **54**, 951 (1989).

7. J. Clarke, Nato ASI Series Vol. 59, Superconducting Electronics, Ed.M. Nisenoff and H. Weinstock (Springer-Verlag, Berlin, 1989) p87.

8. J. E. Zimmerman and N. V. Frederick, *Appl. Phys. Lett.* **19**, 16 (1971).

Chapter 2

High T_c Superconducting Microelectronic Circuit Concepts

2.1 General Construction Principles and Requirements

The difficulties that one encounters in using high-T_c materials depend strongly on the particular application. For example, to fabricate magnet wire, one wishes to obtain a strong and flexible wire which can carry a large current in a high magnetic field. The problems encountered are quite different from, say, the growth of very pure samples for research purposes or the construction of thin-film electrical circuits from high-T_c materials. For the construction of circuits, these difficulties divide into three highly interdependent areas: circuit-related factors, materials-related factors, and processing-related factors.

2.1.1 Circuit-Related Factors

As discussed in Ch. 1, a complete superconducting microelectronics technology requires the development of just a few key components. Since it is essential that all of the components be built on the same chip, it is required that a technique or process used for the construction of one component not prevent the construction, or lead to the destruction, of some other component. In addition, to provide flexibility and generality in design, a technology should allow the components to be placed anywhere on a substrate. Together, these conditions mean that the technology should allow the construction of circuits with an arbitrary placement and combination of components: this is the requirement of extendibility.

The physical size of a component is an important parameter which affects the electrical characteristics and performance of the circuit, for example, the speed, electrical

impedance and current carrying capacity. As a result, real circuits typically use a range of feature sizes to achieve the desired characteristics; when the number of individual components is large, it is generally advantageous to shrink the size of each so that the overall circuit does not become too large. Thus, a useful technology should allow one to scale the component size over a large range. Additionally, the components must generally be connected together. Since microelectronic circuits are built on one surface of a chip, to connect together a number of components, it is generally necessary to use more than one wiring layer. We thus require the technology to allow wiring to be made between any two conducting layers.

Circuits which require a large number of components are common in many digital applications. The main difficulty associated with such circuits is not the number of components, *per se*, but that they must all have nearly identical parameters. In such circuits, the reproducibility and reliability of the components often become the limiting factors. The reproducibility from one chip to the next affects the yield of a process, so that both the on-chip and chip-to-chip reproducibility are of great importance for the commercial viability of a technology.

Finally, the superconducting wires must be capable of carrying an acceptable level of supercurrent. For a given film thickness and required current, the critical current density of the film determines the minimum linewidth that can be used. To construct circuits with very small line widths or high current carrying capacity, it is essential to use films with a large critical current density.

2.1.2 Processing-Related Factors

The construction of multilayer circuits differs substantially from the task of depositing multiple layers of films, largely because in a typical circuit each layer must be patterned individually. Thus one cannot generally build a circuit with a single patterning of

a multilayer stack of unpatterned films. By processing-related factors, we mean those difficulties which arise from the individual patterning of each layer.

One can pattern a film in five distinct ways:

(i) By controlling where the material lands during deposition, for example, with shadow masks [1] as will be discussed in Sec. 2.2.3.

(ii) By using a liftoff procedure. This involves first depositing and patterning a layer of material which will act as a stencil layer. One then deposits the film and dissolves away the stencil, leaving film at places where the stencil was removed during patterning. A CaO_2 stencil layer, which is soluble in water, has recently been developed to allow liftoff patterning of YBCO.[2]

(iii) By etching away material after it has been deposited. This is the most highly developed patterning technique, and a wide range of techniques are available for etching YBCO, including selective chemical etching,[3] non-selective chemical etching,[4] reactive ion beam etching,[5] focused ion beam etching,[6] and laser patterning.[7] Focused ion-beam etching and non-selective chemical etching using weak solutions of HNO_3 have been most widely used to pattern YBCO. Selective chemical etches have recently been used for YBCO and $SrTiO_3$, and also for gold on YBCO.[8] On the other hand, laser patterning is unlikely to be of general use for forming multilayer circuits. Not only is underlying material damaged, but the etched material is expelled onto neighboring regions where it can interfere with the deposition of subsequent layers. We will discuss the use of non-selective chemical etching and ion beam etching techniques, in combination with photolithography, to pattern YBCO films in Ch. 8.

(iv) By implanting material into a deposited layer. While patterning by implantation is used widely for the growth of semiconductor structures, because relatively small doping levels can produce large changes in the conductivity, it has been used infrequently for superconductors. Although the high-T_c superconductors have much lower carrier densities than ordinary metals, compared to a semiconductors they still require much higher doping

concentration to produce a significant change in the conducting properties. Also, since the dopant works by "poisoning" the YBCO to form an insulating layer, it is important that a dopant not diffuse into adjacent superconducting layers, or prevent the epitaxial growth of upper layers.

(v) By damaging the crystal structure or stochiometry. This approach is possible because, unlike an ordinary metal, the high-T_c materials are insulating in the amorphous state. Damage has been induced by using an ion beam[9] to create disorder. One can also remove O_2 from the film selectively, thus turning portions into insulators. Unfortunately, because the resistivity depends sensitively on the oxygen content, this form of damage is readily reversed by a high temperature process, and thus can only be used in a final layer. One can pattern by damaging the crystal structure of an underlying layer or by depositing and patterning a buffer layer underneath a YBCO film. Either the buffer layer or the substrate does not support the epitaxial growth of a high-T_c material deposited on top.[10,11] Patterning by damage leaves behind a non-crystalline layer which generally cannot support the epitaxial growth of an upper layer. A damaged layer will probably also exhibit a higher rate of interdiffusion with adjacent layers.

It should be noted that patterning by implantation and damage tend to leave a planarized circuit. For a multilayer system, this would be distinctly advantageous if the other difficulties can be overcome.

One of the most important factors in the patterning of individual layers by the first three techniques is the production of edges that will generally need to support the growth of subsequent layers. For the upper films to be continuous, it is important that their growth not be disordered at such edges. Where high current carrying capacity is required, it is important that underlying edges do not lead to high angle grain boundaries in an overlying superconducting material. Thus, one desires epitaxial growth over edges as well as over flat surfaces.

Resist-based patterning consists of two distinct steps: (1) a definition step where the pattern is transferred to the resist, and (2) an etching (or liftoff) step where material is removed and the pattern is transferred to the material. This separation of the patterning procedure into two steps allows one to use an etchant which is best suited for the structure or material at hand. There are a number of constraints affecting the choice of an etching technique. First, it is important to use techniques which limit the etching to individual layers, that is, chemically selective etches or timed etches. Second, it is important that the etching procedure not damage unetched materials or leave behind damaged surface material or residue which will tend to prevent epitaxy in subsequent layers. Thus the etch must contain only materials which are chemically compatible with layers it contacts. In practice, this constraint can be relaxed if an appropriate cleaning step is employed after an etch to remove any damaged material or residue.

The construction of multilayer structures requires that the surface of each layer be of high integrity to allow growth of subsequent layers. Conducting layers should be free of dirt, deposited particles, or growths which might prevent the epitaxy of overlying insulating layers and produce shorts. Similarly, insulating layers should be free of pinholes or cracks that cause shorting between layers.

2.1.3 Materials-Related Factors

Although there are only three components in an interconnect technology, the physical properties of the high-T_c materials impose a number of strong constraints. Some of these factors arise from the chemical interactions between the high-T_c materials, the substrate and insulating layers. Others arise from the growth behavior of the layers as they are deposited on an underlying substrate or layer.

For the superconducting layers to ahieve a high-T_c, they must have the correct crystalline structure. In addition, for a film to have a substantial critical current density the

microcrystalline structure should be free of high angle grain boundaries. An exception is the twin-boundary, which has little afffect on the critical current density. Thus each layer must be epitaxially matched to any layer which it grows on. Furthermore, this epitaxial relationship should be maintained up to the highest deposition temperature encountered so that the insulator or lower superconducting layer does not tend to recrystallize and disrupt growth.

Because the high-T_c materials are composed of planes which are only weakly-coupled together, the superconducting properties are highly anisotropic. In particular, the current carrying capacity is greatest in the direction parallel to the a-b plane, implying that interconnects should be made from c-axis oriented films. The use of a-axis films would produce a large anisotropy in the substrate plane, which would be undesirable in most circuits. It should also be noted that while extended defects such as grain boundaries are detrimental to the current carrying capacity of a film, point defects act as pinning sites for flux vortices and produce a high critical current density.

The superconducting properties of a material are a function of the temperature, T. In particular, as T increases towards T_c, the critical current density, J_c, decreases while the surface resistance and penetration depth increase. The current carrying capacity of a wire is determined by J_c, while the penetration depth affects the inductance. Thus to maintain a reasonably high value of J_c and to prevent temperature variations producing too large of a variation in parameters, one prefers to operate circuits well below T_c.

Each film in a multilayer must be chemically compatible with adjacent films so that unfavorable reaction products or phases are not formed. This chemical compatibility must exist at temperatures as high as needed to deposit the layers, typically 750°C. It is also important that elements from one layer do not diffuse into and damage other layers. A lack of crystallinity or the presence of grain boundaries can lead to substantial increases in the interdiffusion of layers and the rate at which a film is attacked by chemicals. Thus it is important that films be of high crystalline quality as judged by x-ray or channeling

measurements. Such films are also more resistant to degradation by water or other chemicals used in processing. Because interdiffusion increases rapidly with temperature and lattice defect density, it is probably essential to use "*in situ*" processes in which films crystalize as they are deposited. *In situ* films do not require annealing after deposition and are generally deposited at temperatures substantially lower than those required to anneal the film; for an *in situ* process, growth proceeds by the arrangement of the deposited atoms on the oriented surface of the film, rather than the rearrangement of atoms in the bulk of a disordered film.

Because the layers must undergo substantial temperature changes after deposition, each layer must have a thermal expansion coefficient, α_i, which is compatible with that of the substrate, α_s. A substrate with a smaller thermal expansion coefficient puts tensile stress on a film as it cools following a deposition, tending to produce cracking in the film.[12] This is detrimental to insulating layers where it produces electrical shorts, and to conducting layers where it produces open lines.

At typical deposition temperatures, oxygen rapidly diffuses through the high-T_c materials. In order to achieve a high T_c, the film must have the correct oxygen stochiometry by the time the sample cools to room temperature. For example, at 760 Torr of oxygen, significant oxygen re-incorporation occurs in YBCO at around 450°C. It is important that any insulating layer which is deposited over a high-T_c film have a substantial diffusion coefficient for O_2 in the appropriate temperature range. Fortunately, re-oxygenation is often not a very serious constraint. Thin-films are geometrically poor diffusion barriers, so that even a modest diffusion coefficient should suffice. Furthermore, MgO and perovskites such as $SrTiO_3$ have sufficient oxygen permeability.

It is essential that the insulating layers have acceptable electrical properties, in particular, a high resistivity at 77K. As a rough guide, the resistivity should be at least $10^6\Omega$cm; yielding a resistance of 2kΩ between two 1x1mm^2 films separated by a 200nm thick film. Also, the dielectric constant of the insulation layer provides a limit to the

maximum frequency at which a circuit can operate. For low frequency applications, the dielectric constant is generally not important, but for microwave applications, dielectric constants and losses in the insulation layer and substrate must be kept small. Typically, one would like a dielectric constant of less than 10 and a loss tangent of less than 0.001 at the frequency of interest.

2.2 Selection of Materials, Deposition Technique, and Patterning Technique

2.2.1 Selection of Materials

Of the high-T_c superconductors, only YBCO has so far been developed for interconnect applications. The reasons for this are numerous, and we list the most important. First, the physical properties of YBCO are now well-known, providing a good basis for selecting compatible materials and processes. Fortunately, there are many insulating materials that can be used for multilayer structures. Second, there are now available a wide variety of deposition techniques for single layer films, enabling one to produce relatively smooth, crack-free thin films on a variety of substrates. Some of these techniques can produce excellent quality *in situ* thin films. Third, crystalline YBCO is relatively inert and, with proper care, films can withstand many resists and chemical processes. Finally, the critical current density can be as large as $10^7 Acm^{-2}$ at 77K, more than adequate for most applications.

In principle, it should be possible to develop multilayer structures from other high-T_c materials. The second most promising candidate is $Bi_2Sr_2CaCuO_{8+y}$ (BSCCO) although it is highly anisotropic and tends to form several different phases with different superconducting properties. The properties of single layer films will probably need to be improved considerably before BSCCO can be incorporated into useful and reliable multilayer structures. On the other hand, it appears that multilayer circuits using

$Tl_2CaBa_2Cu_2O_{8+y}$ (TCBCO) will be difficult to construct: TCBCO requires the introduction of two volatile components, O_2 and Tl, and relatively high temperature processing (900°C).

This choice of YBCO is not without its problems. One disadvantage, if one wishes to operate at 77K, is that the transition temperature is only 92K (or about 88K on MgO substrates), so that one one needs to consider the reduction in J_c, the increase in surface resistance, and the effect of temperature variations on the circuit parameters.

There are a number of suitable substrates for growing YBCO, including $SrTiO_3$, MgO, YSZ, $LaAlO_3$, $LaGaO_3$, $NdGaO_3$ and CeO_2. Table 2.1 lists crystal structures, lattice constants, thermal expansion coefficients, dielectric constants, and loss tangents for YBCO and several insulators. Unfortunately, the a and b lattice constants of YBCO are not equal, so that even materials which are closely lattice matched, such as (100) $SrTiO_3$ and (100) $LaAlO_3$, will produce twinned regions. On the other hand, materials which are less closely lattice matched, such as MgO and YSZ, can have additional epitaxial relationships, and 45° angle grain boundaries are common.[13] The prevalence of one orientation over another is a function of the temperature and deposition conditions.

Reffering to Table 2.1, we note that the thermal expansion coefficients of MgO and $SrTiO_3$ are only sightly larger than that of YBCO. This means that after cooling from a high temperature deposition, YBCO films tend to be under compressive stress when grown on these substrates, and cracking should not occur. On the other hand, YBCO has a larger thermal expansion coefficient than silicon and sapphire, and hence there is a limit to the thickness of films that can be grown on these materials without cracking.[12]

We have mostly used MgO substrates because they are inexpensive and can be obtained in suitable sizes (typically 12.5mmx12.5mm), but they have some difficulties. In addition to generating 45° angle grain boundaries in YBCO, the lattice mismatch also depresses the transition temperature to 88K and generates defects. The surface is easily

damaged by exposure to water vapor or by improper polishing techniques. A buffer layer of $SrTiO_3$ reduces lattice mismatch, improves the in-plane epitaxy, and allows the patterning of YBCO layers by acid etch, but cannot overcome all the potential problems associated with this material.

Table 2.1. Parameters of YBCO and compatible dielectrics.[14-17]

Materials	structure	lattice constant (Å)	thermal expansion coefficient (10^{-6}/°C)	dielectric constant at 25°C	loss tangent (10^{-4})
YBCO	ortho-rhombic	a=3.83 b=3.89 c=11.7	8.5	---	---
$SrTiO_3$	cubic	3.905	9.4	>300	>200 (1MHz)
MgO	cubic	4.213	14	10	91 (1MHz)
YSZ	cubic	5.147	11	27	54 (10GHz)
$LaAlO_3$	cubic	3.792	9.8	15	5.8 (1MHz)
$LaGaO_3$	pseudo-cubic	a=3.888 b=3.884 c=3.888	9	25	18 (1MHz)
$NdGaO_3$	ortho-rhombic	a=5.428 b=5.493 c=7.729	a: 12 b: 7 c: 6	25	18
CeO_2	cubic	5.411	9.5	26	---

The choice of the superconductor and substrate restricts the choice of possible insulators. It is highly desirable that the insulator can be deposited using the same technique and at temperatures not significantly higher than those required to deposit YBCO.

The obvious choices for insulators are those which are used for substrates. Laser deposited $SrTiO_3$ films are are of high quality when grown at deposition temperatures similar to those used for YBCO.[1] Compared to laser deposited $SrTiO_3$, laser deposited MgO can be grown over a wide range of temperatures up to 200°C cooler,[18] and $LaAlO_3$ and $NdGaO_3$ about 50°C higher.[19,15] All of these materials have a resistivity which is high enough for most applications. In addition, variants of YBCO have also been used as insulation layers, the most well known of these is $PrBa_2Cu_3O_{7-x}$.[20] Unfortunately, these materials tend to have a relatively high conductivity, so they are probably unsuitable for most circuit applications involving insulation between layers.

Of the insulators, we have devoted most of our work to $SrTiO_3$ and CeO_2. The main drawback with $SrTiO_3$ is the extremely large dielectric constant, approximately 10^3 in films at 77K, which makes it unsuitable for rf applications. Since our work was devoted primarily to low frequency applications and to proving feasibility, we did not consider this to be an important issue initially. A number of other insulators with better dielectric properties appear to be suitable, namely MgO, Yttrium Stabilized Zirconia (YSZ), $LaAlO_3$, $LaGaO_3$, $NdGaO_3$, and CeO_2. In Table 2.1, we have sumarized the dielectric constant and loss tangents for these materials.

2.2.2 Selection of Deposition Technique

Many different techniques have been used to deposit thin films of high-T_c materials. From the general requirements discused above, we see that the best deposition process for multilayer structures should be capable of depositing epitaxial YBCO *in situ* , quickly, and at a relatively low temperature. These attributes tend to minimize problems associated with interdiffusion, thermal expansion and chemical interaction. The deposition of the insulating layers should satisfy similar requirements.

We have chosen to use a KrF (248nm) pulsed excimer laser for depositing both the superconducting and insulating layers. We typically deposit material at about 50nm per minute, although far higher rates have been demonstrated by Wu et al.[21] We have found that laser deposition is well-suited to the deposition of $SrTiO_3$, MgO, YSZ and other dielectrics as well as silver for *in situ* normal metal contacts[22]. As an added advantage, the targets are stochiometric and need no special preparation other than occasional surface conditioning as discussed below.

An additional advantage in laser depositing the insulation layer is that the films are relatively pinhole free, whereas pinholes seem to be a common problem in insulating films which have been sputtered onto YBCO. We have found pinhole shorts in sputtered films of $SrTiO_3$ and MgO.[23] The origin of pinholes in sputtered films is apparently not known and may depend on the material. However, it should be noted that the pinholes generally only become apparent when one completes the top contact with the high-T_c material. Our own experience is that when the top layer is a metal which has been deposited in a low temperature process, one does not see any pinholes. This result suggests that, at least in some cases, the pinholes open up during the high temperature deposition of a top layer. While in principle it should be possible to sputter pinhole-free films, this has generally not been the case, and more work is needed on this problem.

Despite the advantages of the laser, there are some significant limitations; in particular, it is time-consuming to deposit thick layers of materials which are transparent in the ultraviolet, such as MgO. However, it is possible in the case of MgO to use a metallic Mg target and with sufficient O_2 in the chamber, to grow epitaxial MgO.[22] Conversely, it should be noted that both YBCO and $SrTiO_3$ are good absorbers at 248nm. Another problem is that the material is typically deposited over a relatively small area (usually about 10 to 20 mm on a side), and there is considerable variation in thickness over this area. The uniformity and coverage can be increased to some extent by using a higher fluence (laser energy density per pulse) on the target. Another drawback of laser deposition is that small

particles of YBCO are ejected from the target and deposited on the sample. We have found that this process is enhanced when the surface of the target is rough, and can be substantially reduced by polishing the target.[1] We will have more to say about this in Ch. 3. Additionally, it is important that the surface of the target not become so hot that melted regions are produced; these lead to the deposition of large drops of material. The target surface is heated by both the laser and by radiation emmited from the heater block. To prevent melting, we use a water-cooled heat shield to block most of the target surface from the heater radiation, and rotate the target in a water-cooled mechanism.

2.2.3 Selection of Patterning Technique

For the patterning of semiconductor circuits, photolithographic techniques are so highly refined that it is inconceivable to use anything else. However, for the preliminary investigation of novel materials, we found that shadow mask techniques to be very useful and have several advantages over photolithographic techniques. First, it is simple to construct masks for crossovers, wires, or other simple features, provided they are not too small or too numerous. Second, the thin-film is never exposed to etching chemicals or resists; if need be, the entire process can be conducted *in situ* with the sample at high temperature. Third, shadow masks produce deposited films with smooth and gently sloping edge profiles, facilitating the crystalline growth of layers deposited subsequently over these edges. Of course, shadow masks are non-extendable and cannot be used to make complicated circuits or small windows which would require an unsupported mask.

In fact, for laser deposition, it is somewhat remarkable that one can use shadow masks at all. During an *in situ* deposition, the ambient O_2 limits the mean free path to about 0.25mm so that if the thickness of the mask is great enough and its opening is narrow enough, material will tend to be deposited on the sidewalls of the mask opening rather than on the substrate. We have found that material deposited under such conditions

has severely degraded superconducting properties, thus limiting the minimum linewidth achievable with shadow masks. The achievable linewidth is also limited by the separation between the mask and the substrate surface. If this separation becomes comparable to the mean free path, significant scattering occurs after the material has passed through the mask, and the linewidth will be larger than the mask opening. By lowering the O_2 pressure, and thus increasing the mean free path, we can achieve finer lines, but decreasing the pressure substantially below 150mTorr degrades the film, presumably because of insufficient oxygen incorporation. By striking a plasma in the oxygen, we have found that sufficient O_2 is incorporated and T_c remains high even for an O_2 pressure as low as 35mTorr. It is likely that lower pressures could be used for more highly ionized plasmas.

We have made masks in a number of ways. For patterns about 1mm wide we used stainless steel foil, cut with scissors, or thin stainless steel sheet, patterned by machining. Thin foil masks tend to warp at high temperature giving poorly defined edges. To pattern structures with finer details, we used photolithography and anisotropic etching to form Si shadow masks.[24] We first coat the wafers with a 200nm thick layer of silicon nitride on both sides, spin on photoreisist, and expose and develop the resist to form the desired pattern. The wafer is then etched in HF to remove the nitride where it is not covered with resist. We strip the resist, and use a KOH solution to etch through the Si where the nitride has been removed. The etchant is anisotropic and leaves the mask opening with 54.7° beveled walls, enabling us to overcome some of the deposition problems associated with thick masks. In addition, these masks are stiffer and lie flatter than the foil masks leading to better line definition.

References

1. J. J. Kingston, F. C. Wellstood, P. Lerch, A.H. Miklich, and J. Clarke, *Appl. Phys. Lett.* **56**, 236 (1990).

2. B. Roas, *Appl. Phys Lett.* **59**, 2594 (1991).

3. W. Eidelloth, W. J. Gallagher, R. P. Robertazzi, R. H. Koch, and B. Oh, *Appl. Phys Lett.* **59**, 1257 (1991).

4. M. Gurvitch, A. T. Fiory, *Appl. Phys. Lett.* **51**, 1027 (1987)

5. S. Matsui, N. Takado, H. Tsuge, K. Asakawa, *Appl. Phys. Lett.* **52**, 69 (1988)

6. D. R. Dykaar *et. al.*, *Appl. Phys. Lett.* **52**, 1444 (1988)

7. Arun Inam *et. al.*, *Appl. Phys. Lett.* **51**, 1112 (1987)

8. W. Eidelloth, and R. L. Sandstrom, *Appl. Phys. Lett.* **59**, 1632 (1991)

9. R. H. Koch, C. P. Umbach, G. J. Clark, P. Chaudhari, and R. B. Laibowitz, *Appl. Phys. Lett.* **50**, 20 July (1987)

10. Q. Y. Ma, E. S. Yang, G. V. Treyz, and Chin-An Chang, *Appl. Phys. Lett.* **55**, 896 (1989)

11. D. K. Fork, A. Barrera, T. H. Geballe, A. M. Viano, and D. B. Fenner, *Appl. Phys. Lett.* **57**, 2504 (1990)

12. D. K. Fork *et al.*, *IEEE Trans. on Appl. Supercond.* **1** (1), 67 (1991); K. Char *et al.*, *Appl. Phys. Lett.* **59**, 2177 (1991)

13. D. H. Shin, J. Silcox, S. E. Russek, D. K. Lathrop, B. H. Moeckly, and R. A. Buhrman, *Appl. Phys. Lett.* **57**, 508 (1990)

14. S. Z. Wang, G. C. Xiong, Y. M. He, B. Luo, W. Su, and S. D. Yao, *Appl. Phys. Lett.* **59**, 1509 (1991)

15. Yu Boikov, G. Brorsson, T. Claeson, and Z. G. Ivanov, *Appl. Phys. Lett.* **59**, 2606 (1991)

16. M. Sasaura, S. Miyazawa, and M. Mukaida, *J. Appl. Phys.* **68**, 3643 (1990).

17. X. D. Wu *et. al.*, *Appl. Phys. Lett.* **58**, 2165 (1991); Thermophysical Properties of Matter: The TRPC Data Series Vol. 13, Pg. 212 (IFI/Plenum 1977); Landolt-Bornstein, Numerical Data and Functional Relationships in Science and Technology, Vol. II/6 Pg. 482

18. K. Char, private communication.

19. A. E. Lee, C. E. Platt, J. F. Burch, R. W. Simon, J. P. Goral, and M. M. Al-Jassim, *Appl. Phys. Lett.* **57**, 2019 (1990)

20. C. T. Rogers, A. Inam, M. S. Hegde, B. Dutta, X. D. Wu, and T. Venkatesan, *Appl. Phys. Lett.* **55**, 2032 (1989)

21. X. D. Wu, *et. al.*, *Appl. Phys. Lett.* **56**, 1481 (1990)

22. J. J. Kingston unpublished

23. F. C. Wellstood unpublished

24. N. Newman, private communication

Chapter 3

Pulsed Laser Deposition of Thin Films

3.1 Laser deposition system

Pulsed laser deposition of films requires a laser, an optical imaging system, and a vacuum system with a chamber, target and sample holder (Fig. 3.1). We use a Questek 2820 Excimer laser which is mounted on a rigid table, but not otherwise vibration isolated. The laser operates on a mixture of Kr, F_2, He and Ne (KrF), and generates a pulsed beam with a wavelength of 248nm, pulse length (full width at half maximum) of 30nsec and maximum energy of approximately 825mJ/pulse. By using an aperture, we produce a uniform beam of dimensions 15mm x 6.7mm ($100mm^2$) and maximum energy of about 250mJ /pulse. During deposition, a monitor displays the total energy of each pulse, and the laser has a mechanism for setting and regulating the total pulse energy to a desired level. We use this mechanism to control the laser so that we obtain the desired energy through the aperture, as determined by an external energy meter. The laser has a peak pulse rate of 15 pulses per second, and to deposit YBCO, we usually operate at 5 pulses per second,.

The purpose of the optical imaging system is to increase the fluence on the target to 2-4Jcm^{-2}, depending upon the material being deposited. The imaging system consists of two planar mirrors with reflective dielectric coatings and a single 0.15m focal length plano-concave lens. The three optical elements are mounted on two parallel tracks which are aligned with the laser beam and the vacuum chamber. The lens and mirrors are positioned so as to focus the image of the aperture to a $6mm^2$ spot on the target,[1] accounting for the 45^o angle of incidence of the laser beam with the target. The mirrors allow the object path length to be adjusted without changing the physical separation between the aperture and the

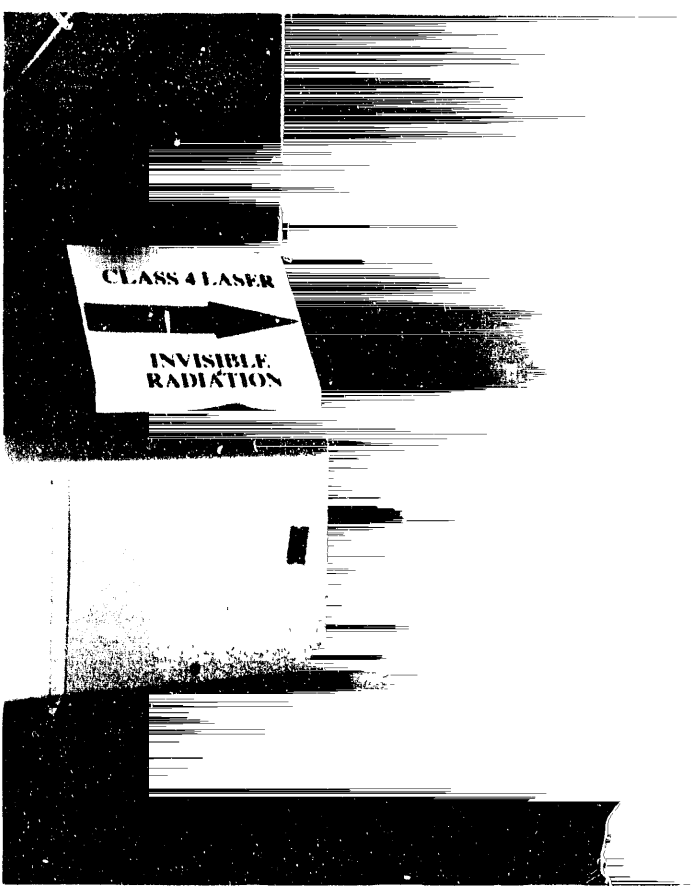

Fig. 3.1 Laser deposition system showing laser,

Pyrometer, on top of chamber, looks down on h

vacuum chamber. The focal length of the lens is chosen to be compatible with our vacuum chamber dimensions: to prevent damage to the quartz window it is important that the beam passing through it not be focused down too much.

The vacuum system consists of a stainless steel vacuum chamber pumped by an oil-based diffusion pump with a liquid nitrogen cold-trap. The base pressure is approximately $5x10^{-7}$ Torr, but the chamber is typically pumped to about $3x10^{-6}$ Torr prior to deposition. The system is roughed out with a mechanical pump which also has a liquid-nitrogen cold-trap. The aluminum top plate, sealed with a Viton o-ring, has a large glass viewport, positioned over the sample heater block, enabling us to monitor its temperature with an infrared pyrometer. The sides of the chamber contain two quartz windows, one to allow the laser beam in and the other for viewing the plume. There are electrical feedthroughs to supply power to the heater and to the plate used to generate an O_2 plasma, and mechanical feedthroughs to operate the shutter and the target holder. There are also feedthroughs for a thermocouple and pressure sensing devices. Mounted on the bottom of the chamber is an ion gauge tube and feedthroughs for O_2 and H_2O.

The chamber contains a sample heater block, a water-cooled holder that rotates targets, and a shutter (Fig. 3.2). The heater block is made from inconel and is heated by an embedded resistive cartridge heater (Fig. 3.3). Except for its front face, the block is surrounded by a stainless steel radiation shield which reflects heat back onto the block, enabling higher temperature operation with lower power settings and reduced heating of other components. A hole in the block, 2mm in diameter and 18mm deep, serves as a blackbody source for monitoring the block temperature with an infrared pyrometer. We also monitor and control the temperature in a feedback loop with a chromel-alumel thermocouple It is pressed into another hole that is symmetrically located and identical in size to the one used for the pyrometer. The block is mounted on a linear motion feedthrough which allows us to vary the target to substrate distance and thereby adjust the position of the substrate in the plume. We typically position the face of the block 60mm

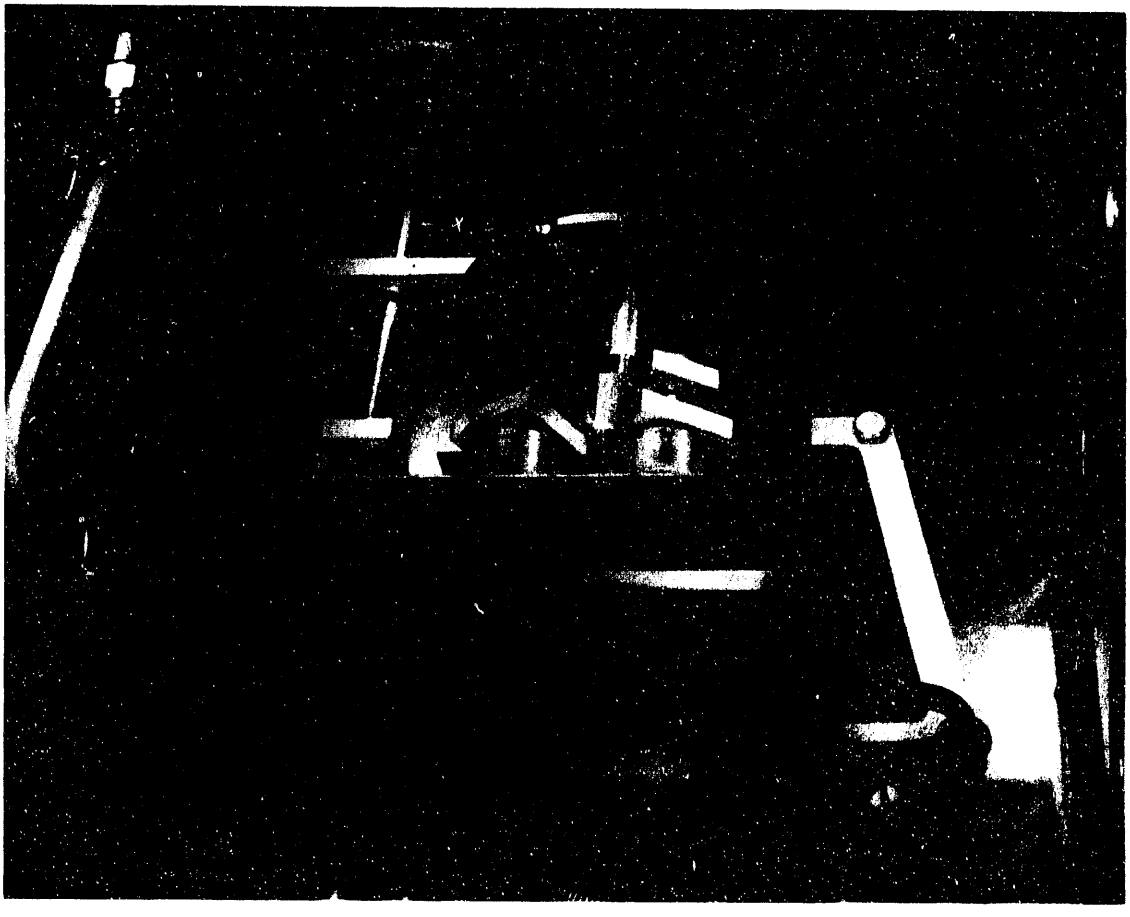

Fig. 3.2 Vacuum chamber containing 6 target exchanger, shutter, and heater block with thermocouple in it. Hole in water-cooled plate allows laser beam to strike target and plume to emerge.

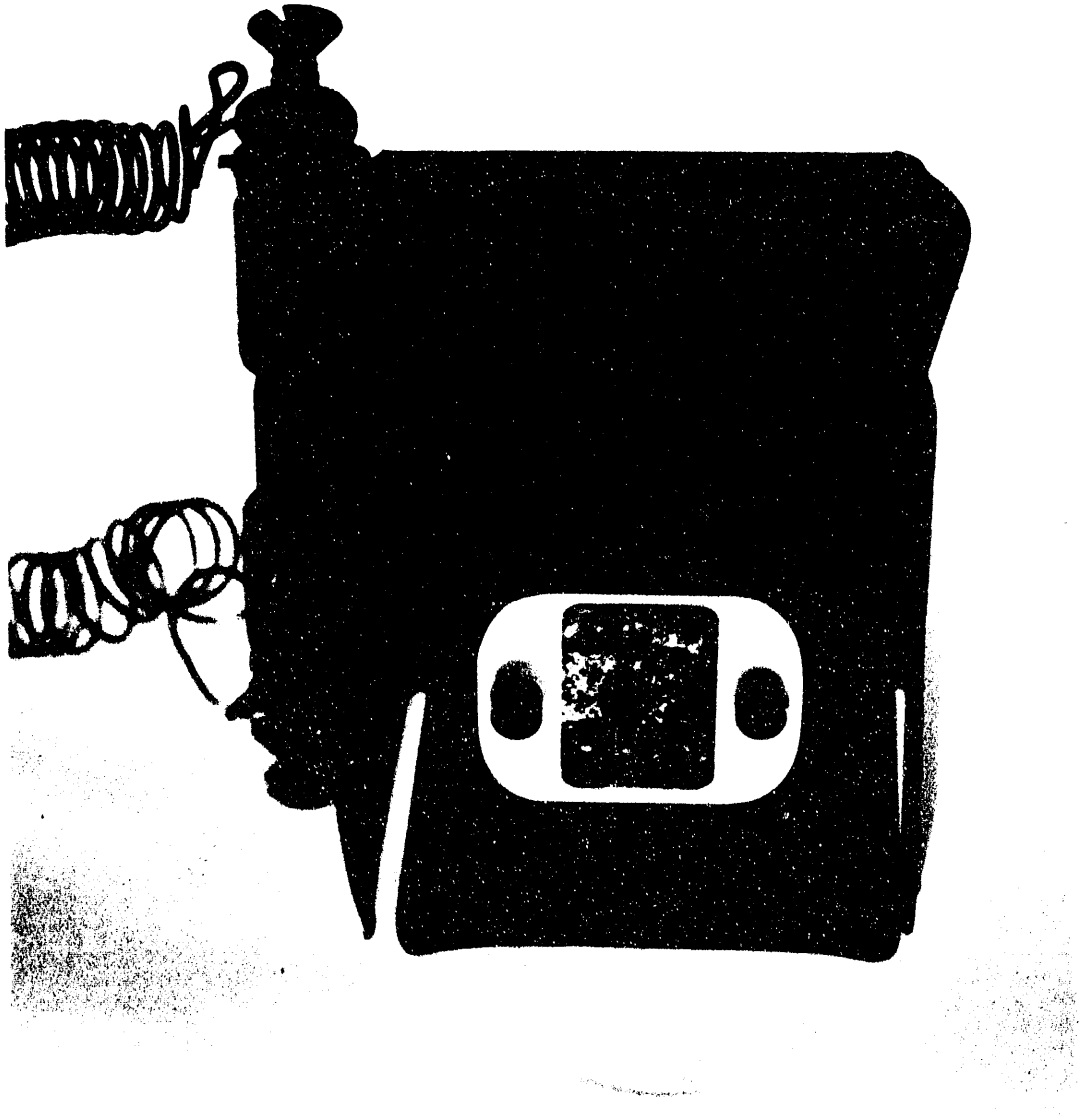

Fig. 3.3 Heater block with clip used to attach substrates. Holes in top used by pyrometer and thermocouple to monitor temperature.

from the target face. The block is readily detached from the feedthrough and removed from the chamber, allowing us to mount or dismount samples easily.

To obtain a more uniform target wear, a longer target lifetime and fewer boulders in our YBCO films, we rotate the target[2] at a rate which is not commensurate with the pulse rate, about 1Hz. We initially used a single target holder, and we had to break vacuum to exchange targets in order to deposit multilayer structures with different materials. Our current system holds six targets, each of which can be positioned for deposition and rotated by means of feedthroughs, enabling us to grow multiple layer structures *in situ* - for example, YBCO on a buffer layer. A water-cooled Cu plate in front of the target reduces heating by radiation from the heater block. A 10x20mm^2 hole in the plate allows the laser beam to strike the target and the plume of ablated target material to emerge. We use a shutter to cover the substrate to prevent material from being deposited while we clean the target. During deposition, we regulate the O_2 pressure at the desired value by means of an automatic gas flow system.

3.2 Film Deposition

We use cleaved and polished substrates that are cleaned successively in an ultrasonic bath with trichloroethane, isopropanol, and methanol, to remove wax and residue left over from the substrate polishing, and blown dry with compressed N_2. We attach the substrate to the the heater with silver paste, clamp it to the block with a bolt on clip (Fig. 3.3) and dry the paste in the chamber while evacuating and heating the heater. Alternately, we dry the silver paste externally, and do not use the clip. The paste insures good thermal contact between the substrate and the heater block. We mount the block in the chamber so that the sample is approximately 60mm from the target, with the face aligned parallel to the face of the target and positioned so that it will intercept the center of the plume. The targets are all stoichiometric and most are made from powder, pressed into

25mm diameter discs, and sintered. However, we use either a single crystal of MgO or a disc of Mg metal to deposit MgO films , and a disc of silver to deposit the silver films used for normal metal contacts.

We evacuate the chamber to about 3 x 10^{-6} while outgassing the heater at about 800°C. We establish the desired O_2 pressure and heater block temperature and, with the shutter blocking deposition, we clean the surface of the target with 600 pulses from the laser while the target is rotated. After rotating the shutter out of the path of the plume, we deposit a film to the desired thickness. For multiple layer *in situ* depositions, we establish the appropriate pressure and temperature, position and clean another target, and deposit the second layer. This can be repeated as desired.

For YBCO, we focus 125mJ of energy (accounting for the losses in all the optics) to a fluence of about 2J/cm^2 on the target, and typically deposit a 300nm thick film in 6min with a laser repetition rate of 5Hz. During deposition, the heater block is held at 760°C and the O_2 pressure at 210mTorr. We deposit $SrTiO_3$ films with the same parameters, except that the O_2 pressure is 150mTorr. When depositing material on YBCO films, we follow a different pumping and heating procedure. To minimize the loss of O_2 in the YBCO film, we evacuate the system with the heater block at room temperature, establish 250mTorr of O_2, and quickly establish the substrate temperature. We clean the appropriate target, establish the desired O_2 pressure, and deposit the film.

After depositing the film(s), we backfill the chamber to about 700 Torr of O_2 and cool the sample to 450°C in 15 minutes and then to room temperature in another 15 minutes. This slow cool down oxygenates YBCO films and lessens the chance of the substrate cracking from thermal stresses.

For contacts we deposit silver at 1mTorr of O_2 onto room temperature YBCO films. To pattern the silver, one can either use shadow masks or photolithographic techniques after the silver has been deposited. In the latter case, the silver can be deposited *in situ* onto a YBCO film that has just been deposited and cooled to room temperature. The

avoidance of wet chemistry prior to the silver deposition eliminates the need for post-annealing.

To determine the optimal deposition conditions for superconducting, dielectric or normal metal films, we use x-ray diffraction and electrical transport measurements. We perform θ–2θ and Φ-scans to determine the crystallographic orientations of the films, and 4-point resistance vs. temperature measurements of the conducting films and critical current vs. temperature measurements of the superconducting films to determine their electrical properties By making a series of samples in which we vary the deposition conditions and then make the x-ray and transport measurements, we thus optimize our films.

Figure 3.4 shows the resistance vs. temperature data for a YBCO film deposited *in situ* on a MgO substrate, the fifth sample that we made in our laser deposition system. At temperatures above the superconducting transition temperature of 85K, the resistance is linear in temperature, a metallic behavior. Ideally, this region of the curve would extrapolate through the origin. The width of the transition is only about 1K, which is quite good. The relatively low T_c is undoubtedly due to insufficient O_2 being present during deposition of the film. We now use 210mTorr of O_2 instead of the 125mTorr used for that sample.

We now routinely fabricate films with T_c = 88K on MgO. To do this we control the heater block temperature at 760°C, the O_2 pressure in the chamber at 210mTorr, set the target to substrate distance at 60mm, and ablate the target with 125mJ/pulse (after passing through all the optics) at a fluence of 2.25J/cm^2. By firing the laser at 5Hz for 6min we deposit a film about 300nm thick. This corresponds to a deposition rate per pulse of 0.167nm. After deposition, we backfill the chamber to about 700Torr of O_2, and cool the sample to 450°C in 15 min, and then to room temperature in another 15 min.

Figure 3.5 shows the θ-2 θ x-ray diffraction spectrum for a YBCO film deposited on a MgO substrate that has been buffered by a $SrTiO_3$ film 100nm thick. Other than two substrate peaks, only YBCO (and $SrTiO_3$) c-axis peaks are observed.

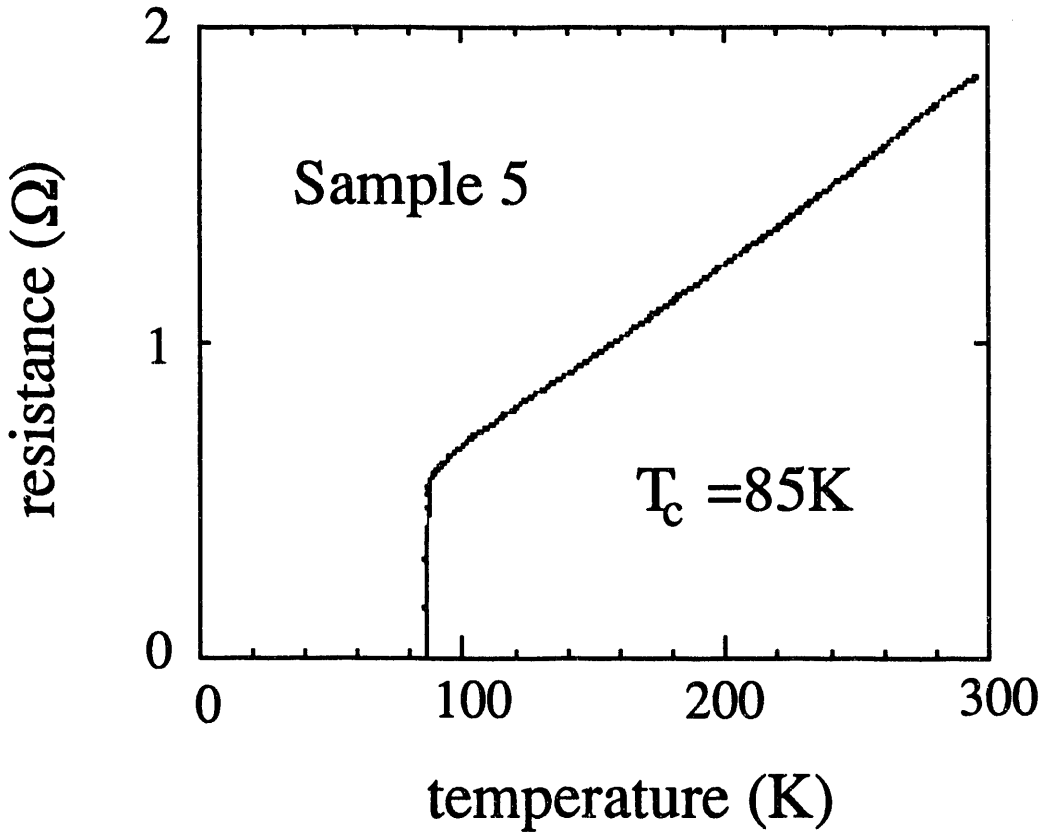

Fig. 3.4 Resistance vs. temperature data for the 5th sample made in the laser deposition system.

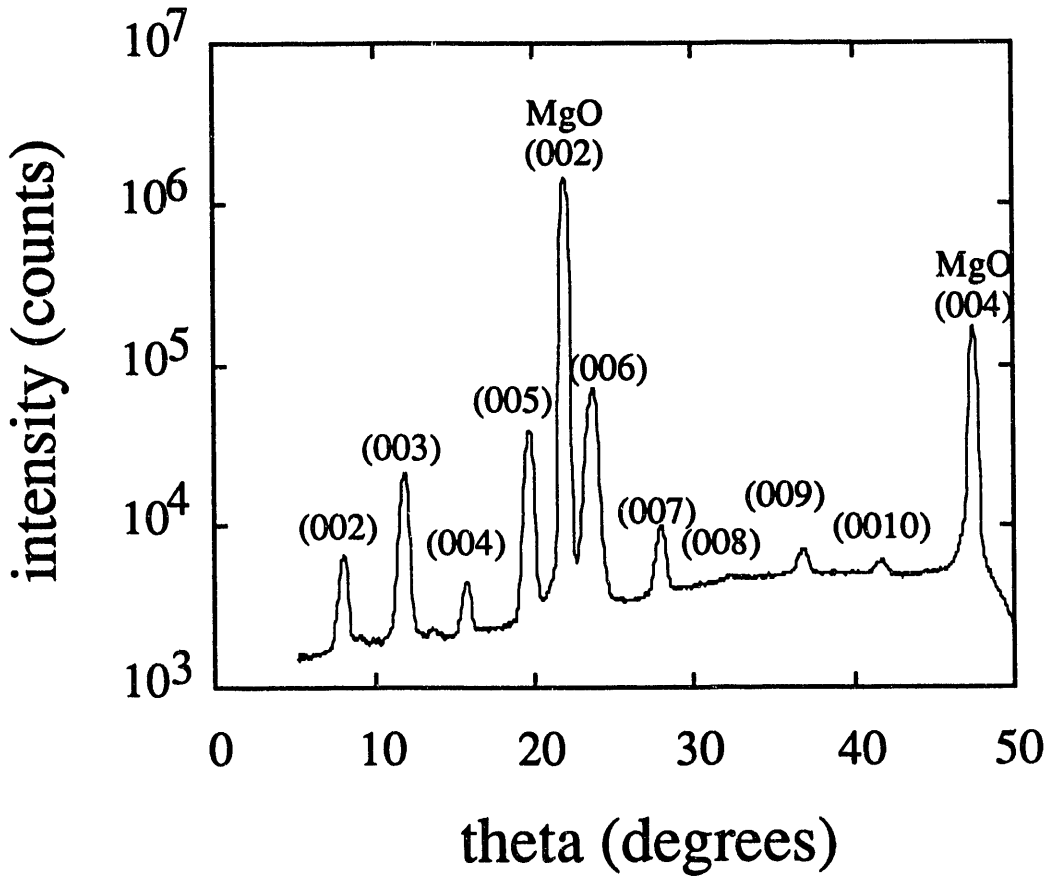

Fig 3.5 θ-2θ x-ray diffraction spectrum of a YBCO thin film deposited onto a MgO substrate buffered by $SrTiO_3$. Peaks are for YBCO unless otherwise noted.

Figure 3.6 shows the Φ-scan x-ray diffraction spectrum on the YBCO (103) peak, for the same sample. It is evident that this film is highly oriented in the plane as well, since the peaks are separated by 90°. No low angle grain boudaries are seen as is common for YBCO deposited directly on MgO. The presence of the $SrTiO_3$ buffer layer substantially improves the alignment of the film. A separate Φ-scan performed on the substrate (not shown) indicates that the a and b axis of the YBCO film are aligned with those of the substrate.

We calibrate the deposition rate by using a profileometer to measure the sample thickness. For transparent insulating layers, we estimate the thickness by using the index of refraction of the material and noting the number and color of the optical interference fringes. It should be remarked that films often have a slightly different index of refraction than bulk samples, so that the method is somewhat inaccurate.

Early laser deposited films were plagued by the presence of a high density of micron-sized embedded particles or "boulders",which can be very detrimental to multilayer structures. After a target has been exposed to many laser pulses, its surface becomes roughened and the deposition of boulders occurs. By lightly sanding the surface smooth and blowing off any dust before each deposition[3], we can largely eliminate such particles, especially if we use a highly dense target[4]. The dense targets retain this boulder-free condition for a longer time but will emit boulders after exposure to enough laser pulses. The emission of particles is delayed by using a low laser fluence, or by ablating material from a larger area on the surface of the target, which can be accomplished by rastering the beam or rotating the target. The key is to reduce the number of laser pulses that strike any spot on the target during the growth of a film.

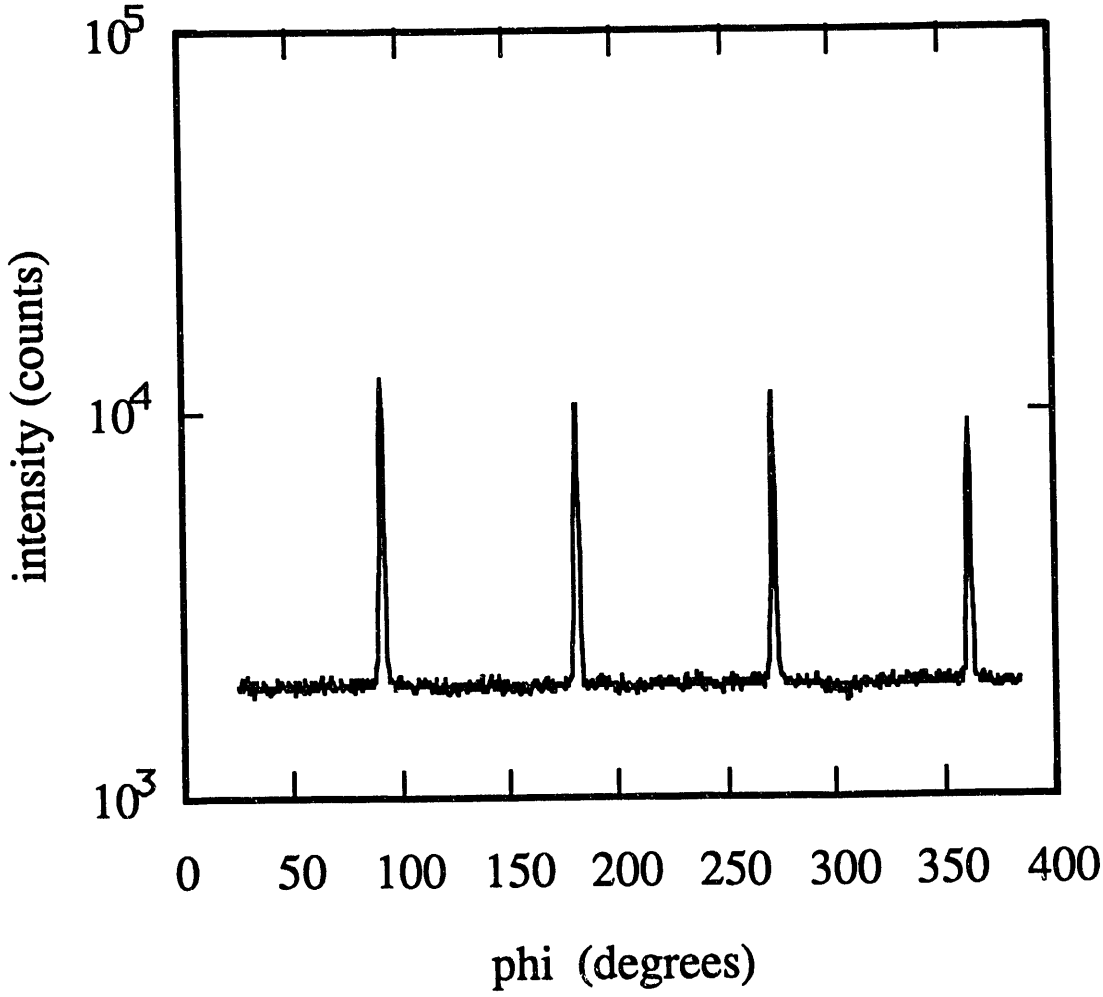

Fig 3.6 Φ-scan x-ray diffraction spectrum of YBCO (103) peak of the same sample as in Fig. 3.5.

References

1. D. Fork, private communication.

2. D. Dijkkamp, T. Venkatesan, X. D. Wu, S. A. Shaheen, N. Jisrawi, Y. H. Min-Lee, W. L. McLean, and M. Croft, *Appl. Phys. Lett.* **51**, 619 (1987).

3. J. J. Kingston, F. C. Wellstood, P. Lerch, A.H. Miklich, and J. Clarke, *Appl. Phys. Lett.* **56**, 236 (1990).

4. Jupiter Technologies, 187 Langmuir Lab, Cornell Business and Technology Park, Brown Road, Ithaca, NY 14850

Chapter 4

$YBa_2Cu_3O_{7-x}$ Interconnects Patterned by Shadow Masks

A wide variety of processes have been described[1] for the deposition of single layers of thin films of the high temperature superconductor YBCO. There are also many reports of YBCO films deposited *in situ* by laser deposition.[2] Rogers et al.[3] have reported the fabrication of YBCO - $PrBa_2Cu_3O_y$-YBCO trilayer junctions that exhibit Josephson characteristics. To produce electronic circuits of any complexity, however, one has to develop techniques to fabricate interconnects. Virtually all superconducting microelectronic circuits require crossovers, and without them, the devices one can fabricate and their interconnections are severely limited.

We describe the process we have developed for producing YBCO - $SrTiO_3$ - YBCO crossovers, which we believe will be suitable for a variety of applications in superconducting microelectronics at 77K.

We first successfully fabricated crossovers by using in situ laser deposition to deposit all thin film layers, shadow masks to pattern them, and $SrTiO_3$ for the insulating material. Laser deposition allowed us to grow all three layers with a minimum of interduffusion and a minimum of degradation of the lower layers during deposition of the upper layers. By using shadow masks to pattern the layers, we avoided the problems of surface contamination of the films and steep edges in them that could result from using photolithography. Our use of $SrTiO_3$ was fortuitous, for we have not found a better material, even to this day.

Initially, we attempted to deposit the insulating films by rf sputtering and to deposit the YBCO films by laser deposition. We achieved heteroepitaxial growth of the

films, but were unable to achieve sufficient insulation between the YBCO films - there were always short circuits.

4.1 Crossover Fabrication Process

We use 12.5 x 12.5 x 1mm^3 cleaved and polished (100) MgO substrates that are cleaned successively in an ultrasonic bath with xylene, trichlorethylene, isopropyl alcohol and ethanol, rinsed with methanol, and blown dry with N_2. Our superconducting films are deposited from stoichiometric YBCO targets pressed and sintered from calcined powder into disks 25mm in diameter and 3mm thick. The insulating layer is deposited from $SrTiO_3$ powder pressed into a disk of the same size.[4] Before each deposition, we grind the surface of the targets with #400 emery paper, polish them on a latex sheet and blow away any loose particles with N_2.

We make the films in a diffusion-pumped vacuum system with a base pressure of 1μTorr. We deposit each layer in turn using the 248nm pulses (18ns full width at half maximum) from a Questek 2820 excimer laser. A 5.4 x 14mm^2 aperture selects the uniform portion of the beam, which is focussed by a 0.15m focal length lens onto the target at an angle of incidence of 45^o. The target is glued to one end of a copper cylinder that rotates at about 60 rpm; the bearings for the shaft are mounted in a water-cooled block. We clamp the substrate to a heater block which is coated with a layer of silver paste to insure good thermal contact. This block is resistively heated, and its temperature is monitored by an imbedded Chromel-Alumel thermocouple. The substrate is 60mm from the target, and aligned to intercept the central portion of the plume emanating from the target. A water-cooled plate partially shields the target from the thermal radiation emitted by the substrate heater block to prevent melting of the surface of the target.

The configuration of the thin-film structure shown in Fig. 4.1 allows us to measure the electrical properties of all three layers. The first layer is an H-shaped YBCO film: the connecting strip is approximately 450μm wide. The second layer is a 9 x 7mm^2 rectangle of $SrTiO_3$ that covers this strip. On top of the $SrTiO_3$ lies the third layer, two strips of YBCO, 450 and 900μm wide, that cross the strip of the first layer of YBCO. The patterns are defined by masks cut from stainless steel foil. Because the deposition occurs in 190mTorr of O_2, the masks must be clamped tightly to the substrate to insure good line definition.

The first step in the process is to outgas the heater and substrate by increasing the temperature to 730°C as we evacuate the chamber to 5μTorr. The temperature is held constant while we throttle the gate valve and bleed in O_2 to maintain a pressure of 190mTorr. We first cover the surface of the substrate with a shutter and clean the target with 300 laser pulses at a rate of 5 per second with an energy density of 1.1Jcm^2 and then deposit the first layer of YBCO for 10 minutes, at the same repetition rate and fluence, to a thickness of about 0.3μm. Immediately after, we turn off the laser, back-fill the chamber with O_2 to 1 atmosphere and reduce the heater power to allow the block to cool to 450°C. In 15 minutes we turn off the heater and allow the sample to cool for another 15 minutes before opening the chamber.

In preparation for the insulating layer, we exchange masks and replace the YBCO target with a polished $SrTiO_3$ target. We outgas the substrate at 200°C while pumping the chamber to 5μTorr; this relatively low temperature minimizes the loss of oxygen from the YBCO layer. We then rapidly raise the block temperature to 660°C, bleed in O_2 to 190mTorr, and clean the target as before. After opening the shutter, we deposit $SrTiO_3$ for 7 minutes at 5 pulses per second at an energy density of 1.4Jcm^{-2}, to produce a film that varies in thickness from 0.4 - 0.45μm. We have found that 660°C is the lowest temperature at which we obtain good growth of the $SrTiO_3$, and have avoided the use of higher temperatures in order to limit interdiffusion. In an

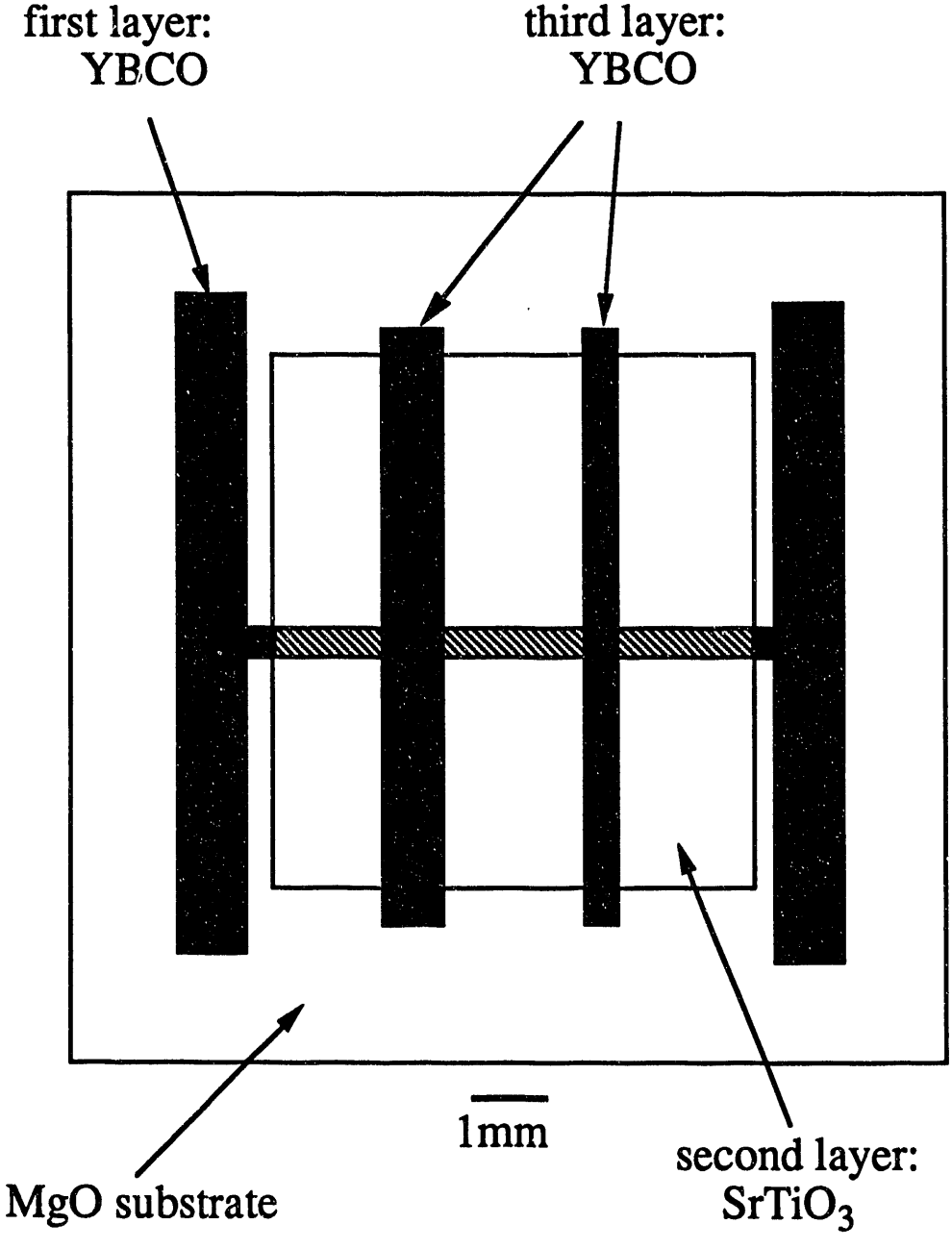

Fig. 4.1 Configuration of YBCO - $SrTiO_3$- YBCO thin-film crossover.

attempt to replenish the O_2 content of the underlying YBCO film and to insure sufficient incorporation of O_2 in the $SrTiO_3$, we use the same cooling procedure as before.

After changing masks and inserting a polished YBCO target, we outgas the substrate at 200°C until the pressure falls to 5μTorr. We quickly raise the temperature to 730°C, bleed in O_2 to 190mTorr, clean the target for 1 minute, and deposit a third layer approximately 0.25μm thick. After the usual cooling procedure, we remove the sample for testing.

4.2 Results

Under an optical microscope, the insulating layer appears smooth and featureless, while the YBCO layers contain some sub-micron grains and small particles up to 1μm in diameter. We have sought to reduce the density of these particles, in an effort to lessen the probability of developing short circuits between the top and bottom layers of YBCO. We have found that after deposition of a film, the face of a target contains many stalactite-like structures that remain after the surrounding material has been vaporized. We believe further erosion of the target surface causes some of the stalactites to break off, resulting in the deposition of the particles. By polishing the target face before deposition, minimizing the number of laser pulses fired, and using a low laser fluence and large spot size on the target, we are able to reduce the particle density to typically 1 per 2500μm^2. A further reduction can be achieved by increasing the area of the target that is ablated by the laser, or perhaps by polishing the target face during deposition thereby eliminating the formation of the stalactite-like structures. The elimination, or at least the minimization of the density, of 1μm particles is desirable in multilayer structures such as an insulated crossover, and it is probably essential in structures such as a tunnel junction.

Figure 4.2 shows the x-ray diffraction spectrum for a trilayer. The plot indicates that the YBCO is predominantly c-axis oriented. However, there is an impurity phase peak located at $2\theta = 32.39^{o}$ that may have contributions from YBCO (103) and (110) and $SrTiO_3$ (110). It is likely that both the YBCO and the $SrTiO_3$ have some random orientation.

We measured the electrical properties using a 4-terminal arrangement, making contacts to the films with pressed In pellets. In Fig. 4.3(a), for comparison, we show a representative plot of resistance (R) vs. temperature (T) for a single layer of YBCO deposited on MgO. Zero resistance is at $T_{CO} = 87.8K$ and the transition width ΔT_C is 2K (10% to 90%). The critical current densities of our patterned single-layer films are typically $J_C \approx 10^6 Acm^{-2}$ at 77K. Figures 4.3(b) and 4.3(c) show R vs. T for the lower and upper YBCO film of our best crossover: the properties have degraded only slightly, to $T_{CO} = 87.3K$ and 87.7K and $\Delta T_C = 1K$ and 3K, respectively. The resistance of the $SrTiO_3$, measured between the lower and upper YBCO strips, increases as the temperature is lowered [see Fig. 4.3(d)]. At 77K, the resistance is approximately 100MΩ, corresponding to $\rho \approx 4 \times 10^9 \Omega cm$. The resistivity of high quality $SrTiO_3$ at room temperature is typically $10^9 \Omega cm$, whereas the film yields $\rho \approx 4 \times 10^4 \Omega cm$, suggesting that impurities or defects are present.

The process described above has proved reproducible. Because of the number of layers involved and the nature of their interactions, the optimization process is complicated. The fact that the sample can be exposed to air between each deposition is an enormous advantage in the fabrication of complex circuits in that it should allow one to pattern each layer using photolithography and etching. If, on the contrary, one were forced to keep the structure in vacuum for the entire process, the complexity of circuits which could be built would be severely limited. However, we believe the process would work equally well if one were to use two interchangeable targets and a suitable mask changer so that one did not have to open the chamber between depositions.

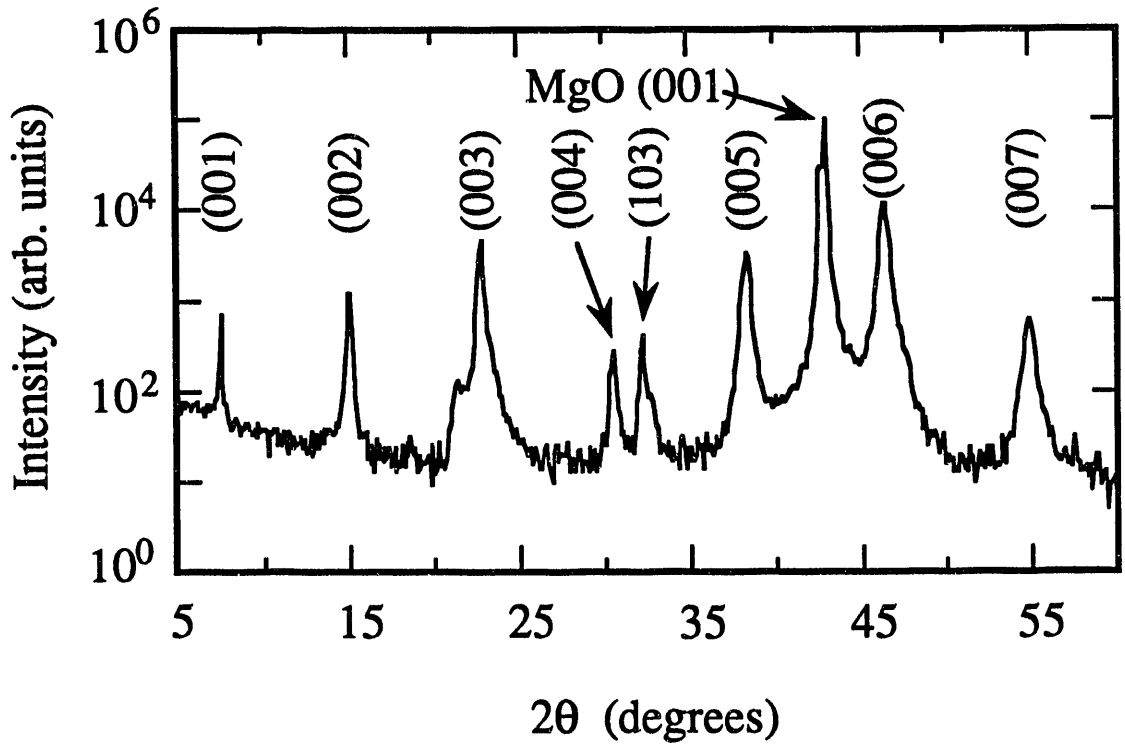

Fig. 4.2 X-ray diffraction spectrum (θ - 2θ scan) of YBCO - $SrTiO_3$ - YBCO crossover on (100) MgO substrate. Orientations refer to YBCO unless labeled otherwise. Impurity phase peak labeled (103) may have contributions from YBCO (110) and (013) and $SrTiO_3$ (110).

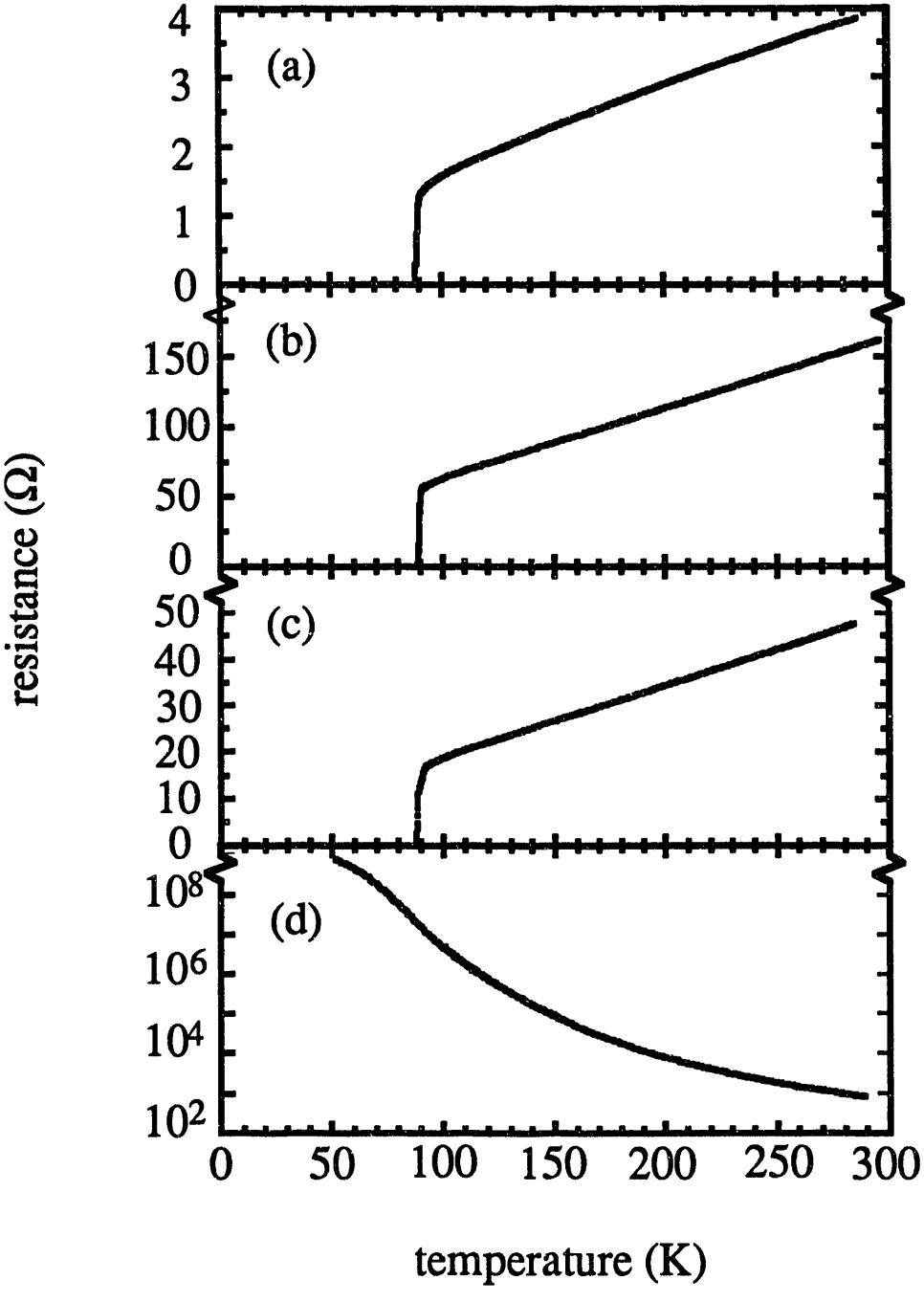

Fig. 4.3 Resistance vs. temperature for (a) single-layer YBCO film deposited on MgO; (b) lower YBCO film of trilayer, (c) upper YBCO film of trilayer, and (d) $SrTiO_3$ insulating layer measured between the upper and lower YBCO films.

4.3 Superconductor - Superconductor Contacts

Prior to the development of the crossover fabrication technique, we had suuccesfully fabricated superconducting contacts between different superconducting layers. Therefore, a complete interconnect technology existed once we had crossovers.

The fabrication procedure is identical to that for a crossover except that the middle insulating layer is omitted. A strip of YBCO is deposited through a shadow mask across the center of the substrate in the usual way. After cooling, the mask is rotated 90° and positioned so that the slit in the mask crosses the YBCO line already deposited. A second layer of YBCO is then deposited and cooled and the sample removed for testing.

By proper positioning of In contacts on each of the crossing YBCO strips, a four contact resistance measurement can reveal the resistance of each of the two strips, of the contact between them, or of the series resistance of the strips and the contact. Our first sample was successful - we could not detect any resistance in the contact below the T_c of the YBCO strips.

Armed with the interconnect technology, we proceeded to attack our goal of fabricating multi-turn coils and flux transformers for use with SQUIDs. But first, let us turn our attention to Transmission Electron Microscopy (TEM) sudies of our multi-layer structures performed by Mohammed Tidjani and Ronald Gronsky at the National Center for Electron Microscopy at Lawrence Berkeley Laboratory. The studies explain the excellent electrical properties found in the crossovers.

References

1. For a review, see the Proceedings of the Applied Superconductivity Conference, 1988; *IEEE Trans. Magn.* **MAG-25**, 719-2590 (1989).

2. S. Witanachchi, H. S. Kwok, X. W. Wang, and D. T. Shaw, *Appl. Phys. Lett.* **53**, 234 (1988); A. Inam, M. S. Hegde, X. D. Wu, T. Venkatesan, P. England, P. F. Miceli, E. W. Chase, C. C. Chang, J. M. Tarascon, and J. B. Wachtman, *Appl. Phys. Lett.* **53**, 908 (1988); J. Frohlingsdorf, W. Zander, and B. Stritzker, *Solid State Communications* **67**, 965 (1988); B. Roas, L. Schultz, and G. Endres, *Appl. Phys. Lett.* **53**, 1557 (1988); G. Koren, E. Polturak, B. Fisher, D. Cohen, and G. Kimel, *Appl. Phys. Lett.* **53**, 2330 (1988); R. K. Singh, J. Narayan, A. K. Singh, and J. Krishnaswamy, *Appl. Phys. Lett.* **54**, 2271 (1989).

3. C. T. Rogers, A. Inam, M. S. Hegde, B. Dutta, X. D. Wu, and T. Venkatesan *Appl. Phys. Lett.* **55**, 2032 (1989).

4. Electronic Space Products International, 5310-U Derry Ave., Agoura Hills, California 91301-4509.

Chapter 5

Heteroepitaxial $YBa_2Cu_3O_{7-x}$-$SrTiO_3$-$YBa_2Cu_3O_{7-x}$ Trilayers Examined by Transmission Electron Microscopy

In order to fabricate certain kinds of devices from the high transition temperature (T_c) superconductors, it is essential that one be able to deposit multiple layers of an insulator and a superconductor. Such a technique has already been used for interconnects,[1] and may be useful, for example, for constructing Josephson tunnel junctions. In our crossover technology for $YBa_2Cu_3O_{7-x}$ (YBCO), we found that patterned YBCO-$SrTiO_3$-YBCO trilayers deposited on MgO substrates showed high levels of electrical isolation between the superconductors (> $4x10^9$ Ωcm at 77K) while maintaining high T_c (> 87K in both YBCO films). The YBCO films were typically 300 nm thick, while the $SrTiO_3$ was between 200 and 400 nm. The successful fabrication of such multilayer structures depends in part on the properties of the interfaces between the YBCO and $SrTiO_3$ layers. Ideally, one would like a heteroepitaxial system with closely matched lattice parameters, so that crystallinity is maintained in the deposited layers, and the interfacial zones have low stress energy. In addition, for a tunnel junction, one would like chemical bonding across the interface which does not degrade the adjoining superconducting regions by atomic diffusion or oxygen depletion. High Resolution Transmission Electron Microscopy (HRTEM) is a powerful technique for studying such properties, and has recently been applied to single layer films,[2-4] $YBa_2Cu_3O_{7-y}$-$Y_{1-x}Pr_xBa_2Cu_3O_{7-y}$ heterostructures[5], and MgO-YBCO heterostructures.[6] This technique can, in favorable cases, determine the atomic structure of an interface, and, in bulk materials, has yielded information such as the location of misfit dislocations[7], the presence or absence of reaction layers[8], and the degree of surface roughness[9] at interfaces on an atomic scale. We report an HRTEM study of a YBCO-$SrTiO_3$-YBCO trilayer.

We fabricated the trilayer test structure using *in situ* laser deposition onto a cleaved and polished (001) MgO substrate, choosing the layer thicknesses so that we could simultaneously view all three layers with HRTEM. The excimer laser was operated at 248nm with 1.3Jcm^{-2} incident on a stoichiometric target of YBCO or $SrTiO_3$. We first deposited 150nm of YBCO in 220mTorr of O_2 while the substrate heater block was held at 740°C. After cooling the substrate to room temperature over a 30min period in one atm of O_2, we opened the vacuum chamber and exchanged the YBCO target for a $SrTiO_3$ target. The chamber was re-evacuated, the substrate heated rapidly to 690°C, and 80nm of $SrTiO_3$ deposited in 200mTorr of O_2. Again, the sample was cooled to room temperature, the targets exchanged, and the vacuum chamber evacuated before the sample was heated rapidly to 740°C for deposition of the top YBCO layer, 150nm thick. After it had cooled to room temperature, the sample was removed from the vacuum chamber. We then prepared cross-sectional specimens by mechanically thinning and ion milling until electron transparency was obtained,[10,11] so that we could view the multilayers with high spatial resolution in the plane of their interfaces. Phase contrast imaging and selected area diffraction (SAD) were performed on a JEOL JEM 200CX transmission electron microscope equipped with an ultrahigh resolution goniometer at an accelerating potential of 200 kV.

A typical low magnification lattice image of the YBCO-$SrTiO_3$-YBCO trilayer is shown in Fig.5.1, and the SAD patterns of the upper and lower YBCO-$SrTiO_3$ interfaces are shown in Figs.5.2(a) and 5.2(b). The micrograph in Fig.5.1 clearly shows that the upper interface exhibits fine scale roughness; however, the (001) (ab) planes of YBCO remain strictly parallel to the macroscopic interface plane over the full lateral extent of the image. Furthermore, the SAD pattern in Fig.5.2a reveals that YBCO exhibits a preferred orientation relationship with $SrTiO_3$ in which the c- and a-axes of YBCO are perfectly parallel to those of $SrTiO_3$:

$$(001)_{YBCO} \,//\, (001)_{SrTiO_3} \quad \text{and} \quad [010]_{YBCO} \,//\, [010]_{SrTiO_3}\,. \tag{5.1}$$

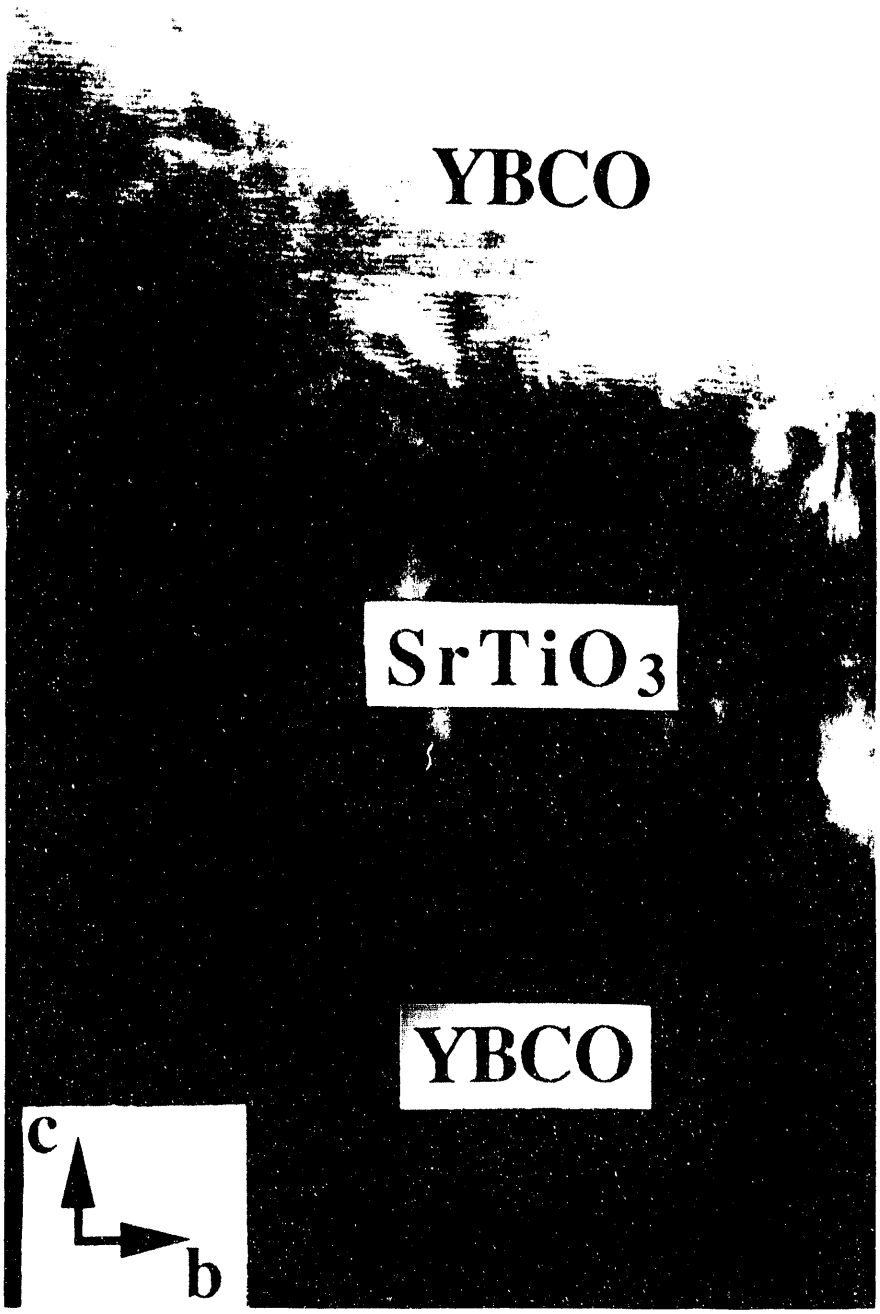

Fig. 5.1 Low magnification TEM micrograph showing a trilayer of YBCO-$SrTiO_3$-YBCO; the lower layer is adjacent to the MgO substrate. No intermediate layer is visible at either the lower or upper interface. The $(001)_{YBCO}$ planes in the uppermost layer are parallel to the interface in spite of the columnar growth of the $SrTiO_3$ layer.

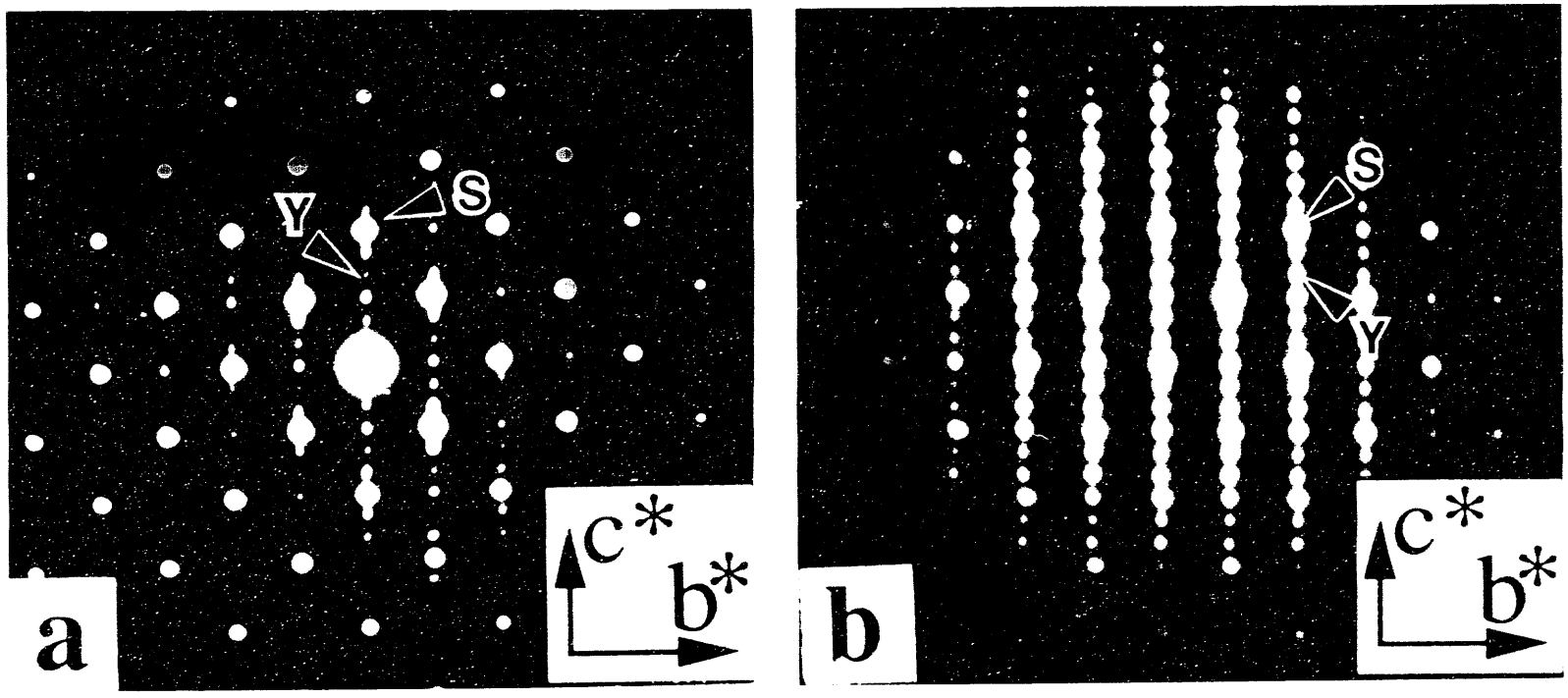

Fig 5.2 Selected area diffraction (SAD) patterns of (a) the lower interface YBCO-SrTiO3, and (b) the upper SrTiO3-YBCO interface. Labels S and Y refer to SrTiO3 and YBCO, respectively.

This observation indicates a complete crystallographic compatibility between the superconducting and the insulating layers, most likely because the lattice paramaters of YBCO (a_o=3.82Å, b_o=3.89Å) and $SrTiO_3$ (a_o=3.91Å) are nearly identical.

In Fig. 5.3, we show a lattice fringe image of the upper $SrTiO_3$-YBCO interface in which both close-packed planes $\{001\}_{SrTiO_3}$ and $(001)_{YBCO}$ are resolved and are clearly parallel. This is also revealed in the SAD pattern in Fig 5.2(a), and indicates a preferred oriented growth of the $SrTiO_3$ layer on YBCO. However, closer examination of Fig.5.3 shows that the $SrTiO_3$ layer exhibits columnar growth, that is, there are elongated grains perpendicular to the YBCO-$SrTiO_3$ interface. These grains appear to be slightly rotated relative to one another around a common [001] direction, and are thus separated by low-angle twist boundaries that appear as shadows in Fig. 5.3. The parallelism of the $(001)_{YBCO}$ planes in the upper layer of YBCO is interesting, since it indicates that YBCO grows epitaxially on $SrTiO_3$ in spite of the obvious polycrystalline morphology of the $SrTiO_3$ film.

While we see a sharp boundary extending over large areas without any intermediate layer, Fig. 5.3 also shows that the $SrTiO_3$-YBCO interface is continuously curved because of local growth perturbations at the $SrTiO_3$ surface as well as a number of interfacial steps. The micrograph also shows regions of dark contrast randomly distributed along the $SrTiO_3$-YBCO interface; these are probably related to the strain fields caused by mismatch and misorientation between the two lattices.

A segment of the lower YBCO-$SrTiO_3$ interface is examined at higher magnification in Fig.5.4(a). Both (010) and (001) cross fringes of $SrTiO_3$ and YBCO layers are visible over the entire micrograph. The image clearly shows a clean interface with no evidence of any second phase formation. In both YBCO and $SrTiO_3$ layers, crystallinity is maintained up to the interface with a sharp transition from YBCO to $SrTiO_3$ and no interfacial amorphous phase anywhere along the entire interface. The $(010)_{SrTiO_3}$ planes maintain the same orientation regardless of the number of steps along curved

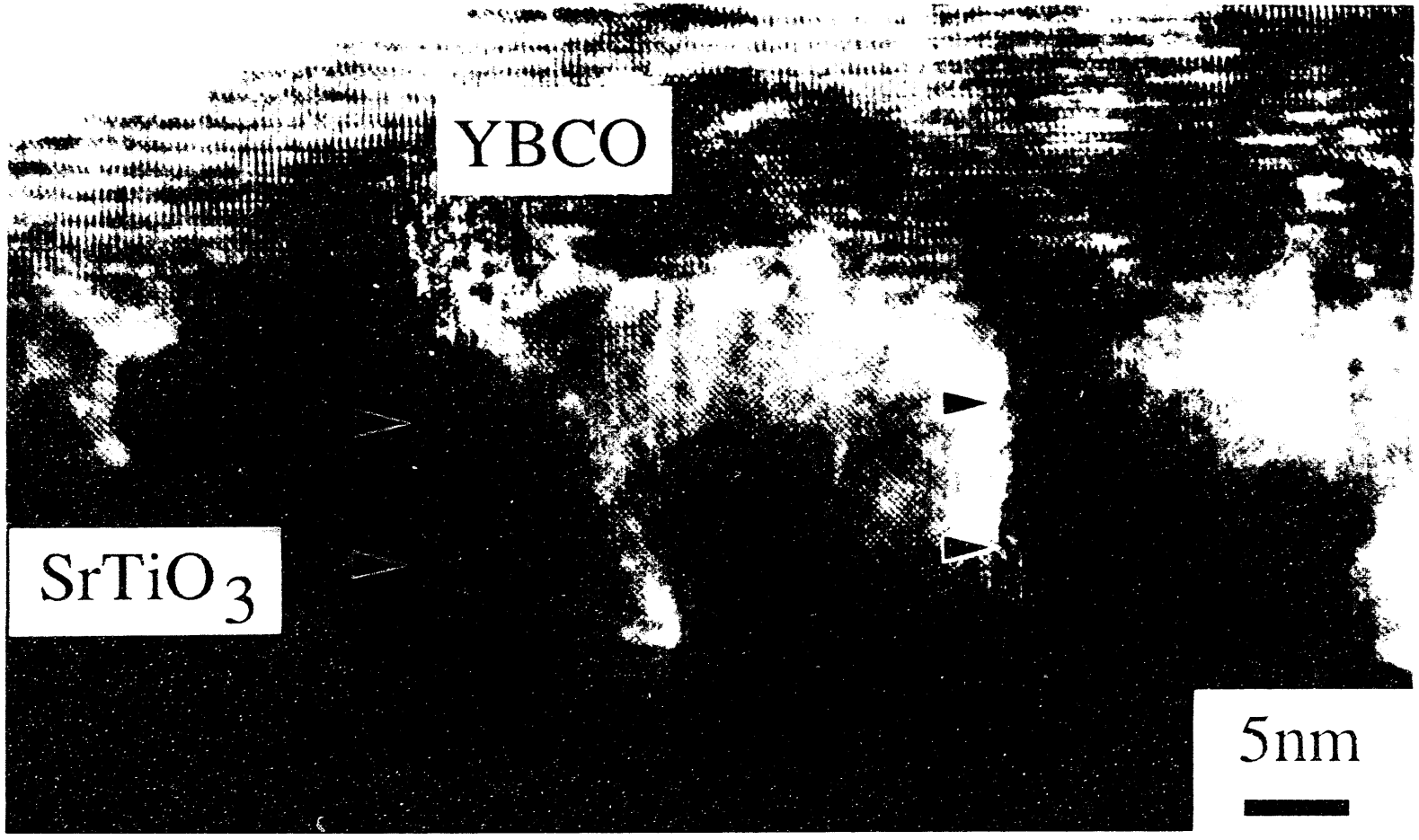

Fig. 5.3 High resolution image of upper YBCO layer deposited on SrTiO3. Notice grain boundaries in SrTiO3 layer at the arrows, and parallelism of the (001)YBCO planes to the interface in spite of the roughness of SrTiO3-YBCO interfacial plane.

interfaces. The YBCO layer contains stacking faults, for example at the arrows, and exhibits occasional bending of the (001) planes. However, away from the interface the regular periodicity of the structure indicates that the lattice of YBCO is free from distortion.

An interesting feature observed in this example and in all the HREM images recorded during this study is the apparent in-plane interface coherency and atomic smoothness along the planar interfaces such as that illustrated in Fig.5.4c. There is an exact one-to-one correspondence between the $(010)_{YBCO}$ and $(010)_{SrTiO_3}$ planes at the interface and, as shown in the SAD pattern in Fig.5.2b, both families of planes are exactly parallel. Dark regions occasionally observed along the interface are strain centers arising from the lattice mismatch between $(010)_{YBCO}$ (3.89Å) and $(010)_{SrTiO_3}$ (3.91Å) with a resultant elastic distortion of 0.5%.

The epitaxial relationship Eq. (5.1) is maintained even along the stepped surface of YBCO. Such interfaces are apparently stabilized by well-defined faceting along the $(011)_{SrTiO_3}$ // $(031)_{YBCO}$ plane, indicating this also to be a preferred interface plane. An example of a stepped interface is examined at higher magnification in Fig.5.4b and shows a coarse ledge (labeled "d") in which an extra plane normal to the ledge plane is observed. As determined by a Burgers circuit construction around this extra plane, the closure failure is attributed to a $(011)_{SrTiO_3}$ plane along the $[011]_{SrTiO_3}$ direction within the projection of this image. The interplanar spacings of $(011)_{SrTiO_3}$ and $(031)_{YBCO}$, 2.7648 Å and 2.7506Å respectively, are again very close and result in an elastic strain of about 0.5%. Hence mismatch between the two lattices is likely to be accommodated by dislocations in the $SrTiO_3$ to preserve the epitaxial growth of the $SrTiO_3$ layer.

In summary, both YBCO and $SrTiO_3$ films grow epitaxially on each other, and we have detected no disordered regions or impurity phases at either interface. Although the $SrTiO_3$ layer exhibits columnar growth, a definite crystallographic orientation relationship is preserved along the entire interface, even at ledges or steps. Along rough interfaces, misorientation of the planes of the two contiguous lattices is accommodated by edge

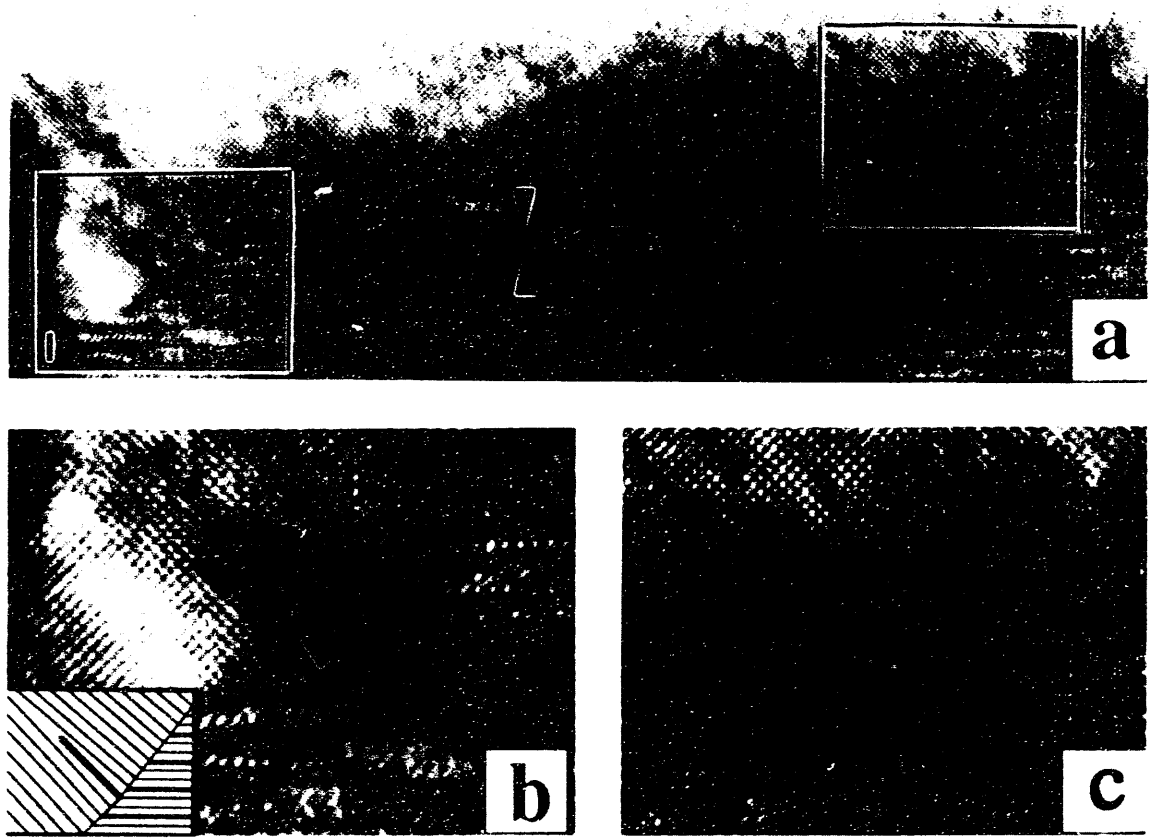

Fig. 5.4 (a) Lattice fringe image of SrTiO3 grown on YBCO; regions I and II are shown magnified as b and c. (b) Example of stepped interface showing an edge dislocation, labeled "d", in which the associated extra half-plane is normal to the interface. (c) High resolution micrograph showing a perfectly planar interface.

dislocations in which the associated extra half-plane is normal to the interface. We find that the close-packed directions are parallel across interfaces, even in the presence of steps and ledges, suggesting that these are low energy interfaces. The observed epitaxy undoubtedly leads to the high quality insulating and superconducting properties we have found in such trilayer structures, and suggests that it may be possible to fabricate structures of comparable quality with much thinner insulating layers.

References

1. J. J. Kingston, F. C. Wellstood, P. Lerch, A.H. Miklich, and J. Clarke, *Appl. Phys. Lett.* **56**, 236 (1990).

2. L. A. Tietz, C. B. Carter D. K. Lathrop, S. E. Russek, R. A. Buhrman, and J. R. Michael, *J. Mater. Res.*, **4 (5)**, 1072 (1989).

3. E. S. Hellman, D. G. Schlom, A. F. Marshall, S. K. Streiffer, J. S. Harris, Jr., M. R. Beasley, J. C. Bravman, T. H. Geballe, J. N. Eckstein, and C. Webb, *J. Mater. Res.*, **4 (3)**, 476 (1989).

4. R. Ramesh, D. Hwang, T. S. Ravi, A. Inam, J. B. Barner, L. Nazar, S. W. Chan, C. Y. Chen, B Dutta, T Venkatesan, X. D. Wu, *Appl. Phys. Lett.* **56(22)**, 2243 (1990); R. Ramesh, D. M. Hwang, T. Venkatesan, T. S. Ravi, L. Nazar, A. Inam, X. D. Wu, B. Dutta, G. Thomas, A. F. Marshall, and T. H. Geballe, *Science* **247**, 57 (1990).

5. T. Venkatesan, A. Inam, B. Dutta, R. Ramesh, M. S. Hegde, X. D. Wu, L. Nazar, C. C. Chang, J. B. Barner, D. M. Hwang, and C. T. Rogers, *Appl. Phys. Lett.* **56**, 391 (1990).

6. S. Tanaka, H. Nakanishi, K. Higaki, and H. Itozaki, *Jap. J. Appl. Phys.*, **29**, 1059 (1990)

7. H. W. Zandbergen, R. Gronsky, and G. Thomas, *J. Micr. Spec. Electron.* **13**, 307 (1988).

8. H. W. Zandbergen, R. Gronsky, and G. Thomas, *Nature*, **331**, 596 (1988).

9. H. W. Zandbergen, R. Gronsky, and G. van Tendeloo, *J. Superconductivity*, **3**, 103 (1989).

10. A. Garulli, A. Armigliato, and M. Vanzi, *J. Microsc. Spectrsc. Electrn.* **10**, 135 (1990).

11. K. Burger, W. Mader, and M. Ruhle, *Ultramicrosc.* **22**, 1 (1987).

Chapter 6

Superconducting Thin-Film Multiturn Coils of $YBa_2Cu_3O_{7-x}$

Armed with our interconnect technology, we proceed to fabricate and test thin-film multi-turn coils of $YBa_2Cu_3O_{7-x}$ (YBCO) that are suitable for coupling to planar SQUIDs. Whereas a single-turn loop can be constructed from a single-layer film, a multiturn coil requires a minimum of three layers, since a superconducting path must connect the innermost turn of the coil to the pick-up coil without producing an electrical short to the remaining turns (see Fig. 6.1). Furthermore, one must pattern each layer of the coil individually, since it is not possible to fabricate a multiturn coil by post-patterning a three-layer stack of films. In order to produce efficient coupling, the linewidth of the turns must be reasonably fine, say 20μm or less, so that all of the turns fit within the outer dimension of the SQUID. In addition, the upper and lower YBCO films must make a superconducting contact at the inner turn of the coil, and the upper YBCO film must remain superconducting where it "climbs" over the edges of earlier layers. Accordingly, a high degree of compatibility is required between the design of the coil, the materials, the deposition techniques and the patterning methods.

To a large extent, the above requirements determine the details of the process. Having developed our crossover technology using YBCO and $SrTiO_3$,[1] we naturally chose to use the same materials. Because the linewidth of the line making contact to the inner turn can be relatively large and no fine patterning is required for the $SrTiO_3$, we use shadow masks to pattern these two layers.[1] The choice has two advantages: we have found that the masks do not contaminate the surfaces of the films significantly, so that epitaxial growth of subsequent films is achieved, and the edges of the patterned

films are smooth, so that subsequent films can easily climb them. On the other hand, the fine linewidth required for the turns of the coil is most easily accomplished using photolithography and an etch, processes that are best left for the last step so that the resist does not come into contact with surfaces that must subsequently support epitaxial growth. Accordingly, the top YBCO layer is used to form the turns, and the bottom layer the contact line ("crossunder").

Figure 6.1 shows the design of a square spiral coil with 10 turns of 20μm linewidth, an outer width of 1mm and an inner width of approximately 150μm; we have also made coils with 19 turns and a 10μm linewidth. We choose a relatively large linewidth to minimize the chance of a defect breaking the coil, and to provide a higher coupling efficiency if used in a flip-chip arrangement.[2] For testing purposes, we pattern 1mm^2 contact pads on the ends of the leads to the coil.

We have used two kinds of masks for patterning the first two layers. Some were made from Si_3N_4 coated 50mm diameter Si wafers using photolithography and a KOH etch. The others were made from 50μm and 100μm thick stainless steel foils patterned with an electro-discharge machine. While the steel masks have proven to be more robust, the Si masks produce a sharper line definition because they are considerably flatter and stiffer, and can be clamped more tightly to the substrate. The first layer mask defines the YBCO crossunder, which is a 100μm wide line stretching almost to the edges of the chip. The second layer mask defines a rectangle of $SrTiO_3$ that covers the central portion of the crossunder, leaving the ends exposed (Fig. 6.1). The second YBCO layer covers the entire chip. The final patterning step is made with an Ar ion mill using photoresist as a stencil mask. This process defines the turns of the coil, forms the pads, and removes the portion of the crossunder line not covered by $SrTiO_3$ that would otherwise short the turns. The mill is stopped from etching through the remainder of the crossunder by the layer of $SrTiO_3$.

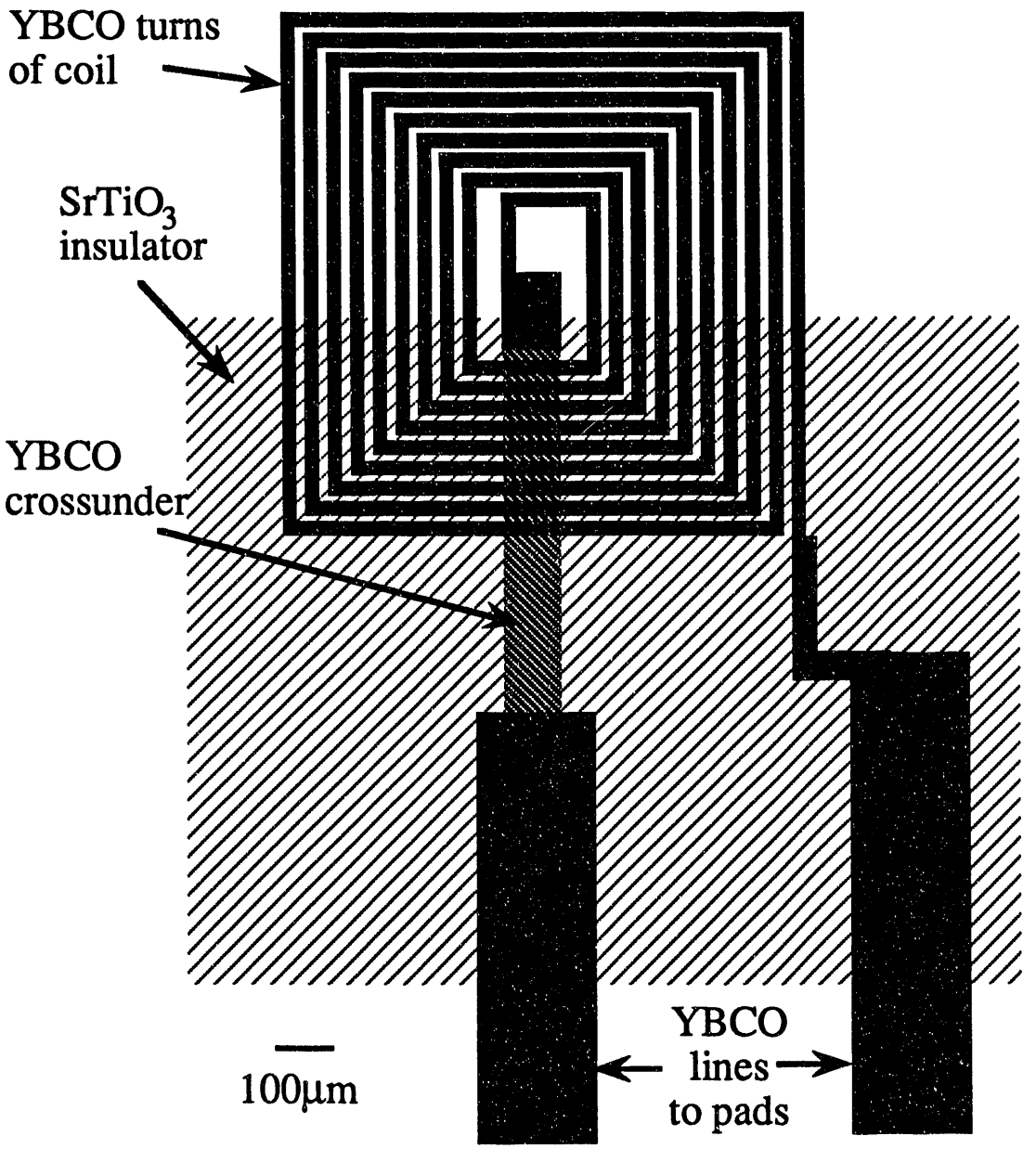

Fig. 6.1 Layout of thin-film 10-turn coil with 20μm linewidth. The bottom layer of YBCO forms the crossunder, the middle layer is of $SrTiO_3$, and the top layer is of YBCO (solid fill).

We deposit the films on (100) cleaved and polished 12.5 x 12.5 x 1 mm^3 MgO substrates, opening the vacuum chamber to change masks and targets between each deposition. All layers are deposited with a Questek 2820 KrF pulsed excimer laser. While the upper two layers are grown with a standard laser deposition technique,[1,3] the bottom layer is grown with an rf plasma assisted laser deposition technique that we developed to allow the deposition of 0.1mm wide lines through a shadow mask. Instead of backfilling the vacuum chamber to 200mTorr as is usual, we strike a 60W rf plasma with 40mTorr of O_2 in the vacuum chamber during deposition, thereby increasing the sharpness of the line definition while insuring sufficient O_2 incorporation into the film. Our attempts to deposit 0.1 mm lines in 200mTorr of O_2 resulted in YBCO with a lowered T_c.

Although we have made coils of various thicknesses using different deposition parameters, for convenience we describe a typical procedure that yields layers about 400nm thick. We deposit the first layer of YBCO with the rf plasma using a laser fluence of 1.3Jcm^{-2} at 5Hz for 6 min, while maintaining the heater block at 700°C as indicated by an optical pyrometer. The chamber is then quickly filled with 700Torr of O_2 and the heater block is allowed to cool to 450°C in 15min before cooling to room temperature in another 15 min. After exchanging targets and masks, the chamber is evacuated to $3x10^{-6}$ Torr as the temperature of the heater block is raised to 200°C. The temperature is then increased to 680°C in about 3 min, during which time the chamber is filled with 190mTorr of O_2 and the surface of the $SrTiO_3$ target is cleaned with 300 laser pulses. We then deposit $SrTiO_3$ for 6 min at 5Hz with a laser fluence of 1.3Jcm^{-2} before cooling in O_2 as in the previous step. After removing the mask and again exchanging the targets, we evacuate the chamber as before, raise the temperature to 735°C and deposit YBCO for 6 min at 5Hz in 200 mTorr of O_2 prior to cooling.

After removing the chip from the vacuum chamber, we pattern it with a 2-3μm thick layer of Microposit 1400-31 resist, and ion mill the surface for a total of 25-35

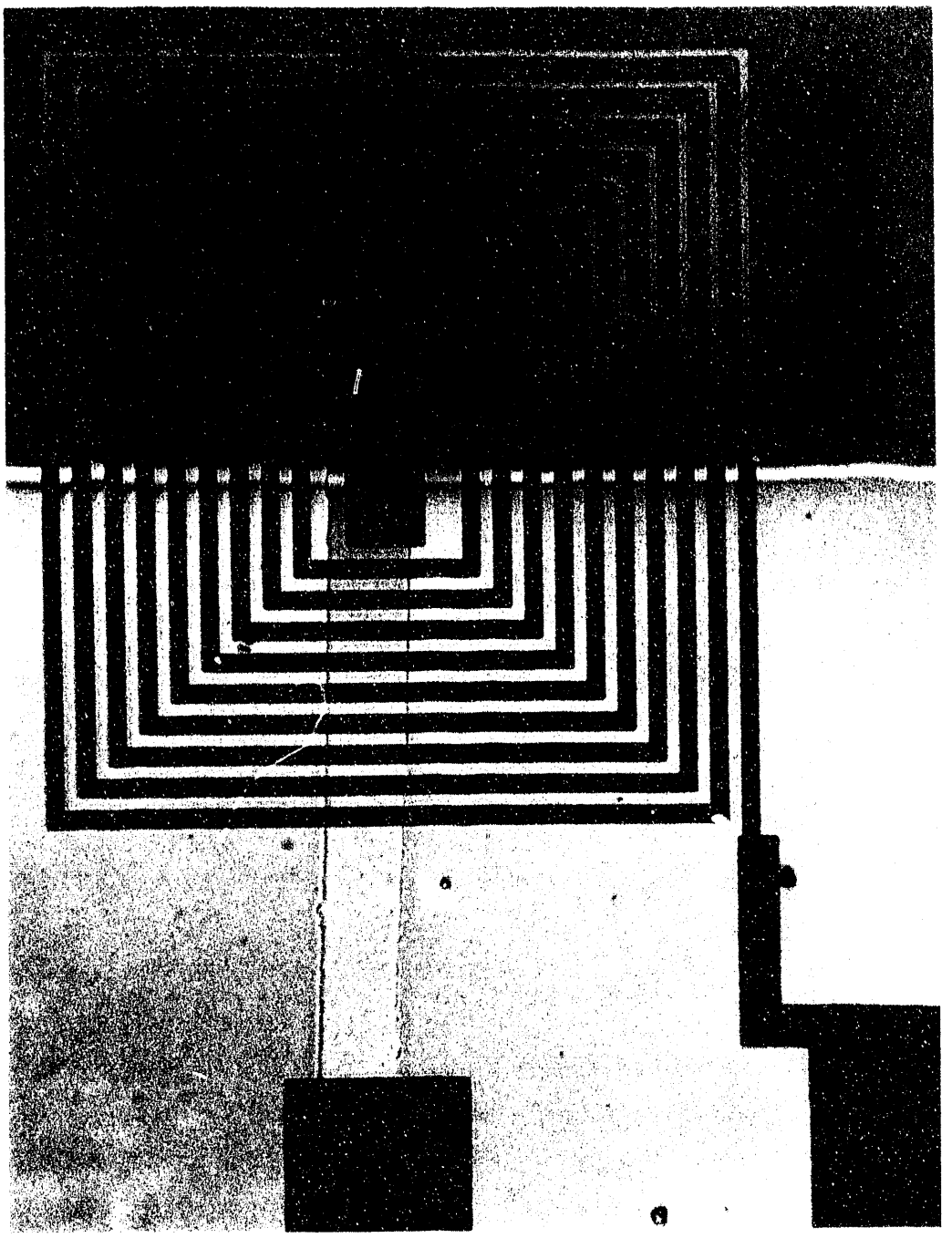

Fig. 6.2. Photomicrograph of completed 10-turn coil. Coil is 1mm on a side.

min in a 600V, 1.5mAcm^{-2} beam of Ar ions. To minimize heating, we clamp the chip to a Cu block and typically perform the ion milling in 5 min steps separated by 15 min cooling intervals. Figure 6.2 shows a completed coil. Finally, we press In contacts onto the pads and use a 4-terminal arrangement to measure the resistance and critical current.

Figure 6.3 shows resistance vs. temperature T for a 10-turn and a 19-turn coil. Initially, as the temperature is lowered from 300K, the resistance decreases slowly (b) or even increases (a). We believe that this effect is due to parallel conduction through the $SrTiO_3$ and along the turns of the YBCO coil. At room temperature, the $SrTiO_3$ can have appreciable conductivity, whereas at lower temperatures the resistance of the $SrTiO_3$ becomes very large and conduction along the YBCO coils dominates. Figure 6.4 shows the critical current I_c, measured using a 10mV detection criterion, as a function of T for six coils. At 77K, the large variations in I_C are mostly the result of differences in T_C between the coils. We believe that the critical currents and transition temperatures of coils 1 and 2 were lowered by heat degradation during ion milling: the milling was performed in 18 min intervals. Each film in coils 3 and 4 was only about 200 nm thick, about one-half the thickness of the films in the other coils. Coils 5 and 6 have the highest transition temperatures, but their critical currents differ by an order of magnitude. We suspect that this difference is due to defects in the films caused by defects or dirt on the surface of the substrate. Of the six coils, coil 5 (10 turns, 20μm linewidth, T_C=82K) had the largest critical current, approximately 1.4mA at 77K and 40mA at 4.2K. These values correspond to critical current densities of about 2 x 10^4 and 5 x 10^5A cm^{-2} in the turns of the coil, respectively.

Figure 6.5 shows the resistance between the crossunder and the turns of coil 4. To measure this resistance, we opened the innermost turn of the coil by patterning with photoresist and ion milling. The resistance increases steadily as the temperature is lowered, becoming approximately $10^7\,\Omega$ at 77K. This value exceeds the minimum

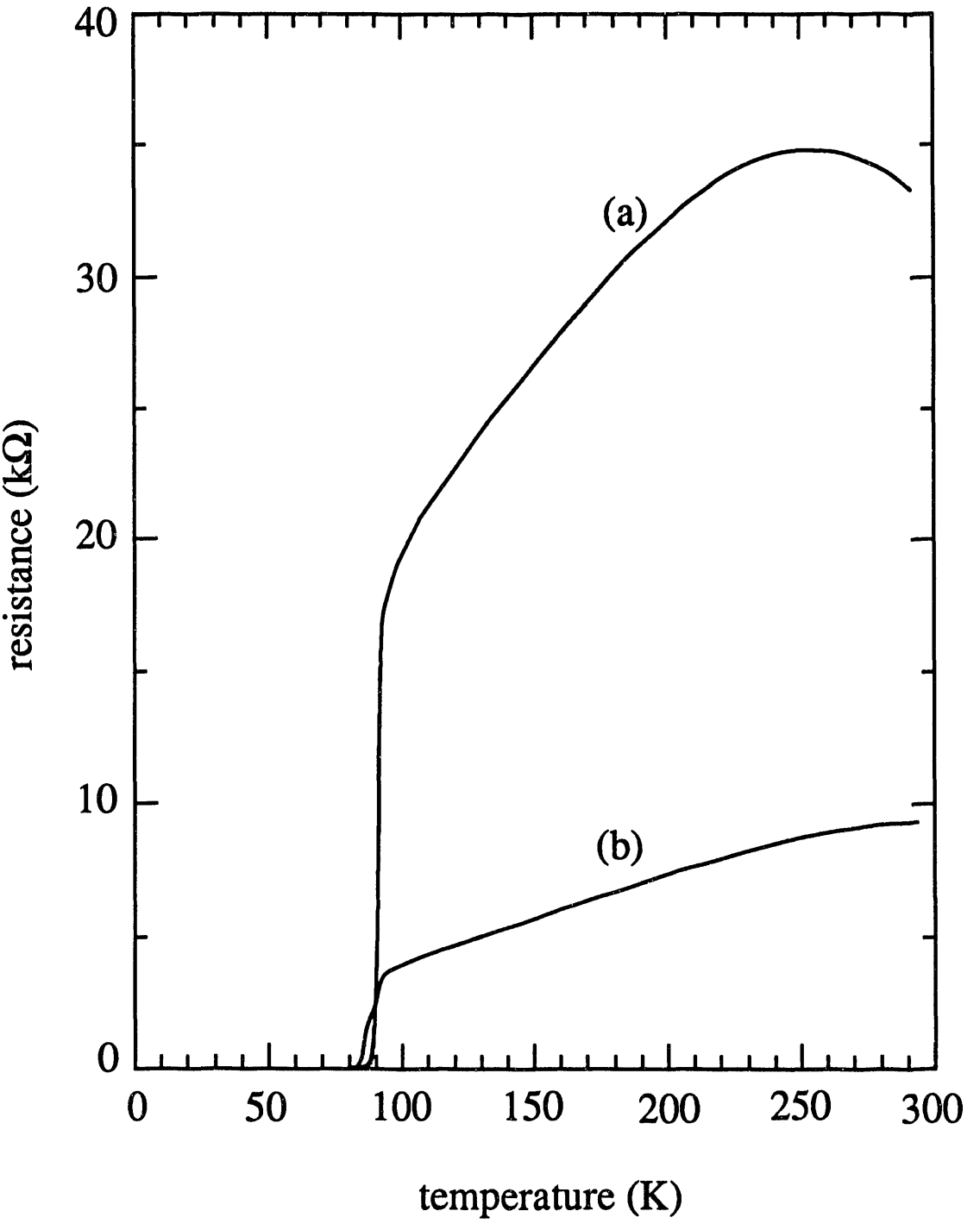

Fig. 6.3 Coil resistance versus temperature for (a) coil 2 (19-turn, 10μm linewidth), (b) coil 5 (10-turn, 20μm linewidth).

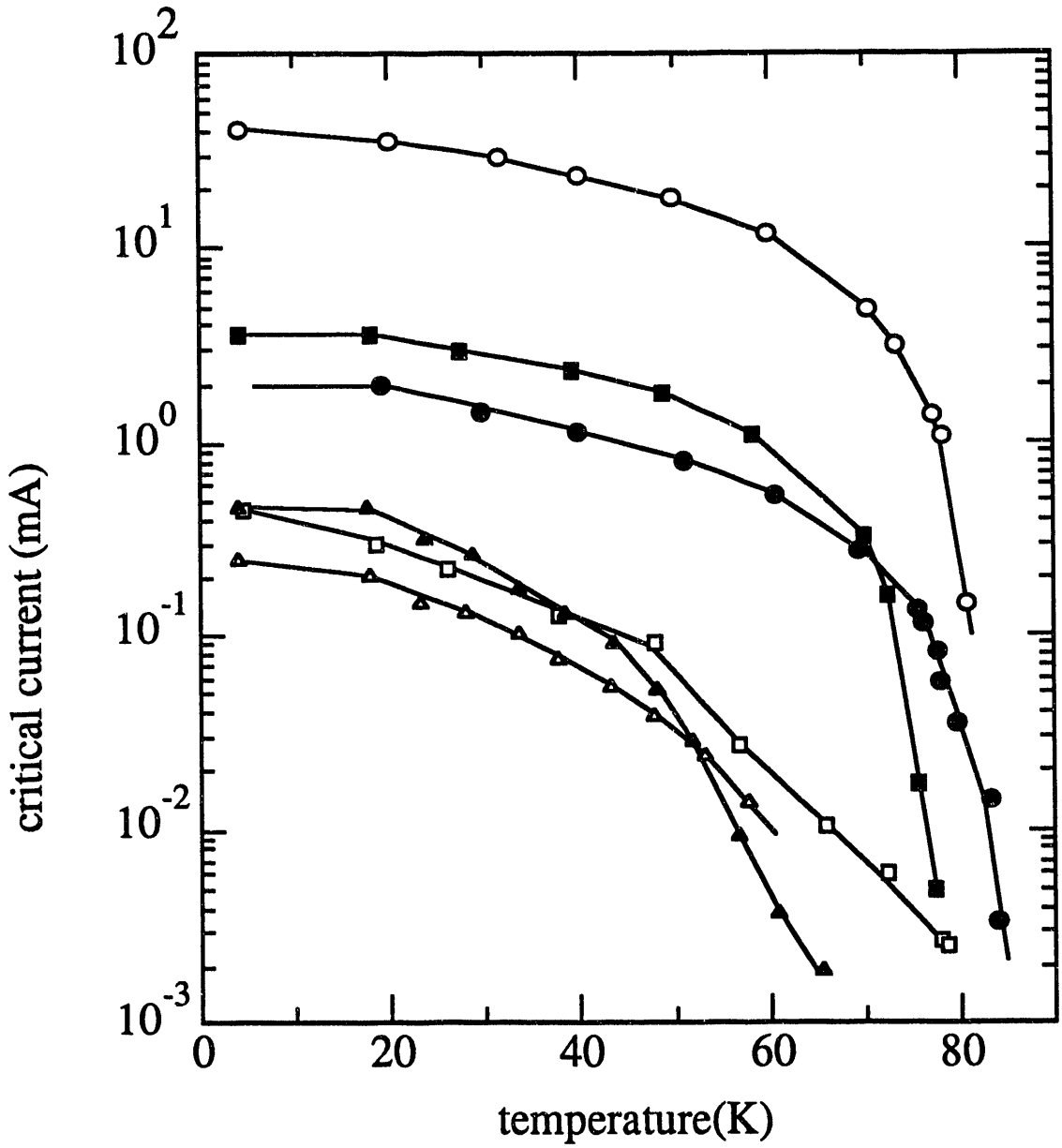

Fig. 6.4 Critical current versus temperature for: coil 1, open triangles; coil 2, closed triangles, coil 3, open squares; coil 4, closed squares; coil 5, open circles; coil 6, closed circles. Coils 1 and 2 have 19 turns of 10μm linewidth, while the remaining coils have 10 turns of 20μm linewidth.

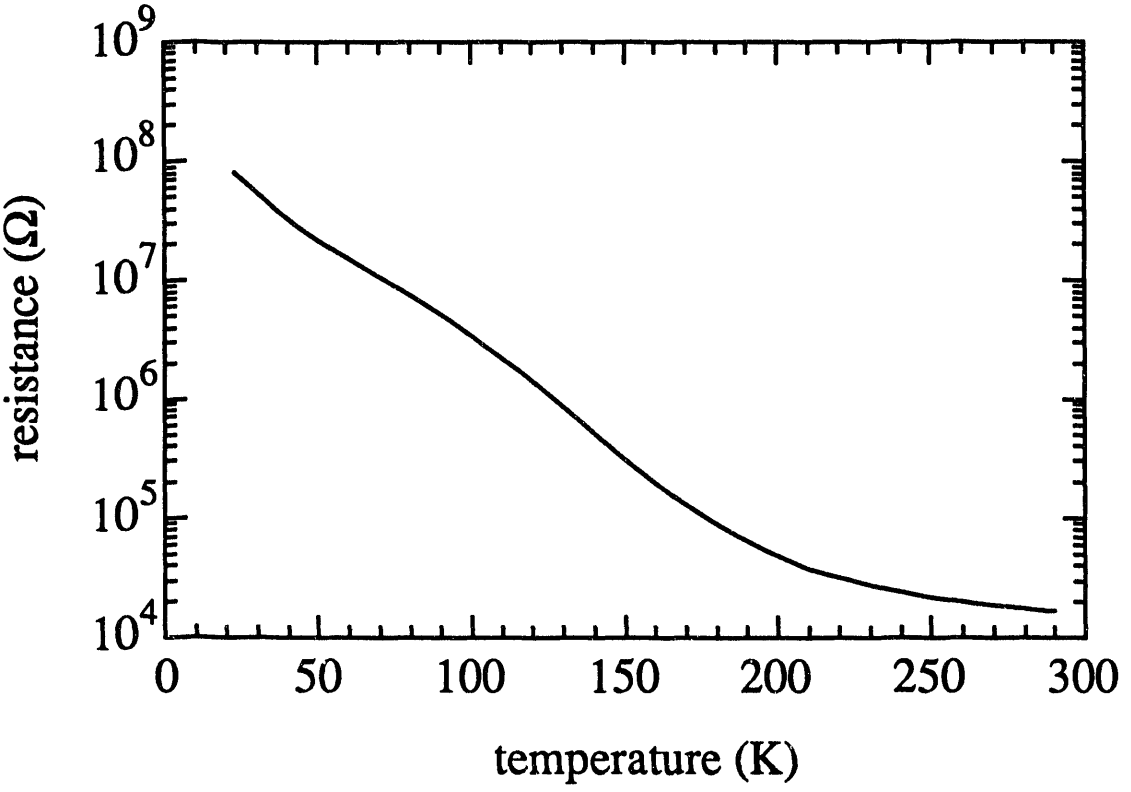

Fig. 6.5 Resistance versus temperature of the $SrTiO_3$ between the crossunder and 9 crossovers of coil 4.

acceptable parallel resistance for use in flux transformers by several orders of magnitude: a resistance of 10 kΩ would produce a negligible Nyquist current noise. Given that there are 9 crossovers, this implies that the $SrTiO_3$ resistivity was about $10^8\Omega$cm at 77K. At 290K, the $SrTiO_3$ has a resistivity of approximately $1.6x10^5\Omega$cm, whereas single crystal $SrTiO_3$ has a resistivity of about $10^9\Omega$cm. We suspect that the lower $SrTiO_3$ resistance obtained in the coil is the result of small defects in the insulation.

In conclusion, the measured properties of the coils make them promising candidates for use in flux transformers, and should enable one to construct sensitive magnetometers from high-T_c SQUIDs. Most importantly, these results demonstrate that relatively sophisticated multilayer high T_c circuits are now well within reach.

References

1. J. J. Kingston, F. C. Wellstood, P. Lerch, A. H. Miklich and J. Clarke, *Appl. Phys. Lett.* **56,** 189 (1990).

2. V. P. Koshelets, A. N. Matlashov, I. L. Serpuchenko, L. V. Filippenko, Y. E. Zhuravlev, *IEEE Trans. Magn* . **MAG-25,** 1182 (1989).

3. See for example: S. Witanachchi, H. S. Kwok, X. W. Wang, and D. T. Shaw, *Appl. Phys. Lett.* **53**, 234 (1988); A. Inam, M. S. Hegde, X. D. Wu, T. Venkatesan, P. England, P. F. Miceli, E. W. Chase, C. C. Chang, J. M. Tarascon; and J. B. Wachtman, *Appl. Phys. Lett.* **53**, 908 (1988); J. Frohlingsdorf, W. Zander, and B. Strizker, *Solid State Communications* **67**, 965 (1988).

Chapter 7

Superconducting Thin-Film Flux Transformers of $YBa_2Cu_3O_{7-x}$

We describe the design, construction, and magnetic field response of thin-film flux transformers with multiturn input coils, constructed from the high-temperature superconductor $YBa_2Cu_3O_{7-x}$ (YBCO).[1]

Having already discussed this in more detail in the introduction, I simply remind you that the design of a flux transformer involves a few simple considerations: (i) the magnetic field response increases as the area of the pickup coil increases; (ii) the pickup coil should have the smallest possible inductance, L_p, for its area; (iii) the magnetic field response is largest when the input coil inductance, L_i, is set equal to L_p; (iv) the input coil should have approximately the same overall size and shape as the SQUID in order to be efficiently coupled to it. We note that if one is to obtain substantial gain in magnetic field response, the area of the pickup loop should be much greater than that of the SQUID. Consequently, in an optimized transformer, the input coil should generally be multiturn; a single-layer transformer, which necessarily has a single turn input coil[2,3], gives a lower than optimum response.

We show the design of our thin-film YBCO flux transformer in Fig. 7.1(a), and summarize its parameters in Table 7.1. The area of the pickup loop was limited by the size of the MgO substrate, and we kept the inductance small by choosing a large linewidth, 1mm. The size and shape of the input coil were designed for good coupling to our thin-film, low-temperature dc SQUID, which is a square washer[4] with an outer width of 1mm and an inner width of 0.2mm (see Table 7.1). In practice, it is somewhat difficult to match L_i and L_p accurately because we do not know L_p exactly,

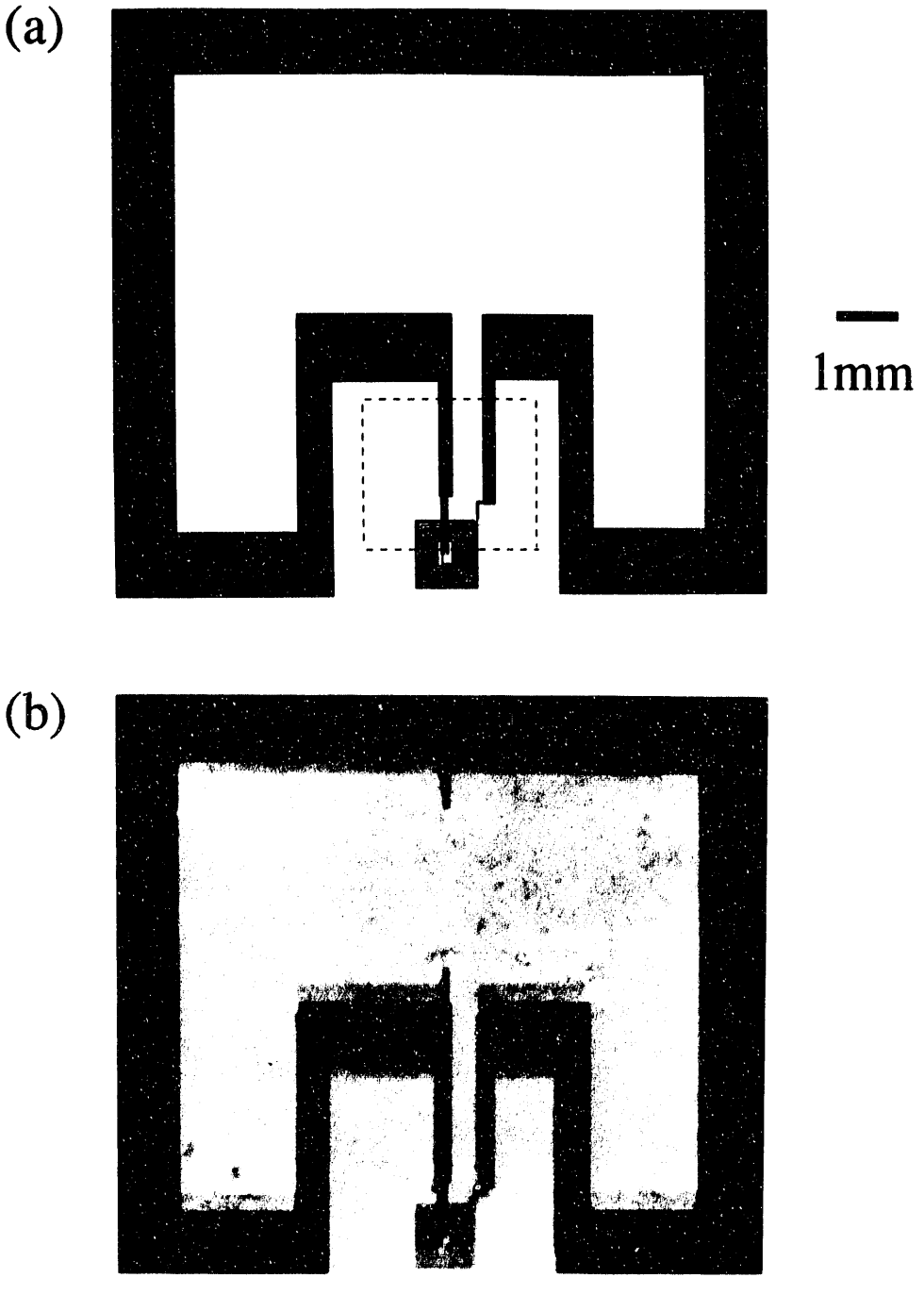

Fig 7.1 (a) Configuration of planar thin-film YBCO flux transformer; dashed lone outlines $SrTiO_3$ film. (b) Photograph of completed transformer.

and L_i depends strongly on the distance of the input coil from the square washer SQUID, which provides a superconducting groundplane.[4] Given these uncertainties, we somewhat arbitrarily chose 10 turns for the input coil. If it were tightly-coupled to the SQUID, we estimate this coil would have an inductance of about 40nH, a factor of 2 larger than our estimate for the pickup loop; in the present experiments, the weaker coupling to the SQUID increases the inductance to about 75nH. We chose a relatively large linewidth for the input coil, 20μm, to reduce the chances of a defect breaking the coil and to ensure a more than adequate critical current.

Table 7.1 Parameters of SQUID and flux transformers.

	pickup coil	input coil	SQUID
sensing area (mm^2)	≈70	---------	≈0.2
number of turns	1	10	1
line width (mm)	≈1	0.02	---------
inductance (nH)	≈20	≈ 75[a]	0.44
outer width (mm)	≈11	1	1
inner width (mm)	≈9	≈ 0.15	0.2

[a] depends on coupling to SQUID.

Because a superconducting connecting line must be made to the inner turn of the input coil, at least two patterned and electrically isolated superconducting layers are needed, and we thus require multilayer processing techniques[5,6]. Each transformer was

made on a 12.5 x 12.5 x 0.75 mm^3 (100) cleaved, polished and cleaned MgO substrate. We deposited the layers *in situ* using a Questek 2820 excimer laser operating on the KrF 248nm line with a 5Hz repetition rate. The beam was focussed to a fluence of 1.3Jcm^{-2} onto 25.4mm diameter pressed, sintered, and polished targets which rotated at about 1Hz on a mount attached to a water-cooled block. The MgO substrate was clamped to a heater block 60mm from the target.

We first deposited 300nm of YBCO in 45mTorr of O_2 in the presence of an rf discharge[6] with the substrate at 690°C; this layer forms the connecting line or "crossunder" to the innermost turn of the input coil. The second film, 300nm of $SrTiO_3$ deposited in 190mTorr of O_2 at 680°C, provides electrical insulation between the crossunder and the turns of the coil. The third layer, 300nm of YBCO deposited in 190mTorr of O_2 at 740°C, forms the pickup loop and the turns of the input coil. After each layer was deposited, the substrate was cooled to room temperature in O_2, and exposed to air while the masks and targets were changed. The first two layers were patterned by shadow masks consisting of etched Si chips clamped directly to the face of the substrate, while the last layer was patterned with photolithography and an Ar ion mill etch. Figure 7.1(b) shows a completed flux transformer.

We tested each flux transformer by mounting it on a temperature-controlled stage[7] less than 100μm from the conventional Nb-PbIn dc SQUID at 4.2K. The assembly was inserted in a superconducting shield and enclosed in a vacuum can surrounded by liquid ^4He. We aligned the input coil of the transformer with the SQUID to ensure good coupling, and operated the SQUID in a flux-locked loop that produced an output voltage proportional to the applied flux. The transformer was placed above the center of a 10-turn, 19mm diameter coil which we used to apply a magnetic field.

In Fig. 7.2, we plot the response of the SQUID to a quasistatic magnetic field B as a function of the temperature of the transformer. The two transformers shown, 1

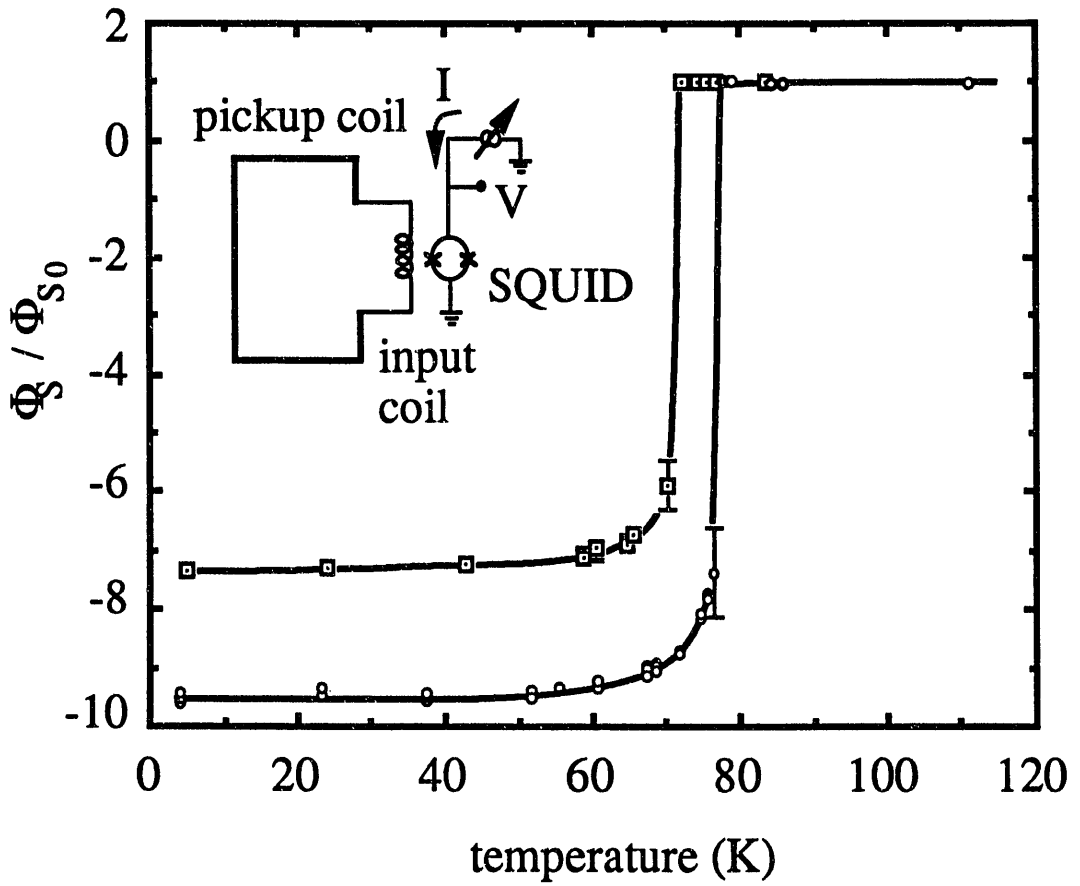

Fig. 7.2 Φ_S/Φ_{S0} vs. temperature for transformers 1 (squares) and 2 (circles). Solid lines are guides to the eye. Inset shows schematically a flux transformer coupled to a dc SQUID.

and 2, have transition temperatures T_c of 71K and 77K, respectively. Above T_c, the response is due to the SQUID alone, and is positive. Below T_c, the response includes contributions from the transformers, and is -7.3 and -9.5 times that of the SQUID alone for transformers 1 and 2, respectively. The sign change is due to our deliberate choice of the winding sense between the pickup and input coils, made so that there would be a clear signature that the flux transformer was functioning.

The total flux induced in the SQUID by an applied magnetic field B is

$$\Phi_S = BA_S - BA_p\alpha\,(L_i\,L)^{1/2}/(L_i + L_p), \qquad (7.1)$$

where L is the SQUID inductance, $A_s = \eta A$ and A_p are the effective pickup areas of the SQUID loop and pickup coil, respectively. Here, α is the coupling coefficient, A is the inner geometric area of the SQUID, and η is a flux focussing factor,[8] which we estimate to be 5. We have assumed that B is uniform, and neglected any direct coupling of the field into the input coil, which gives a small correction. The first term in Eq. (7.1) is the flux Φ_{so} coupled directly into the SQUID in the absence of the flux transformer, while the second is the flux coupled by the transformer; the latter is zero above T_c. We now define $g = \Phi_S(T<<T_c)/\Phi_{S0}$ and use Eq. (7.1) to find

$$\alpha = (1 - g)\,(A_S/A_p)(L_i + L_p)/(L_i\,L)^{1/2}\,. \qquad (7.2)$$

Using the measured values of g and the estimated values of A_S, A_p, L, L_i and L_p (see Table 7.1), we find $\alpha = 0.39$ and 0.50 for transformers 1 and 2, respectively. Since the SQUID and transformer are physically separated, we consider these values of α to be quite reasonable.

We measured the response of transformer 1 at 59K and of transformer 2 at 67K over the range $\pm$ 5nT, and found the hysteresis was less than 0.1%. At somewhat higher applied fields, the response was strongly hysteretic, implying that the induced screening current in the transformer had exceeded the critical current. The open symbols in Fig. 7.3 show the estimated critical current of the transformers, which we inferred from the largest field at which the response was nonhysteretic. Transformer 2 had a

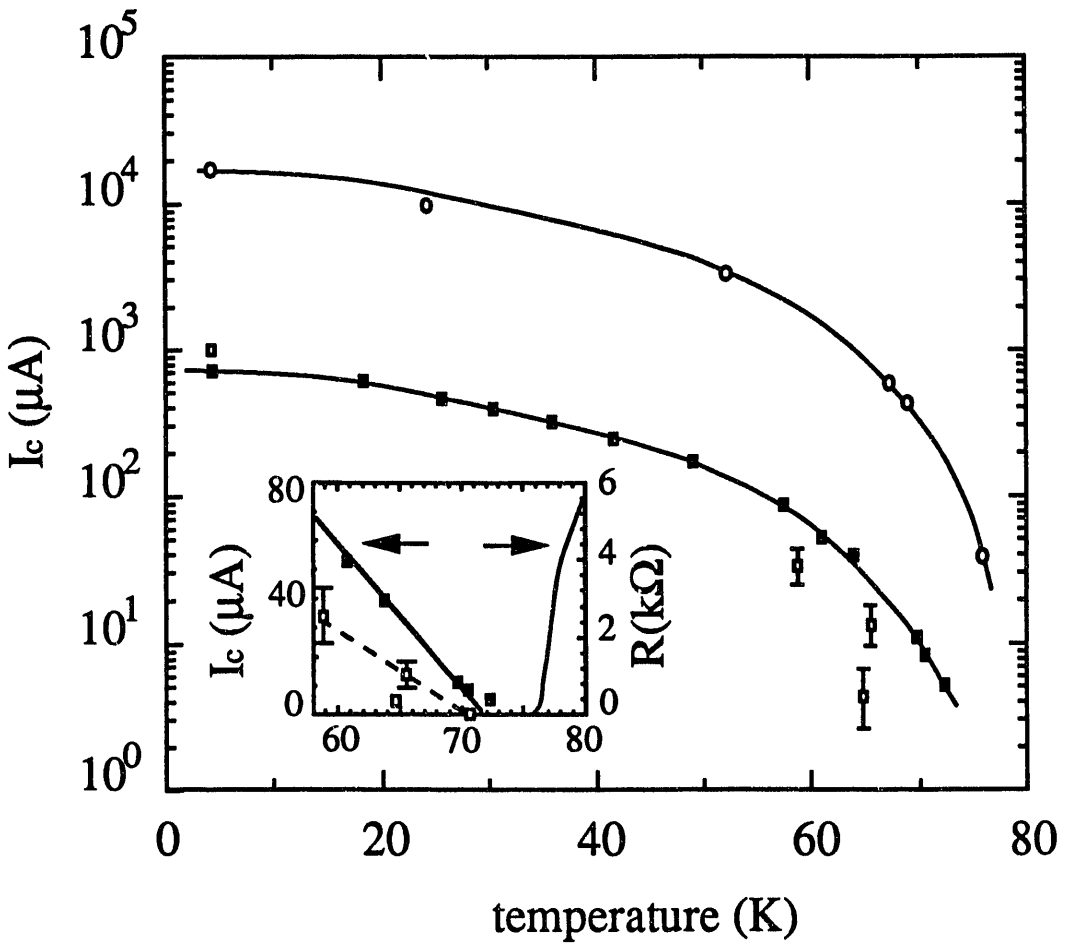

Fig. 7.3 Critical current Ic vs. temperature for transformers 1 (squares) and 2 (circles) measured by a dc SQUID (open symbols) or by direct transport measurements (filled symbols). Inset shows Ic and R vs. T near Tc.

higher critical current, about 16mA at 4.2K, corresponding to a critical current of $2.5x10^5 Acm^{-2}$ in the turns of the coil.

After completing the SQUID measurements on transformer 1, we scribed open the pickup loop and attached electrical leads to make direct transport measurements of the critical current and coil resistance. The solid points in Fig. 7.3 show the critical current vs. temperature, determined with a 10μV criterion, and Fig. 7.4(a) plots the resistance vs. temperature. We note that near T_c the inductively measured critical current lies somewhat below that measured with a transport current, as one might expect, and that both measurements extrapolate to zero at a temperature well below the rapid drop in resistance (see inset to Fig. 7.3). These results suggest that the critical current of the coil is determined by relatively short regions of poor quality film or by a weak link in the coil. Well above T_c, the resistance of the coil increases approximately linearly with T [Fig. 7.4(a)]. Subsequently, we opened the inner turn of the spiral coil and measured the resistance of the $SrTiO_3$ insulation between the crossunder and the turns of the coil [see Fig. 7.4(b)]. At 77K, the resistance is about 150MΩ indicating that the crossovers are well-insulated.

We suspect that the somewhat low values found for the transition temperatures of the transformers are the result of damage incurred during the ion-mill etching. The etching involves the removal of a considerable thickness of film, up to 800nm, and may produce substantial heating of the film. Transformer 1 was milled with 600V Ar^+ ions at $1.5mAcm^{-2}$ in 5 min bursts separated by 15 min cooling intervals. For transformer 2, we reduced the beam energy to 450 V and kept the other parameters fixed. We believe that the reduced beam energy in the second case resulted in less damage and a higher transition temperature and critical current.

In conclusion, we have operated thin-film, multiturn YBCO flux transformers that have zero resistance at temperatures as high as 77K. The magnetic field response of the SQUID was enhanced by a factor of 9.5 by transformer 2. We note that had we

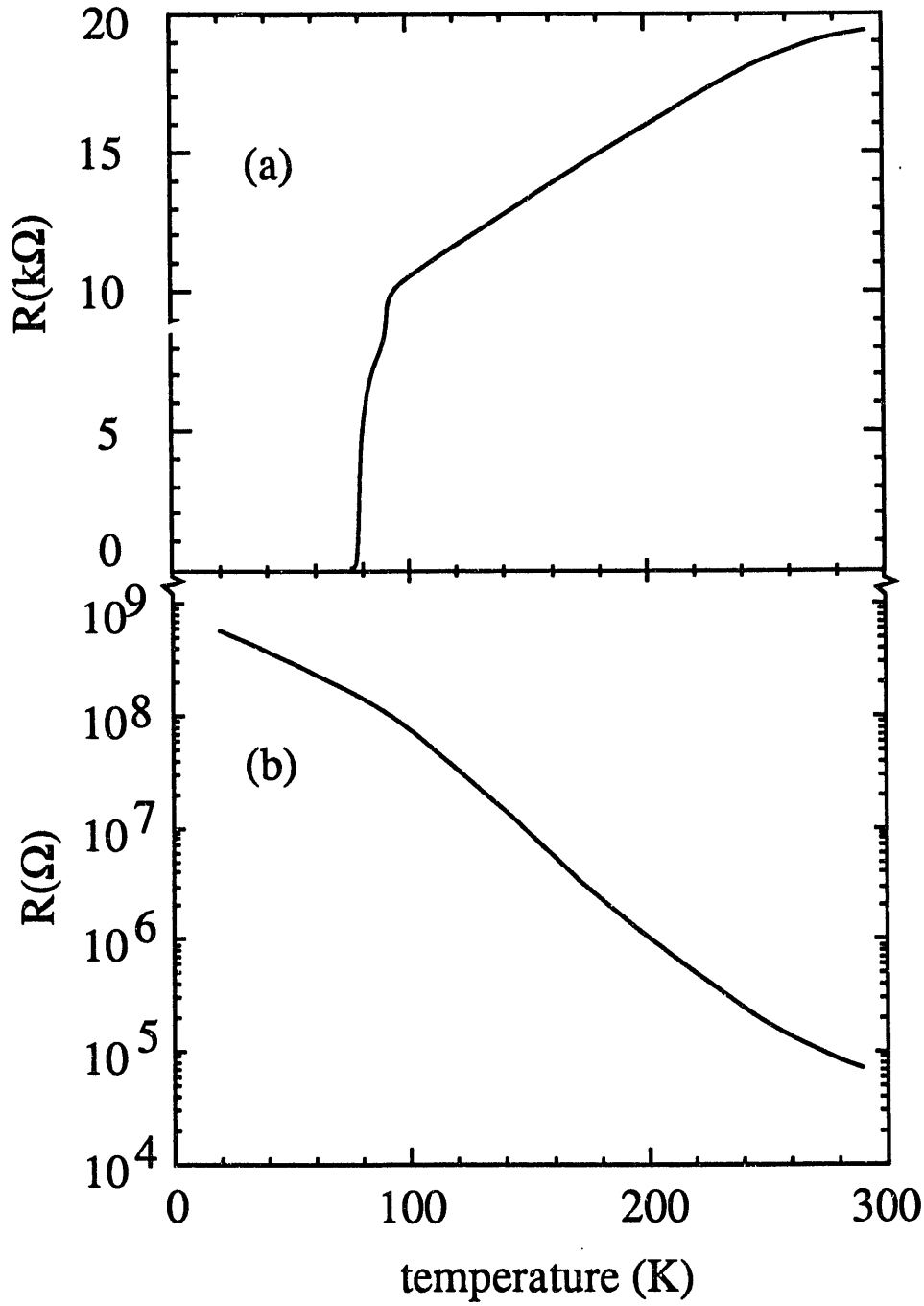

Fig. 7.4 Resistance vs. temperature of flux transformer 1, measured by opening the pickup loop; (b) resistance vs. temperature of the insulating $SrTiO_3$ layer of transformer 1 measured between the turns of the input coil and the crossunder.

wound the input coil in the opposite sense, the enhancement would have been about 12, and that a further factor of about 2 could be realized with the same transformer if the input coil were more tightly pressed to the SQUID.

References

1. F. C. Wellstood, J. J. Kingston, and J. Clarke, *Bull. Am. Phys. Soc.* **35**, 377 (1990).

2. B. Oh, R. H. Koch, W. J. Gallagher, V. Foglietti, G. Koren, A. Gupta, and W. Y. Lee, *Bull. Am. Phys. Soc.* **35**, 377 (1990); *Appl. Phys. Lett.* (25 June, 1990).

3. M. S. Diorio, K-Y. Yang, A. N. Erickson, L. Warden, D. S. Buchanan, and D. N. Paulson, *Bull. Am. Phys. Soc.* **35**, 377 (1990).

4. M. B. Ketchen and J. M. Jaycox, *Appl. Phys. Lett.* **40**, 736 (1982).

5. J. J. Kingston, F. C. Wellstood, Ph. Lerch, A. H. Miklich, and J. Clarke, *Appl. Phys. Lett.* **56**, 189 (1990).

6. F. C. Wellstood, J. J. Kingston, and J. Clarke *Appl. Phys. Lett.* **56**, 2336 (1990).

7. M. J. Ferrari, M. Johnson, F. C. Wellstood, J. Clarke, P. A. Rosenthal, R. H. Hammond, and M. R. Beasley, *Appl. Phys. Lett.* **52**, 695 (1988).

8. M. B. Ketchen, W. J. Gallagher, A. W. Kleinsasser, S. Murphy, and J. R. Clem, SQUIDs - Superconducting QUantum Interference Devices and their Applications (Walter de Gruyter, Berlin, 1985) p. 865.

Chapter 8

Photolithographically Patterned Interconnects and Flux Transformers

The vast majority of electronic circuits require a thin-film multilayer technology to provide interconnects between devices.[1] Previously, we described crossovers in which two films of $YBa_2Cu_3O_{7-x}$ (YBCO) were isolated from each other by an intervening film of $SrTiO_3$ while retaining a high transition temperature (T_c). Subsequently, we fabricated multiturn coils[2] and flux transformers[3] suitable for coupling magnetic flux to thin-film high T_c SQUIDs.[4] In the original crossover process,[5] however, all three layers were deposited through shadow masks, and, in the coils,[2,3] only the last layer was patterned photolithographically. However, for most practical applications it is highly desirable to define each layer with photolithography so that one can "step and repeat" patterns with small or complicated features and achieve precise alignment of different layers. We now describe processes in which all three films are patterned independently by photolithography; as an example of this technology, we describe the fabrication of a flux transformer with $T_c \approx 87K$.

8.1 Photolithograpically Patterned Interconnects

8.1.1 Crossovers

There are two distinct problems that arise when one tries to use photolithography rather than shadow masks to pattern the lower layer of YBCO. First, while a shadow mask produces a line with rounded edges, photolithography followed by an etch tends to produce

sharp edges that are more difficult to insulate. Second, we have found that exposure of the surface of YBCO to photoresist leaves a layer of contamination that often prevents the epitaxial growth of subsequent layers. We have found that both problems can be ameliorated by etching the surface in a 2% solution of Br in methanol.[6] This process removes the surface contamination and thins the film, thereby making insulation easier.

We now describe the process used to fabricate the crossover shown in Fig. 8.1, in which only the first YBCO film is patterned photolithographically. The films are deposited using *in situ* laser deposition onto cleaved and polished (100) MgO substrates.[2,3,5] After depositing approximately 300nm of YBCO with the substrate at 740°C, we remove the sample from the vacuum chamber and pattern it into a 100μm wide strip using standard photolithography and either a 0.1% nitric acid solution or an Ar ion mill (450 V, 1.5 mA/cm^2) to etch the film. We strip the resist with acetone, immerse the substrate in the Br solution for up to 30s, rinse the substrate with methanol to stop the etch and blow it dry with N_2 before remounting it in the vacuum chamber. After evacuating the chamber with the substrate at 200°C, we rapidly raise its temperature to 690°C and deposit 600nm of $SrTiO_3$ through a shadow mask. We break vacuum to exchange targets and shadow masks, and, after a similar evacuation procedure, deposit approximately 400nm of YBCO. As we see in Fig. 8.2, the transition temperature of the lower YBCO film was 85K, the insulation between the lower and upper YBCO films at 77K was greater than 100MΩ at 77K, and the critical current of the lower film at the same temperature was 170mA, corresponding to a critical current density of $7x10^5$ A cm^{-2}. The transition temperature of the upper YBCO film (not shown) was 87K. Thus, this process produces satisfactory crossovers on photolithographically patterned YBCO films.

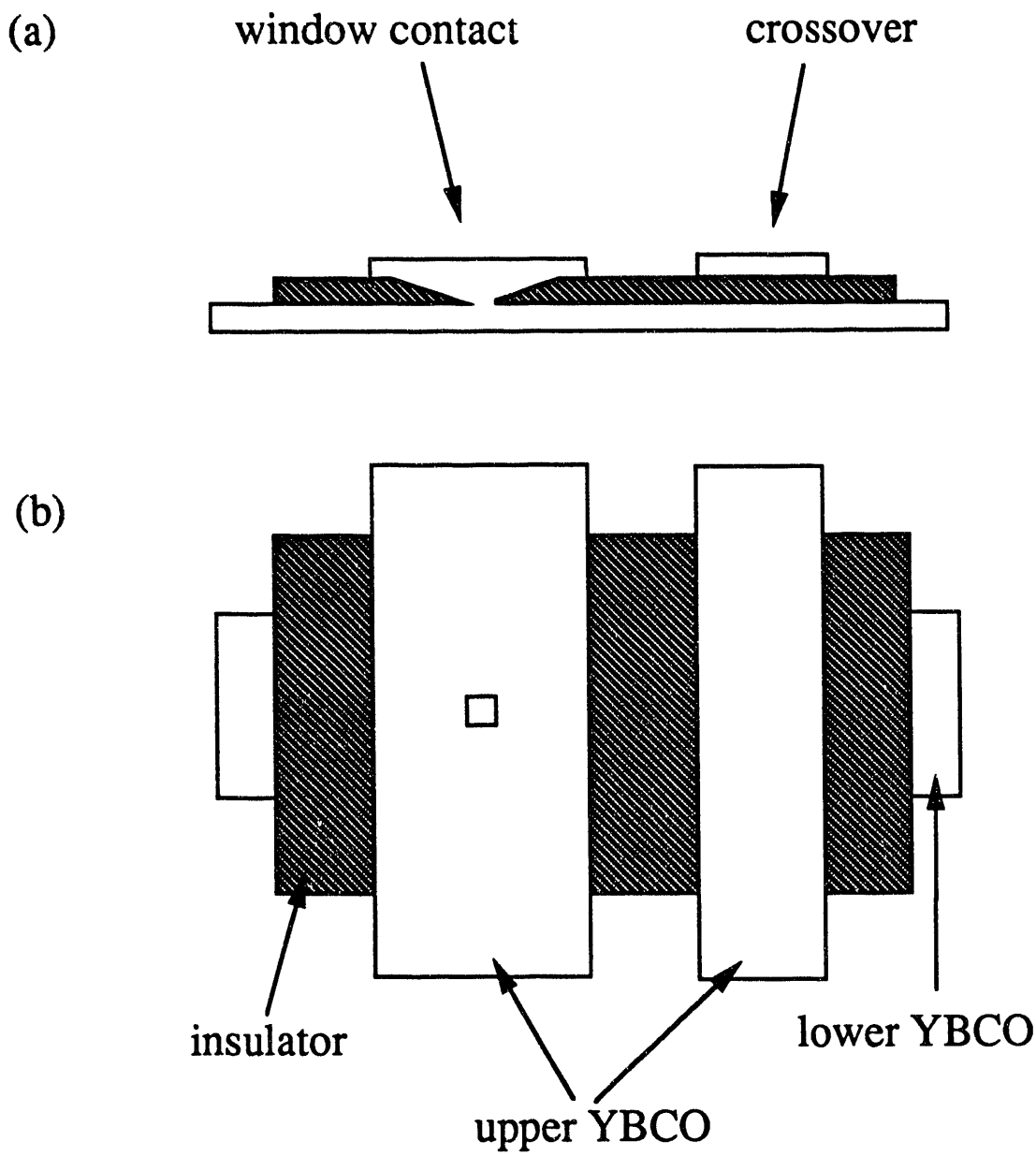

Fig. 8.1 (a) Cross - sectional view and (b) top view of window contact (left) and crossover (right)

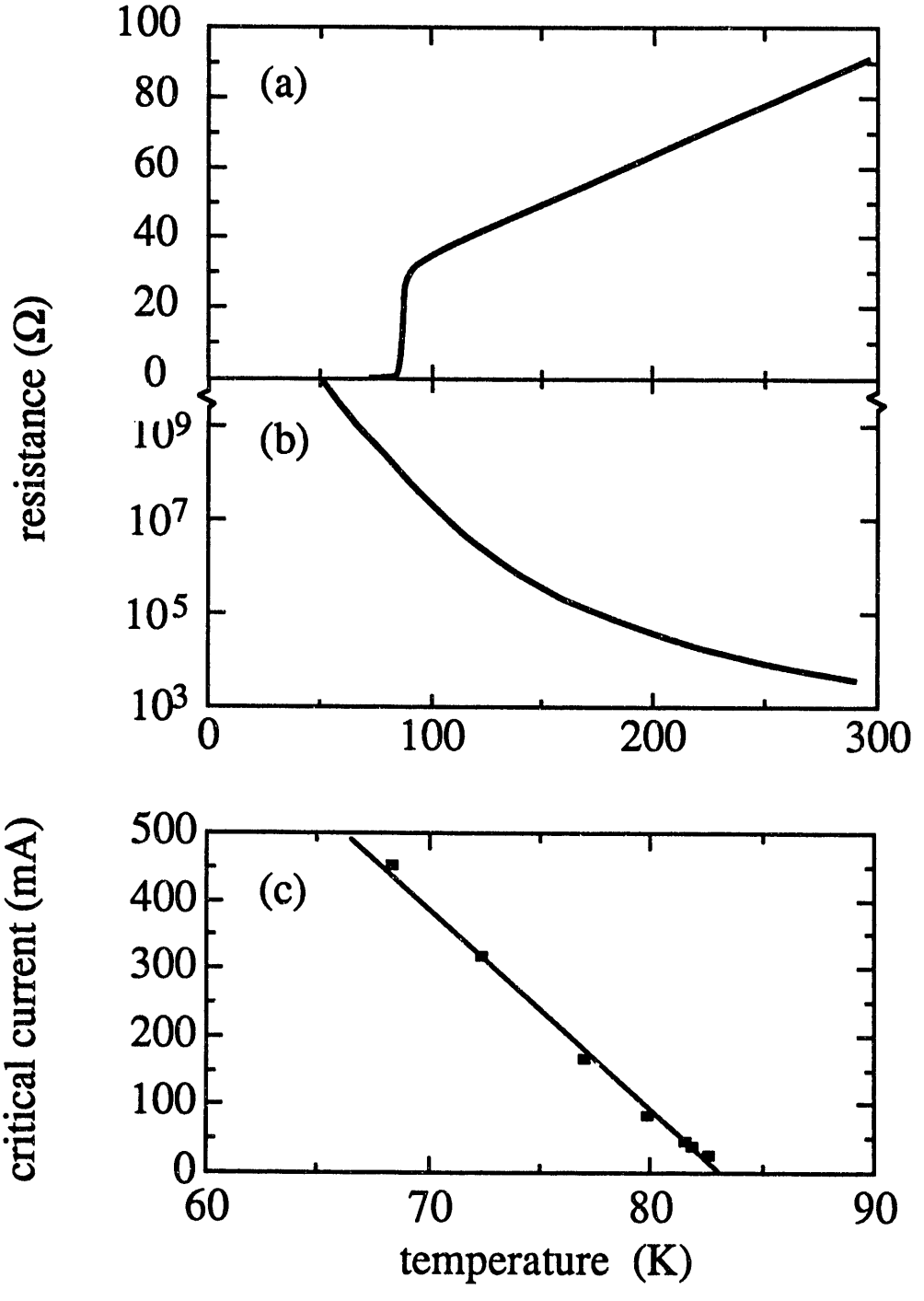

Fig. 8.2 Crossover: (a) resistance vs. temperature of lower YBCO line, (b) resistance between lower and upper YBCO films, and (c) critical current of lower line 100μm wide and 0.3 μm thick.

8.1.2 Window Contacts

The second structure needed for a complete interconnect technology is a superconducting contact. We have fabricated superconducting window contacts, that is, a superconducting connection between two YBCO films made via a window patterned in an intervening $SrTiO_3$ film (Fig. 8.1). Initially we had success fabricating window contacts using relatively thin insulating layers, 100nm or less. However, our first attempts to use thicker $SrTiO_3$ films were unsuccessful, presumably because the upper YBCO film was discontinuous at the edges of the window. Unfortunately, to make window contacts compatible with crossovers, the $SrTiO_3$ film has to be about 400nm thick. To remedy this problem, we have developed a technique for producing beveled walls in the windows in the $SrTiO_3$ layer, thereby obtaining a gently sloping surface that supports the subsequent growth of the upper YBCO film.

Our procedure for constructing a window contact is as follows. We first deposit 300nm of YBCO and pattern it with either shadow masks or photolithography and a nitric acid etch, and clean the surface with the Br etch after stripping the resist. We then typically deposit 400nm of $SrTiO_3$ (less if the bottom layer has been patterned with a shadow mask) and spin on a relatively thick (2μm) layer of photoresist which is subsequently baked at 70°C. We expose the window pattern moderately out-of-focus and develop as usual. This produces a window in the resist with gently sloping walls. We then etch using an ion mill at 600V for up to 40 min, thereby cutting through the $SrTiO_3$ in the window to expose the lower layer of YBCO. We determine when to end the mill by careful examination of the window under a microscope: too little etching leaves an insulating layer, while too much can degrade the quality of the contact. We then finish by milling at 450V for a few minutes to reduce damage to the exposed YBCO. This process leaves beveled walls in the window in the $SrTiO_3$, the steepness of the slope being determined by the relative etching rates of

the photoresist and the $SrTiO_3$ and the initial slope in the resist walls. Finally, we deposit 400nm of YBCO for the upper layer, and pattern with the ion mill or chemical etch.

We note that we do not use the Br etch after cutting the $SrTiO_3$ window because it tends to remove YBCO under the $SrTiO_3$ layer. We believe that this undercutting prevents the growth of a good superconducting connection between the upper and lower YBCO films. Despite the fact that the exposed surface of the lower layer of YBCO must be damaged by the mill, we have found it is possible to achieve good contacts, presumably because the surface damage is annealed out during the deposition of the last YBCO layer.

Figure 8.3(a) shows resistance vs. temperature for a contact, measured between the upper and lower YBCO films; the transition temperature was 87K. This contact was 9 x 15 μm^2, and the lower YBCO layer was patterned using a shadow mask while the 70nm thick $SrTiO_3$ layer and the upper YBCO layers were patterned photolithographically. Figure 3(b) shows the critical current of the contact vs. temperature, measured with a 10μV criterion; the value at 77K is 53mA. The corresponding critical current density of the 135μm^2 contact would be $4x10^4 Acm^{-2}$; however, it is almost certain that the critical current was limited by the 9μm wide YBCO film leading to the upper part of the contact, since there the current density corresponds to $1.6x10^6 Acm^{-2}$.

8.1.3 Photolithograpically Patterned Flux Transformer

In general, one would like to be able to incorporate both photolithographically patterned crossovers and window contacts in the same circuit. To demonstrate that this is possible, we fabricated thin-film flux transformers with small 10-turn input coils (see Fig. 8.4). The first layer of YBCO, 300nm thick, is patterned as shown in Fig. 8.4(a) to form a strip or "crossunder" that eventually will contact the innermost turn of the input coil. We pattern the 400nm thick $SrTiO_3$ film to produce two windows, one on each end of the crossunder, using the procedures described above. Finally, we deposit and pattern the top

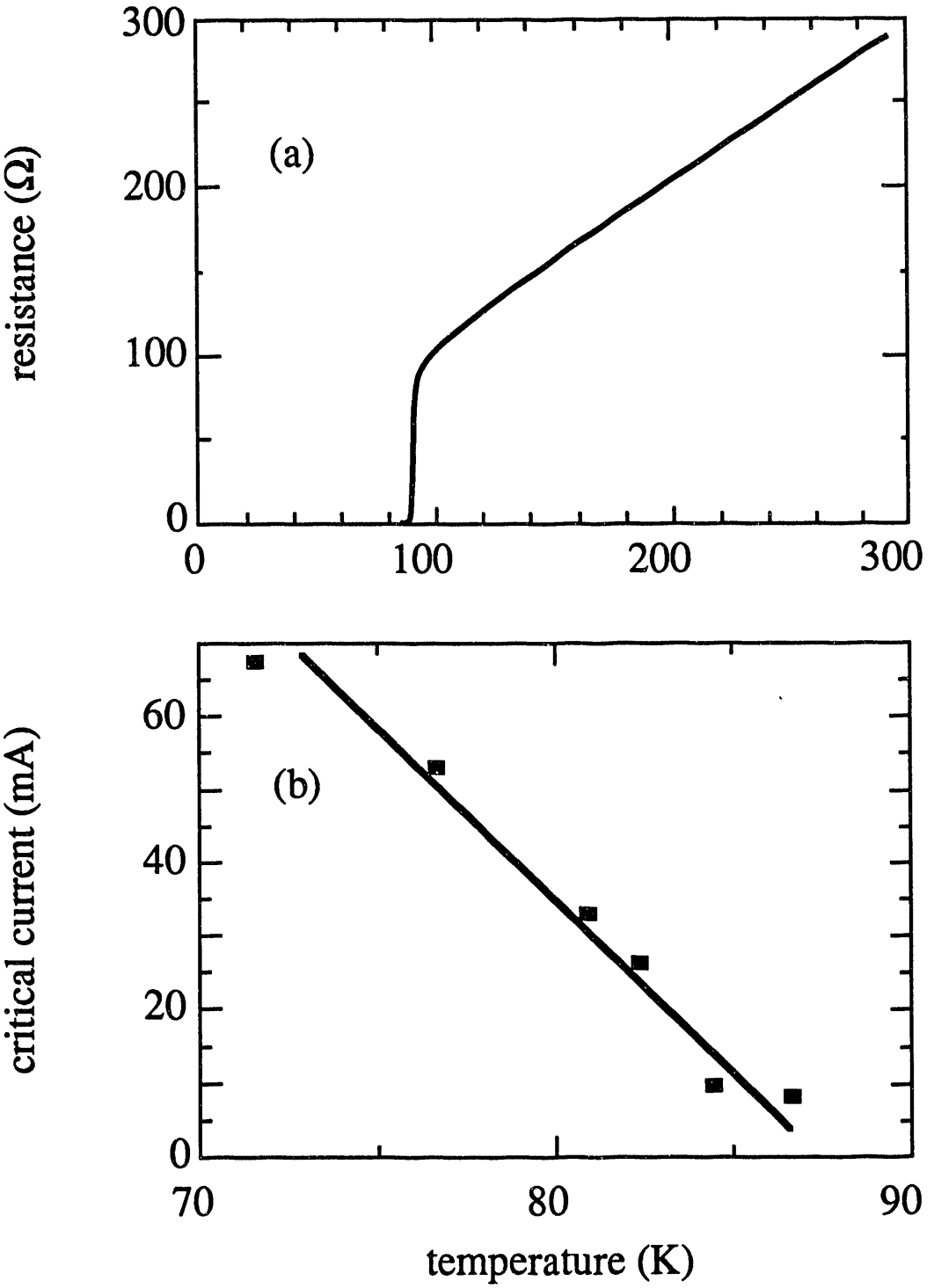

Fig. 8.3 Window contact: (a) resistance vs. temperature and (b) critical current vs. temperature. Measurements include upper and lower YBCO films plus the contact.

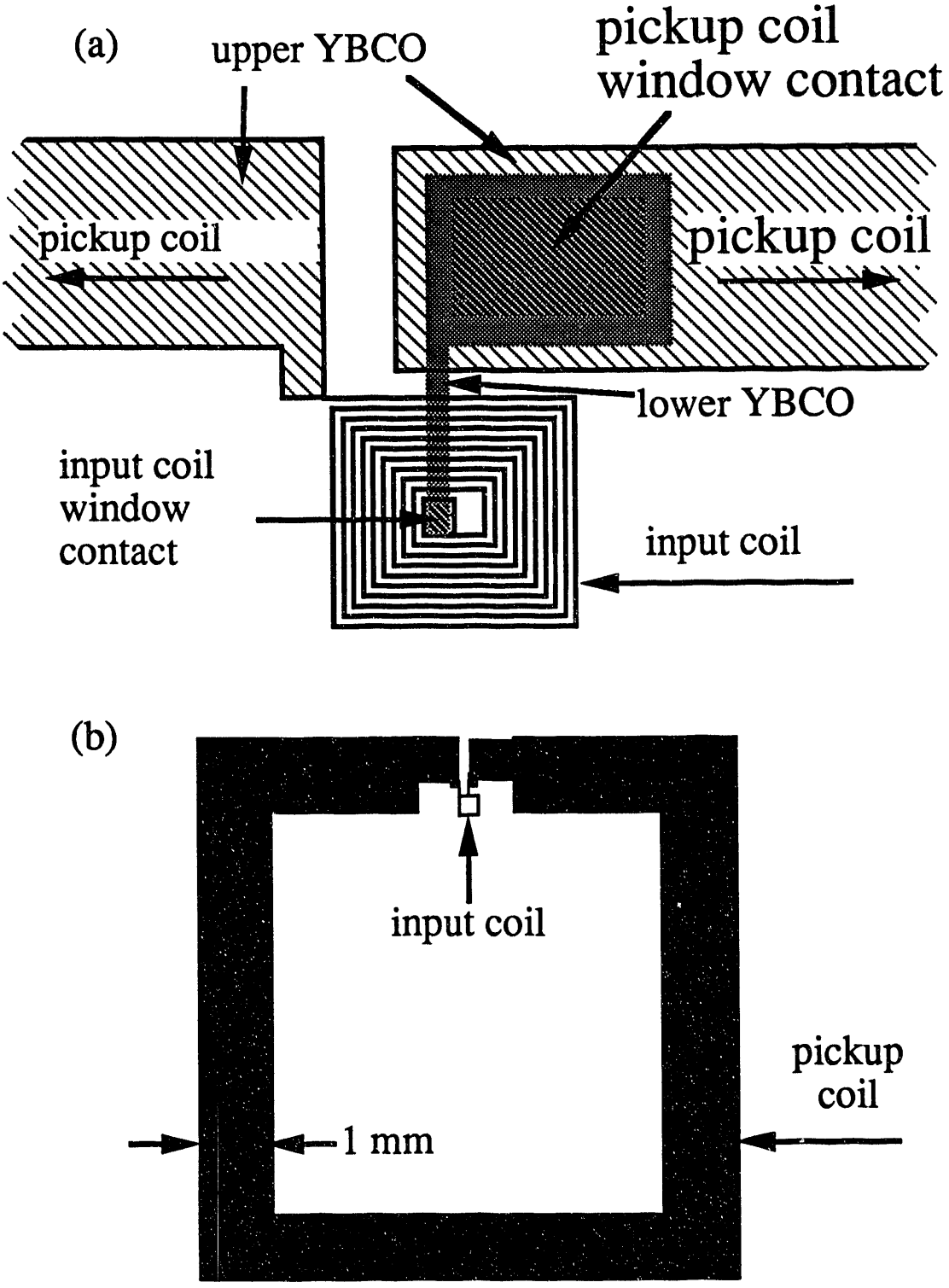

Fig. 8.4 Flux transformer: configuration of (a) input coil and connections to pickup loop, and (b) pickup loop (not to scale).

YBCO layer, which is also 400nm thick, to form the spiral input coil and the pickup loop shown in Fig. 8.4(b). The inner end of the spiral coil and the end of the pickup loop are aligned to contact the lower YBCO layer through the windows. A photograph of a completed input coil is shown in Fig. 8.5; the linewidth of the turns is 2-3μm. The smaller linewidth was due to undercutting during the acid etching of the upper layer; the same photomask yields a 6μm linewidth with ion milling.

Figures 8.6(a) and 8.6(b) show resistance and critical current vs. temperature for a transformer in which we had cut open the pickup loop. The transition temperature was 87K, and the critical current was 135μA at 82K (5μV criterion); the corresponding critical current of the 6μm-wide turns of the input coil was about $3 \times 10^4 Acm^{-2}$. We subsequently opened the innermost turn of the coil as well and measured the insulation between the lower and upper YBCO films. The resistance decreased as the temperature was lowered below T_c [Fig. 8.6(c)], possibly because of poor coverage of one or more edges of the lower YBCO layer by the $SrTiO_3$. Nonetheless, the resistance of about 60kΩ at 77K is more than adequate for this application.

In summary, we have demonstrated the fabrication of superconducting multilayer crossovers and window contacts using photolithographic patterning of each layer. Although the procedures have proved adequate, some improvements could undoubtedly be made: for example, the degree of thinning and any edge-smoothing produced by the Br etch is not very easily controlled. In addition, we should emphasize that most of the parameters such as layer thicknesses and etching times have not been optimized. Furthermore, the relatively low resistance of the insulation shown in Fig. 8.6(b) is probably due to poor edge coverage, indicating that our process needs refining. Nonetheless, our results demonstrate that it is now possible to fabricate relatively complicated superconducting interconnect structures from YBCO.

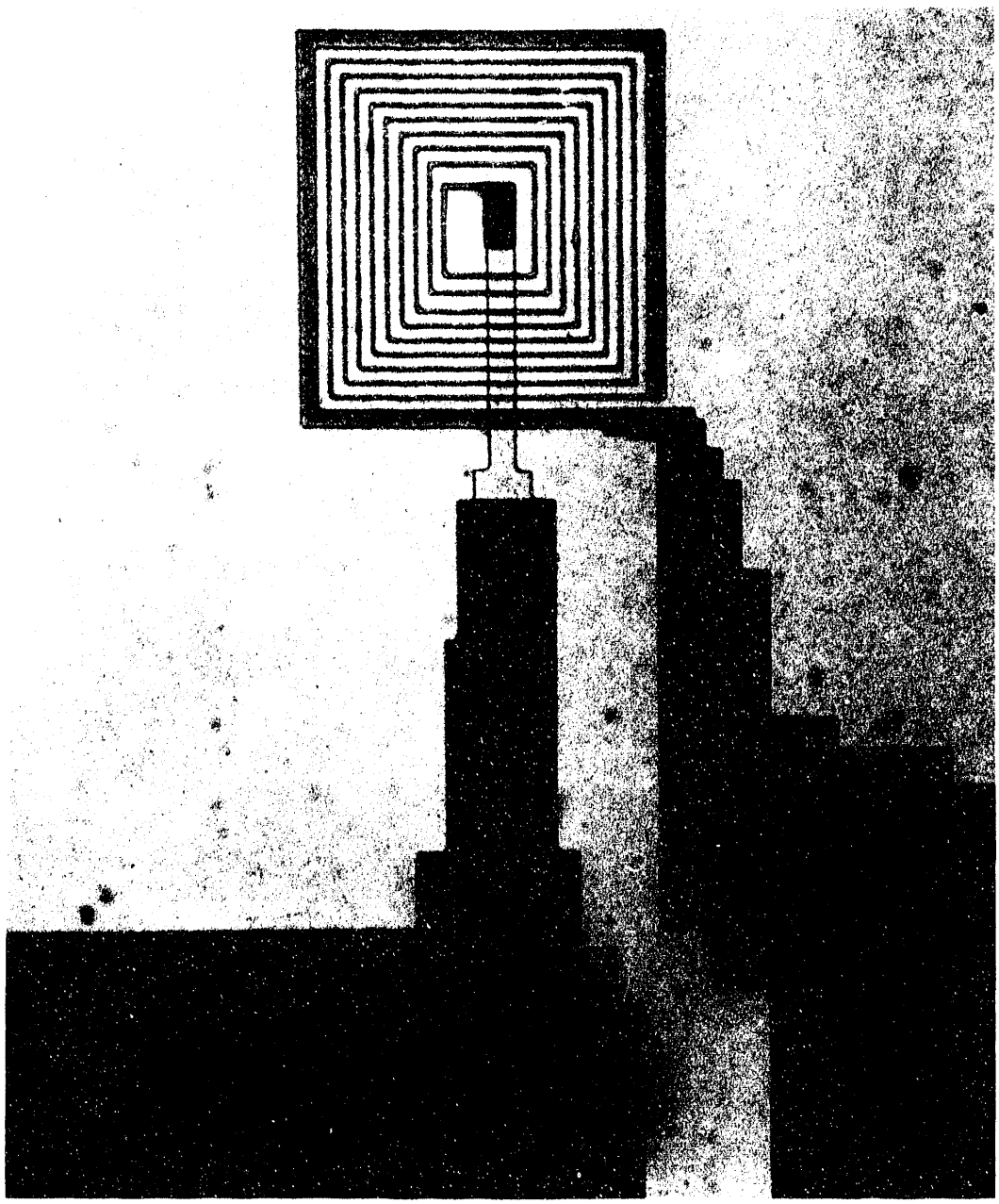

Fig. 8.5 Photomicrograph of a 10-turn input coil. Coil is 250μm on a side.

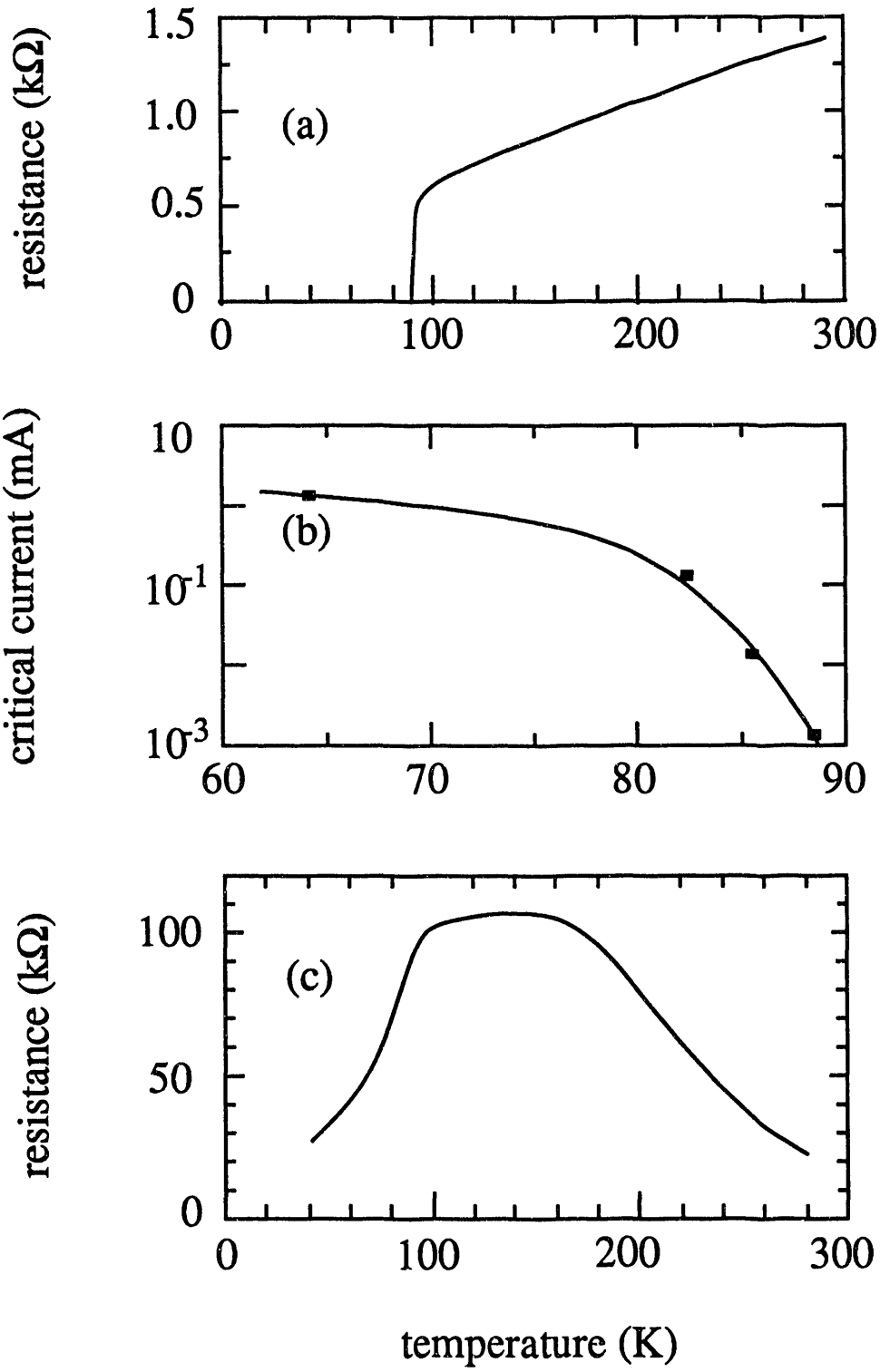

Fig. 8.6 Input coil: (a) resistance and (b) critical current of input coil vs.temperature; (c) resistance between turns of input coil and crossunder vs. temperature.

References

1. See, for example, Y. Tarutani, M. Hirano and U. Kawabe, "Niobium-based Integrated Circuit Technologies", *Proc. IEEE*, 77, 1164-1176 (1989); S. Hasuo and T. Imamura, "Digital Logic Circuits", *ibid.* 1177-1193; Y. Wada, "Josephson Memory Technology", *ibid.* 1194-1207.

2. F. C. Wellstood, J. J. Kingston and J. Clarke, "Superconducting Thin-Film Multiturn Coils of $YBa_2Cu_3O_{7-x}$", *Appl. Phys. Lett.*, **56**, 2336 (1990).

3. F. C. Wellstood, J. J. Kingston, M. J. Ferrari and John Clarke, "Superconducting Thin-Film Flux Transformers of $YBa_2Cu_3O_{7-x}$", *Appl. Phys. Lett.*, **57**, 1930 (1990).

4. See, for example, R. H. Koch, C. P. Umbach, G. J. Clark, P. Chaudhari, and R. B. Laibowitz, "Quantum Interference Devices Made from Superconducting Oxide Thin-films", *Appl. Phys. Lett.*, **51**, 200 (1987); B. Häuser, M. Diegel, and H. Rogalla," Preparation of Thin-film YBaCuO Quantum Interference Devices with a Liftoff Technique", *Appl. Phys. Lett.*, **52**, 844 (1988); H. Nakane, Y. Tarutani, T. Nishino, H. Yamada, and U. Kawabe, "DC-SQUID with High-Critical-Temperature Oxide-Superconductor Film", *Jpn. J. Appl. Phys.*, **26**, L1925 (1987); R. H. Koch, W. J. Gallagher, B. Bumble, and W. Y. Lee, "Low-noise thin-film TlBaCaCuO dc SQUIDs operated at 77K", *Appl Phys. Lett.*, **54**, 951 (1989).

5. J. J. Kingston, F. C. Wellstood, Ph. Lerch, A. H. Miklich and J. Clarke, "Multilayer $YBa_2Cu_3O_x$-$SrTiO_3$-$YBa_2Cu_3O_x$ Films for Insulating Crossovers", *Appl. Phys. Lett.*, **56**, 189 (1990).

6. R. P. Vasquez, B. D. Hunt, and M. C. Foote, "Nonaqueous chemical etch for $YBa_2Cu_3O_{7-x}$", *Appl. Phys. Lett.*, **53**, 2692 (1988)

Chapter 9

High T_c Thin-Film Magnetometer

We now describe our first magnetometer in which both the SQUID and flux transformer were fabricated from high T_c superconductors. Let us first review ideas pertinent to the design of high T_c SQUID magnetometers.

Although Superconducting QUantum Interference Devices (SQUIDs) are extremely sensitive detectors of changes in magnetic flux, planar SQUIDs made from thin films of superconductor are generally not very sensitive to changes in magnetic field. This is because the field sensitivity of the SQUID is

$$B_N^{(S)}(f) = S_\Phi^{1/2}(f) / \eta A_S, \tag{9.1}$$

where $S_\Phi^{1/2}(f)$ is the spectral density of the flux noise, A_S is the geometric area of the hole in the SQUID, and η is the flux focussing factor[1] that depends on the geometry of the device. Thus, ηA_S is the effective pickup area of the SQUID, defined as the flux coupled per unit applied magnetic field. The inductance of a square hole of side d in a large film is given approximately by[2] $L = 1.25\mu_0 d$. For use as a SQUID there is an upper bound on L imposed by the requirement that thermal fluctuations in the flux be much less than $\Phi_0/2$, where $\Phi_0 = h/2e$ is the flux quantum. As a result, the inner dimensions of most high-T_C thin-film SQUIDs[3] are not much more than 50x50 μm^2. To achieve useful sensitivities to magnetic field, all such devices require a superconducting flux transformer[4].

A flux transformer consists of a pickup coil of inductance L_p connected to an input coil of inductance L_i which is inductively coupled to the SQUID of inductance L (see Fig. 9.1). The pickup coil often consists of a single turn, while the input coil usually has many turns. Any magnetic flux, Φ, applied to the pickup coil induces a supercurrent in the transformer and hence a flux in the SQUID given by

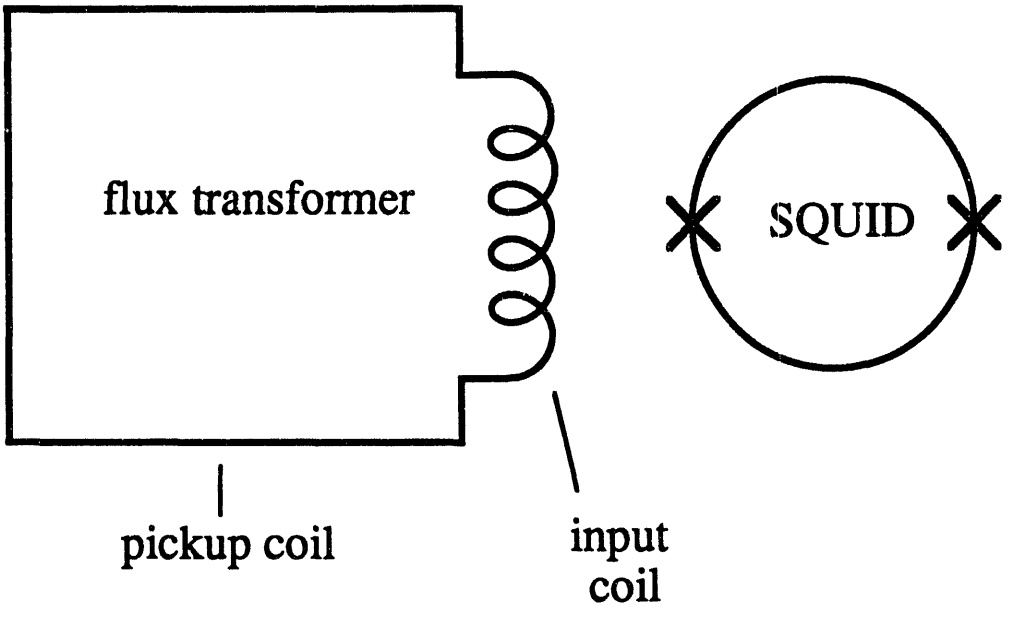

Fig. 9.1 Schematic of a flux transformer coupled to a SQUID.

$$\Phi^{(S)} = -\frac{M_i}{L_i + L_p}\Phi, \qquad (9.2)$$

where $M_i = \alpha(L_i L)^{1/2}$ is the mutual inductance between the input coil and the SQUID, and α is the associated coupling coefficient. The minus sign arises because on the transformers we fabricated we chose the winding of the input coil to be such that in a uniform applied field the flux coupled to the SQUID by the flux transformer is of *opposite sign* to that linking the SQUID directly. This gives us an unequivocal signal that the flux transformer is functioning.

We can express the magnetic field gain, G, of the flux transformer as the ratio of the magnetometer effective area, A_M, to the SQUID effective area, ηA_S:

$$G = \frac{A_M}{\eta A_S} = 1 - \frac{A_p}{\eta A_S}\frac{\alpha(L_i L)^{1/2}}{L_i + L_p}. \qquad (9.3)$$

Here, A_p is the area of the pickup loop. Assuming that the flux transformer itself contributes no noise, we can write the magnetic field sensitivity of the magnetometer as

$$B_N(f) = B_N^{(S)}(f) / |G|. \qquad (9.4)$$

We note that when the flux transformer is functioning and well coupled to the SQUID the second term in Eq. 9.3 dominates and the measured gain is negative.

The dc SQUID we used was fabricated by Superconductor Technologies, Inc. by wet etching a 500 nm thick film of $Tl_2CaBa_2Cu_2O_{8+y}$ (TCBCO) grown on a MgO substrate by laser ablation and post annealing[5]. Before the film was patterned, the transition temperature, determined by magnetic susceptibility, was 103.4 K. The inner hole of the SQUID is a 20×80 μm^2 rectangle, and has two small bridges a few microns wide which contain native grain boundary weak-links (Fig. 9.2). At liquid nitrogen temperatures the noise rounded critical current of the SQUID was 1-2 μA, and the dynamic resistance about 3.8 Ω. The application of a magnetic field to the bare SQUID modulated the critical current with a period corresponding to an effective pickup area of 4.4×10^4 μm^2. This area is about 27 times greater than the geometrical area of the loop; we attribute

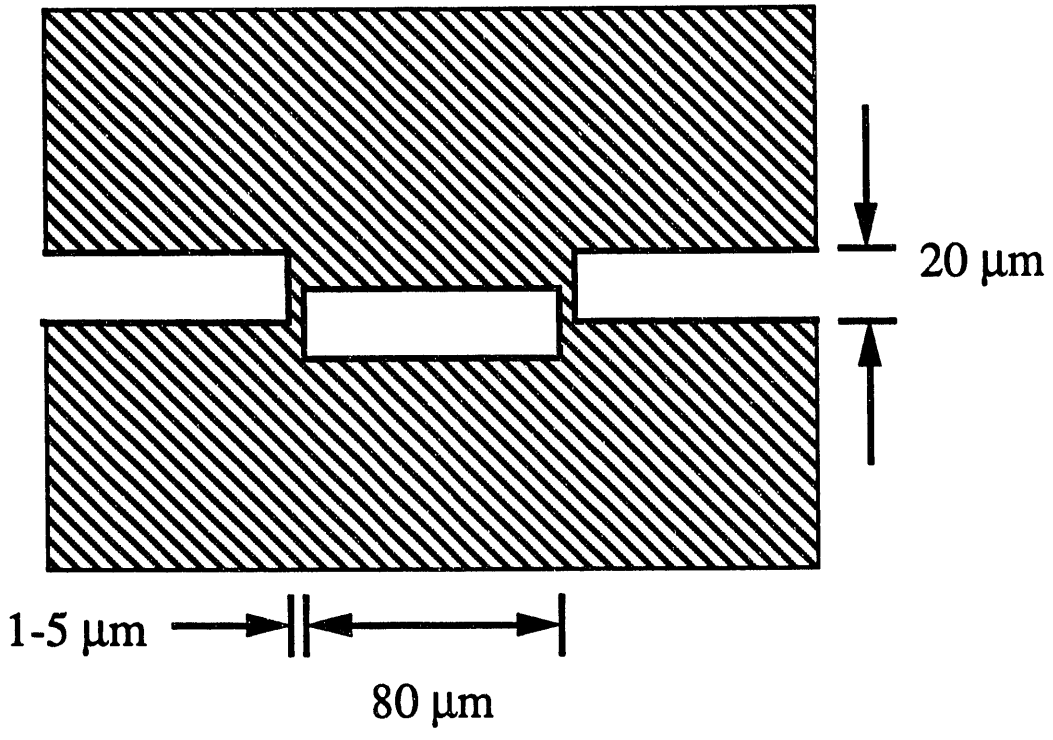

Fig. 9.2 Schematic of SQUID design drawn roughly to scale. The shaded areas are superconductor (which extends beyond the edges of the drawing), the clear areas have been etched away. The SQUID loop is the central rectangle, weak links are formed by native grain boundaries in the narrow bridges on either side

this large flux focussing factor to the large rectangles of superconductor used to provide contacts to the SQUID.

To measure its noise as a function of temperature, we mounted the SQUID on a probe that we could position at a variable height above the surface of liquid helium in a dewar. The end of the probe was surrounded with a thin tube of CO-NETIC brand high-μ metallic foil, a solid copper can, and a further layer of μ-metal, and the cryostat was operated inside an rf shielded room. At low frequencies, this arrangement screened external magnetic fields by a factor of 100. The SQUID was operated in a flux-locked loop, with a flux modulation frequency of 100 kHz. The voltage across the SQUID was amplified by a cooled transformer of turns ratio 1:15 wound from copper wire.

A representative flux noise power spectrum of the SQUID at 55 K is shown in Fig. 9.3. The two noise spikes are due to external noise sources, and demonstrate that the shielding is somewhat inadequate. At low frequencies (< 10 Hz), the noise power is steeper than 1/f (where f is the frequency), and probably arises from a number of sources including external noise and drifts in temperature and ambient magnetic field during the period of the measurement. At 10 Hz, the rms noise is $S_\Phi^{1/2}$ (10 Hz) $\approx$ $7.0 \times 10^{-4}\ \Phi_0\ \mathrm{Hz}^{-1/2}$, while in the white noise region the noise drops to $S_\Phi^{1/2}$ (100 Hz) $\approx 4.5 \times 10^{-4}\ \Phi_0\ \mathrm{Hz}^{-1/2}$. The latter flux noise corresponds to a magnetic field sensitivity of about 21 pT $\mathrm{Hz}^{-1/2}$. These noise levels are appreciably higher than those for the quietest TCBCO SQUID yet reported[6].

We have successfully coupled the SQUID to two $YBa_2Cu_3O_{7-x}$ (YBCO) flux transformers, each with a 10-turn input coil. Each transformer was deposited on a 12.5×12.5×0.75 mm^3 MgO substrate. The first, which we refer to as the "large" transformer, had an input coil of 1×1 mm^2, while the second, the "small" transformer, had an input coil of 250×250 μm^2. The relevant parameters of the two transformers are listed in Tab. 9.1. The multiturn geometry of the transformers necessitated the use of multilayer technologies that have been described elsewhere[7]. The first layer is a strip, or

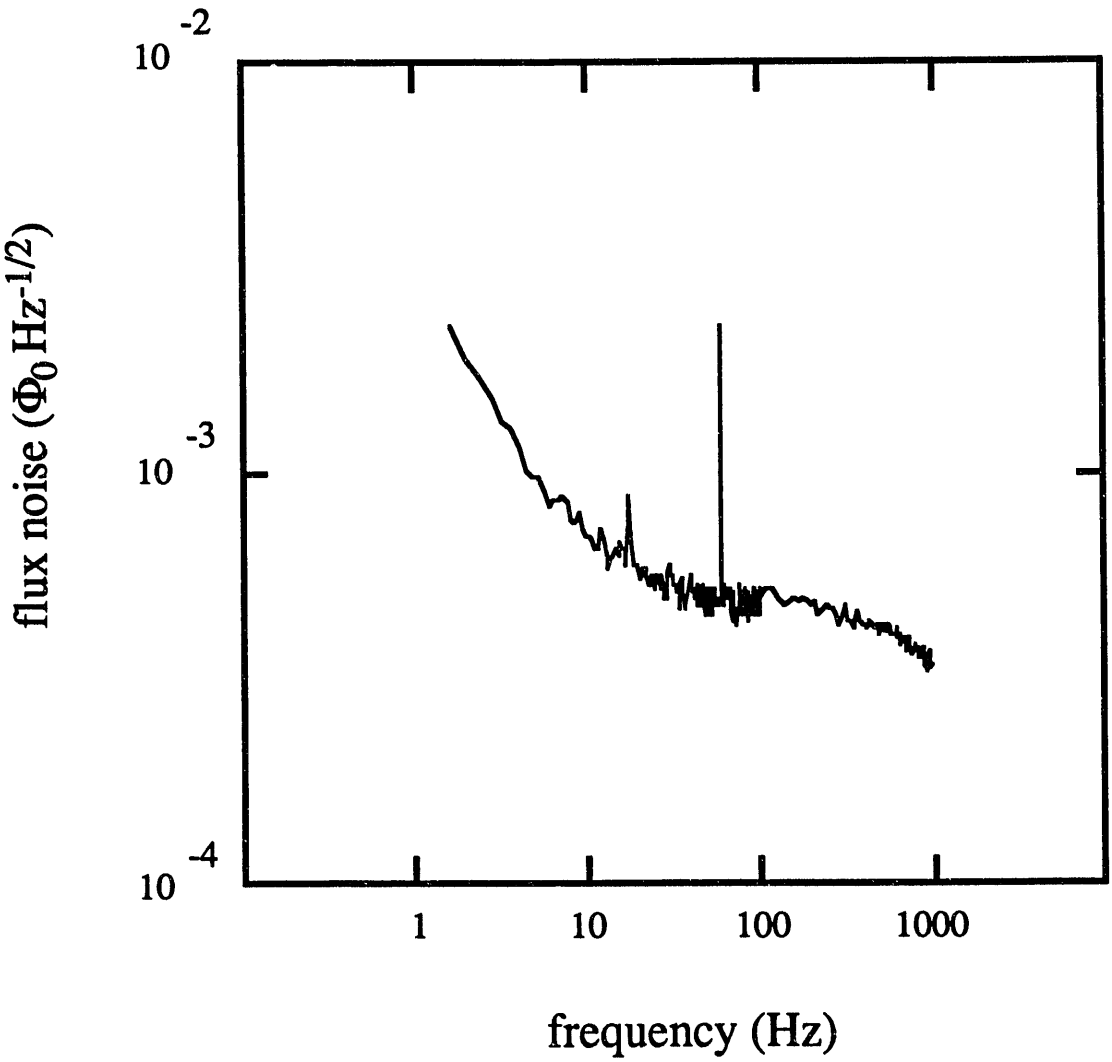

Fig. 9.3 Flux noise $S_\Phi^{1/2}(f)$, of the SQUID without a flux transformer. The data were taken at T = 55K. The measured bandwidth of the flux-locked SQUID was ~ 1kHz.

"crossunder", of YBCO that eventually connects the innermost turn of the spiral input coil to one side of the pickup loop. The second layer is $SrTiO_3$ which insulates the crossunder from the turns of the input coil. The third layer is YBCO, which is patterned to form both the input coil and the pickup loop; it is essential that this layer makes a superconducting contact to each end of the YBCO crossunder. In the case of the large transformer, the first two layers were patterned with shadow masks and the third was patterned photolithographically[8]. For the small transformer, all three layers were patterned photolithographically[9].

Table 1. Flux Transformer Parameters

Parameter	Small Transformer	Large Transformer
Number of Turns on Input Coil	10	10
Linewidth of Input Coil	~ 5 μm†	20 μm
Input Coil Inductance (L_i)*	~ 50 nH	~ 75 nH
Pickup Coil Inductance (L_p)*	~ 20 nH	~ 20 nH
Area of Pickup Coil (A_p)	81 mm^2	70 mm^2

†The lines were set on a 10 μm pitch.

*Estimate based on geometry of the uncoupled coils.

We coupled each flux transformer in turn to the SQUID by pressing the two chips together face-to-face in a flip-chip arrangement. A thin (~ 3 μm) sheet of mylar was placed between the two chips to provide electrical insulation and to prevent scratching, and the two chips were tied together and secured to the probe with nylon twine. By observing the two chips through a microscope with bright transmitted light, we were able to align the centers of the input coil and the SQUID to within 20 μm.

In Fig. 9.4 we show the measured low frequency gain of our two magnetometers vs. temperature. From Eq. 9.3, using the estimated values of L_i and Lp, we used the measured gains to estimate the coefficient α. The maximum gains of the large and small transformers at 4.2 K were -7.5 and -8.7, respectively, and the corresponding values of α were 0.23 and 0.21. The large transformer operated at temperatures up to 79 K, while the small one operated up to only 25 K. It should be noted here, however, that inaccuracies in the calibration of the coil with which we apply the magnetic field to the transformer may have caused us to overestimate the above gains by as much as 30%.

The failure of the small transformer to operate at zero frequency above 25 K is somewhat puzzling, particularly in view of measurements[9] of the transport properties of a second small transformer made by the same process. In this transformer we opened the pickup loop and found that the resistive transition, as measured by a transport current with a voltage resolution of 5 μV, was about 85 K. However, those measurements are not capable of detecting a resistance smaller than 5 mΩ. While the first small transformer did not operate above 25 K at zero frequency, at 26 K it did display a gain for alternating fields with the low frequency rolloff occurring at about 1 kHz. From this frequency and the estimated inductance of the transformer we deduce a series resistance of about 0.4 mΩ, a value too small to have been observed in transport measurements. Since the transformer has a normal state resistance of about 600 Ω at 90 K, this small resistance is probably due to a highly localized failure. Thus, we believe the integrity of most of the transformer was maintained to a very much higher temperature than 25 K. The fact that the transformer exhibited large gain demonstrates that the turns of the input coil were indeed electrically isolated from the crossunder.

In Fig. 9.5 we show the measured power spectra of the magnetic field sensitivity of the two magnetometers. The increase in the magnitude of the spikes compared with those in Fig. 9.3 indicates the higher sensitivity to environmental noise. The noise levels with the large transformer at 38 K were about 3.1 pT $Hz^{-1/2}$ at 10 Hz and 0.34 pT $Hz^{-1/2}$ at 1

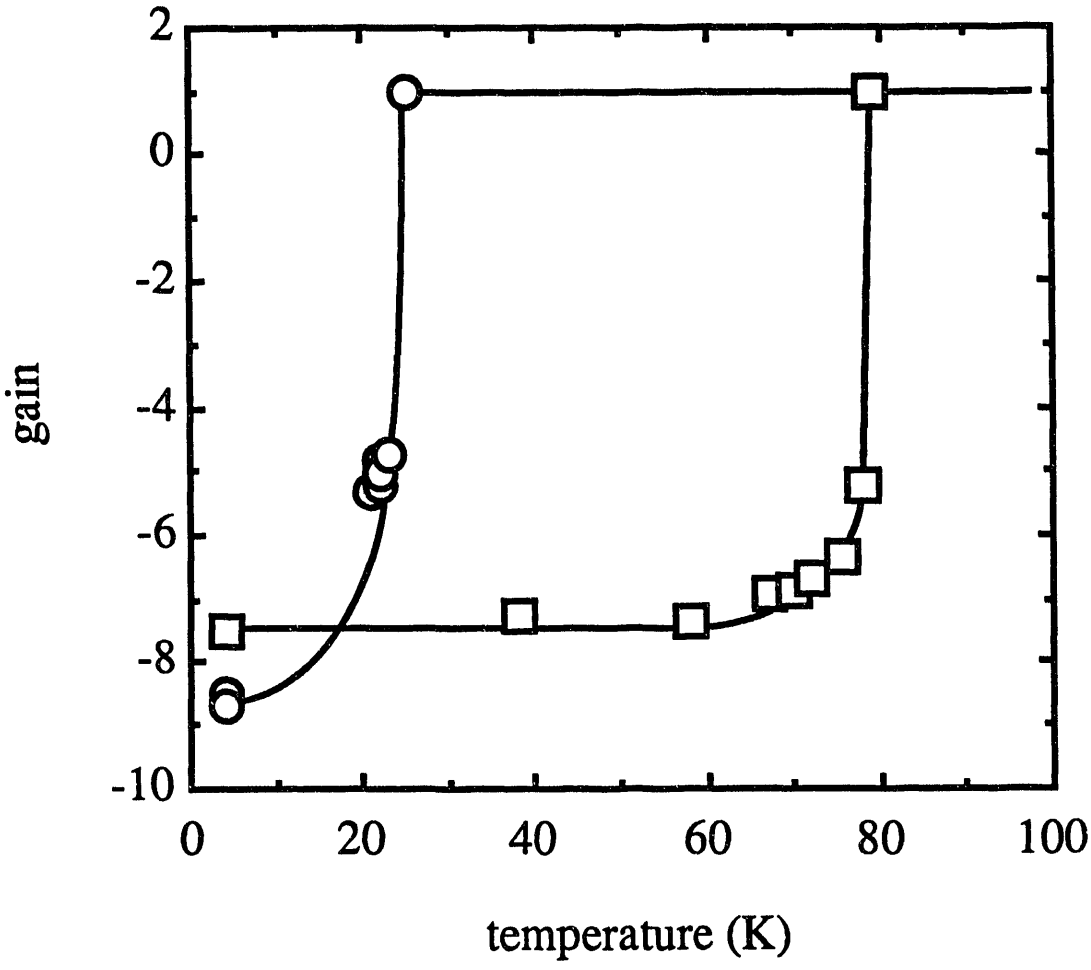

Fig. 9.4 Measured gain, G, of magnetometer (ratio of the magnetometer effective area to the SQUID effective area) vs. temperature. Circles are for the small flux transformer, squares are for the large transformer. The solid lines are guides for the eye. Note that when the flux transformer is operating, the gain is negative because of the sense of the input coil.

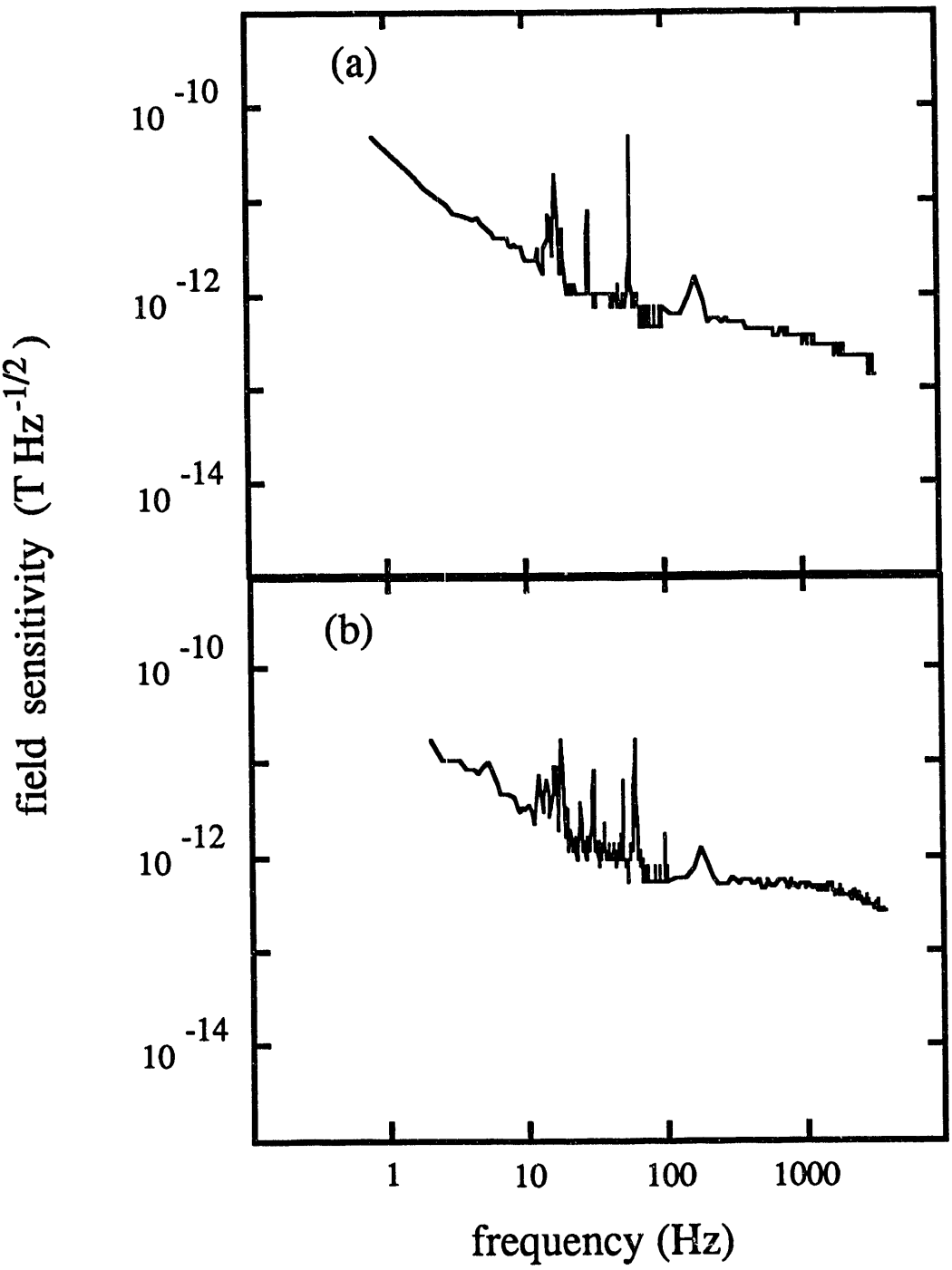

Fig. 9.5 Field sensitivities $B_N(f)$ of the magnetometer with (a) large flux transformer at 38K and (b) small transformer at 4.2K. The measured flux-locked bandwidths were ~ 3.5kHz and 3.8kHz respectively.

kHz. The magnetometer with the small transformer at 4.2 K exhibited very similar values, about 3.5 pT $Hz^{-1/2}$ at 10 Hz and 0.35 pT $Hz^{-1/2}$ at 1 kHz. In both cases, the magnetic field sensitivity was limited by the flux noise in the SQUID. Separate measurements[10] on the large transformer at 60 K with a Nb/PbIn SQUID yielded a magnetic field sensitivity of 0.3 pT $Hz^{-1/2}$ at 10 Hz that was determined to be limited by intrinsic noise in the flux transformer. Thus, a quieter high-T_c SQUID would give an improvement in the magnetic field sensitivity. At this point, we have no measurements with a low-T_c SQUID coupled to the small transformer.

We have successfully constructed two high-T_c magnetometers by coupling high-T_c flux transformers with multiturn input coils to a high-T_c dc SQUID. The large transformer was operated successfully at temperatures up to 79 K, while the small transformer ceased to operate at 25 K, due to a localized failure in its structure. The coupling coefficients between the input coils and the SQUID, in the range 0.2 - 0.25, are lower than desirable and imply that the two chips need to be brought closer together. A reduced spacing would enhance the gain and hence the magnetic field resolution in two ways, one by increasing α, and the other by reducing the inductance L_i of the input coil by means of screening (see Eq. 9.3). The measured gains of the large and small transformers were about -7.5 and -8.7, respectively. We note that these values would have been larger if the body of the SQUID had been narrower and, thus, the flux focussing factor η smaller; however, the overall magnetic field sensitivity of the transformers would not have been very different. The magnetic field noise levels measured in the large transformer at 38 K and in the small transformer at 4.2 K were virtually the same, about 3pT $Hz^{-1/2}$ at 10 Hz and 0.35pT $Hz^{-1/2}$ at 1 kHz.

References

1. M. B. Ketchen, W. J. Gallagher, A. W. Kleinsassar, S. Murphy and J. R. Clem, "dc SQUID flux focuser", in *SQUID '85*, H. D. Hahlbohm and H. Lübbig, Eds., Walter de Gruyter, Berlin (1985).

2. J. M. Jaycox and M. B. Ketchen, "Planar coupling scheme for ultra low noise dc SQUIDs", *IEEE Trans. Mag.*, **17**, 400-403 (1981).

3. See for example: R. B. Laibowitz, R. H. Koch, A. Gupta, G. Koren, W. J. Gallagher, V. Foglietti, B. Oh and J. M. Viggiano, "All high T_C edge junctions and SQUIDs", *Appl. Phys. Lett.*, **56**, 686-688 (1990); D. W. Face, J. M. Graybeal, T. P. Orlando and D. A. Rudman, "Noise and dc characteristics of thin-film Bi-Sr-Ca-Cu-oxide dc SQUIDs", *Appl. Phys. Lett.*, **56**, 1493-1495 (1990); B. Häuser, M. Diegel and H. Rogalla, *Appl. Phys. Lett.*, **52**, 844-846 (1988); H. Nakane, Y. Tarutani, T. Nishino, H. Yamada and U. Kawabe, "dc-SQUID with high-critical-temperature oxide-superconductor film", *Jap. J. Appl. Phys.*, **26**, L1925-L1926 (1987).

4. J. E. Zimmerman and N. V. Frederick, "Miniature ultrasensitive superconducting magnetic gradiometer and its use in cardiography and other applications", *Appl. Phys. Lett.*, **19**, 16-19 (1971).

5. L. C. Bourne, R. B. Hammond, McD. Robinson, M. M. Eddy, W. L. Olson and T. W. James, "Low-loss microstrip delay line in $Tl_2Ba_2CaCu_2O_8$", *Appl. Phys. Lett.*, **56**, 2333-2335 (1990); W. L. Olson, M. M. Eddy, T. W. James and R. B. Hammond, "Preparation of superconducting Tl-Ca-Ba-Cu thin films by chemical deposition", *Appl. Phys. Lett.*, **55**, 188-190 (1989).

6. R. H. Koch, W. J. Gallagher, B. Bumble and W. Y. Lee, "Low-noise thin film TlBaCaCuO dc SQUIDs operated at 77 K", *Appl. Phys. Lett.*, **54**, 951-953 (1989).

7. J. J. Kingston, F. C. Wellstood, P. Lerch, A. H. Miklich and J. Clarke, "Multilayer $YBa_2Cu_3O_x$ films for insulating crossovers", *Appl. Phys. Lett.*, **56**, 189-191 (1990).

8. F. C. Wellstood, J. J. Kingston, M. J. Ferrari and J. Clarke, "Superconducting thin-film flux transformers of $YBa_2Cu_3O_{7-x}$", *Appl. Phys. Lett.*, **57**, 1930 (1990).

9. J. J. Kingston, F. C. Wellstood, D. Quan and J. Clarke, "Photolithographically patterned thin-film multilayer devices of $YBa_2Cu_3O_{7-x}$", Proceedings of the 1990 Applied Superconductivity Conference, *IEEE Trans. Mag.*, **27**, (1991).

10. M. J. Ferrari, J. J. Kingston, F. C. Wellstood and J. Clarke, "Flux noise from superconducting $YBa_2Cu_3O_{7-x}$ flux transformers", *Appl. Phys. Lett.*, **58**, 1106 (1991).

Chapter 10

Sensitive $YBa_2Cu_3O_{7-x}$ Thin-Film Magnetometer

We now describe a high-T_c magnetometer operating at temperatures up to 81K with a magnetic field sensitivity substantially higher than any previously reported. The dc SQUID involves a bi-epitaxial junction process[1], and all layers of the flux transformer are patterned photolithographically.[2]

The configuration of the SQUID, which was fabricated at Conductus Inc., is shown in Fig. 10.1(a). The fabrication procedure, which has been described in detail elsewhere,[1] is briefly as follows. We laser-deposit a 10nm thick seed layer of epitaxial MgO on an r-plane sapphire substrate, and remove it from part of the substrate by photolithographic patterning and Ar ion milling or acid etching. Subsequently, we laser deposit a 10nm thick epitaxial $SrTiO_3$ buffer layer; this film grows epitaxially on both the sapphire and the patterned MgO, but with orientations which are separated by a single 45° grain boundary located at the edge of the MgO. Without breaking vacuum, we deposit a 200-nm thick $YBa_2Cu_3O_{7-x}$ (YBCO) film which grows epitaxially on the $SrTiO_3$, thus replicating the grain boundary. Finally, we use photolithography and an acid etch to pattern the YBCO film into the geometry shown in Fig. 10.1(a).

The current-voltage (I-V) characteristics of the SQUID are close to the predictions of the resistively shunted junction model,[3] although we do observe some structure. The I_oR product is typically 0.2mV at 4.2K, where I_o and R are the critical current and asymptotic resistance of each junction. We have observed operation of the device as a dc SQUID at temperatures up to 88K, and operated it in a flux-locked loop at temperatures up to 83K. We estimate the inductance L of the SQUID to be 110pH, and the resistance (R/2)

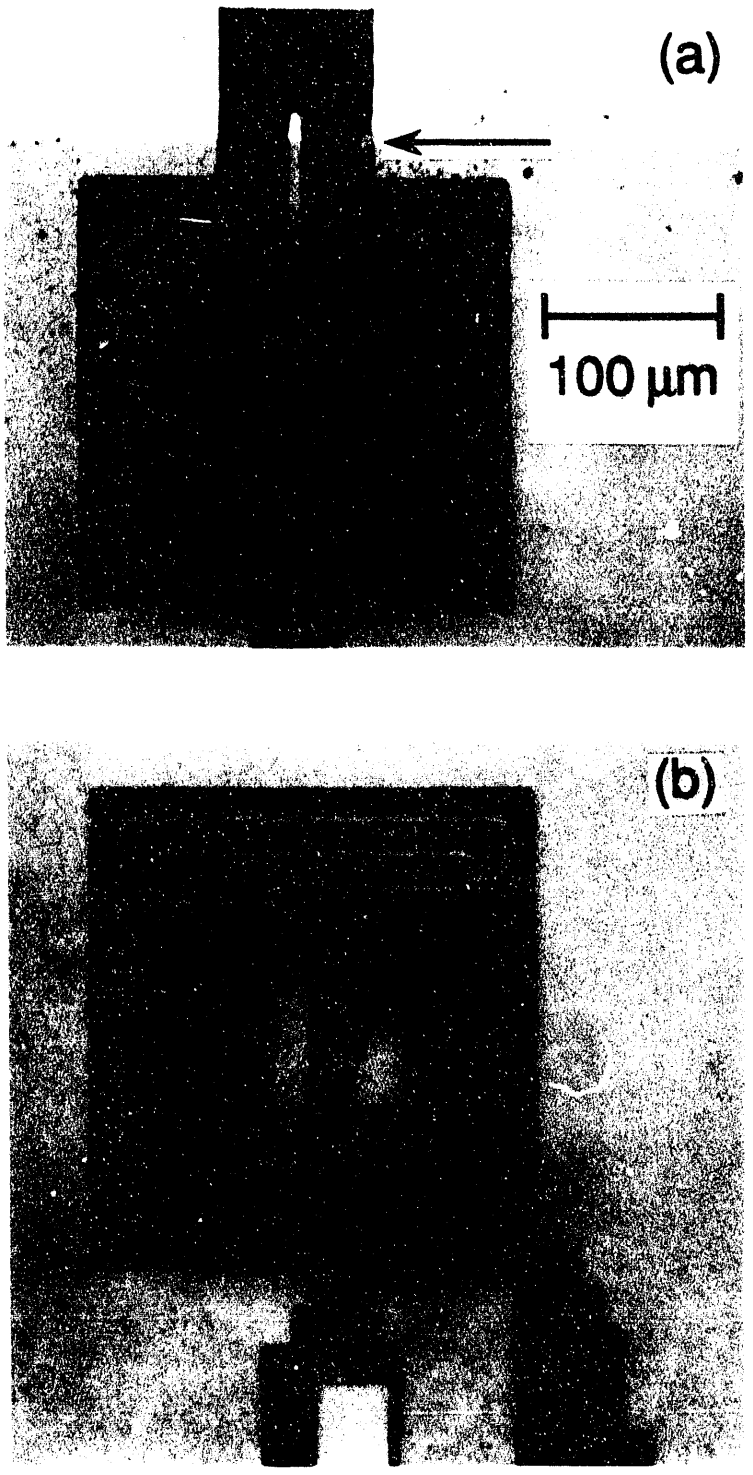

Fig. 10.1 (a) Photograph of YBCO SQUID. The two bi-epitaxial junctions are on the upper side of the square washer on the line (arrow) demarcating the edge of the MgO seed layer. (b) Photograph of 5-turn spiral input coil. The two leads at the lower edge of the figure connect to the single-turn pick-up loop.

is approximately 4Ω. By determining the magnetic field (perpendicular to the SQUID) required to induce one flux quantum, we estimated the effective pick-up area A_s to be 12,000μm^2; this value exceeds the geometrical area of the hole and slit by a factor of 6, and is due to focussing of the flux by the body of the SQUID.[4]

We fabricate the flux transformer [Fig. 10.1(b)] on an MgO substrate following a variation on procedures described earlier.[5] We first laser deposit a 300nm thick film of YBCO and pattern it to form the crossunder, the line that will connect the inner-turn of the input coil to the pick-up loop, using photolithography and a 0.1% nitric acid etch. After stripping the resist, we immerse the sample in a 1% solution of Br in methanol to etch clean the surface of the YBCO film. In the second step, we deposit 450nm of $SrTiO_3$ and open two windows, one at the inner end of the crossunder and a second at the outer end [see Fig. 10.1(b)]. After patterning the windows in the $SrTiO_3$ with photoresist, we etch with an Ar ion mill at an angle of 30° to the substrate; this procedure produces an edge along one side of the window beveled at about 8° to the substrate. We also allow the ion mill to remove roughly 100nm of the YBCO in the window, to ensure that no $SrTiO_3$ remains and to enable the two YBCO films to make contact both in the ab-plane and along the c-axis. Ion milling at an angle yields an optically smooth contact surface and allows the top layer of YBCO to grow in a highly oriented manner on the flat surfaces of YBCO and $SrTiO_3$ as well as on the beveled $SrTiO_3$ edge. The upper layer of YBCO is subsequently patterned with photolithography and the acid etch to produce the five-turn coil, shown in Fig. 10.1(b), and the single-turn pick-up loop (not shown) which is approximately 10mm across and has a pick-up area A_p of 81mm^2. We have deliberately broadened the linewidth of the turns of the input coil (to 11μm) compared with our earlier transformers[5,6] in an attempt to improve the coupling efficiency to the SQUID. We estimate the inductance of the pick-up loop, L_p, to be about 20nH. It is more difficult to estimate the inductance of the input coil, L_i, because of the uncertainty in the separation between the coil and the

SQUID and hence in the reduction in L_i by screening. If we assume that this separation is rather less than the width of the turns, we estimate $L_i \approx 1.5$nH.

To assemble the magnetometer, we carefully aligned the SQUID over the input coil and clamped them together with a 3μm-thick mylar sheet between them. The magnetometer was mounted on a variable temperature insert in a liquid ^{4}He dewar surrounded by a mu-metal shield; in some experiments, we immersed the magnetometer directly in liquid N_2. We determined the critical current of the flux transformer by applying an increasing magnetic field and noting the field at which the period of the oscillations in the SQUID voltage abruptly changed. At this point, the transformer evidently entered a critical state and further increases in the magnetic field produced no increase in the induced supercurrent. Using these measurements, we infer the critical current from the area of the pick-up loop and the estimated value of the transformer inductance. The critical current is plotted as a function of temperature in Fig. 10.2, and, for magnetometer applications, is entirely adequate for temperatures up to at least 86K. At 77K, the critical current density referred to the cross-sectional area of the turns of the input coil is about 5×10^4 Acm^{-2}. Separate transport measurements on window contacts alone indicated that their critical current density, referred to the cross-sectional area of the upper YBCO strip, can be over 10^6Acm^{-2} at 77K. Thus, we believe the critical current density is limited by the steps in the upper YBCO film that occur where the $SrTiO_3$ crosses the edges of the lower YBCO film. We define the gain g of the transformer as the factor by which the flux transformer increases the magnetic field response over that of the SQUID alone. We deliberately chose the sense of the windings of our transformers to produce a flux in the SQUID opposite in sign to the direct flux; hence g is negative. It is straightforward to show that

$$g = 1 - \frac{A_p}{A_s} \frac{M_i}{L_i + L_p}, \qquad (10.1)$$

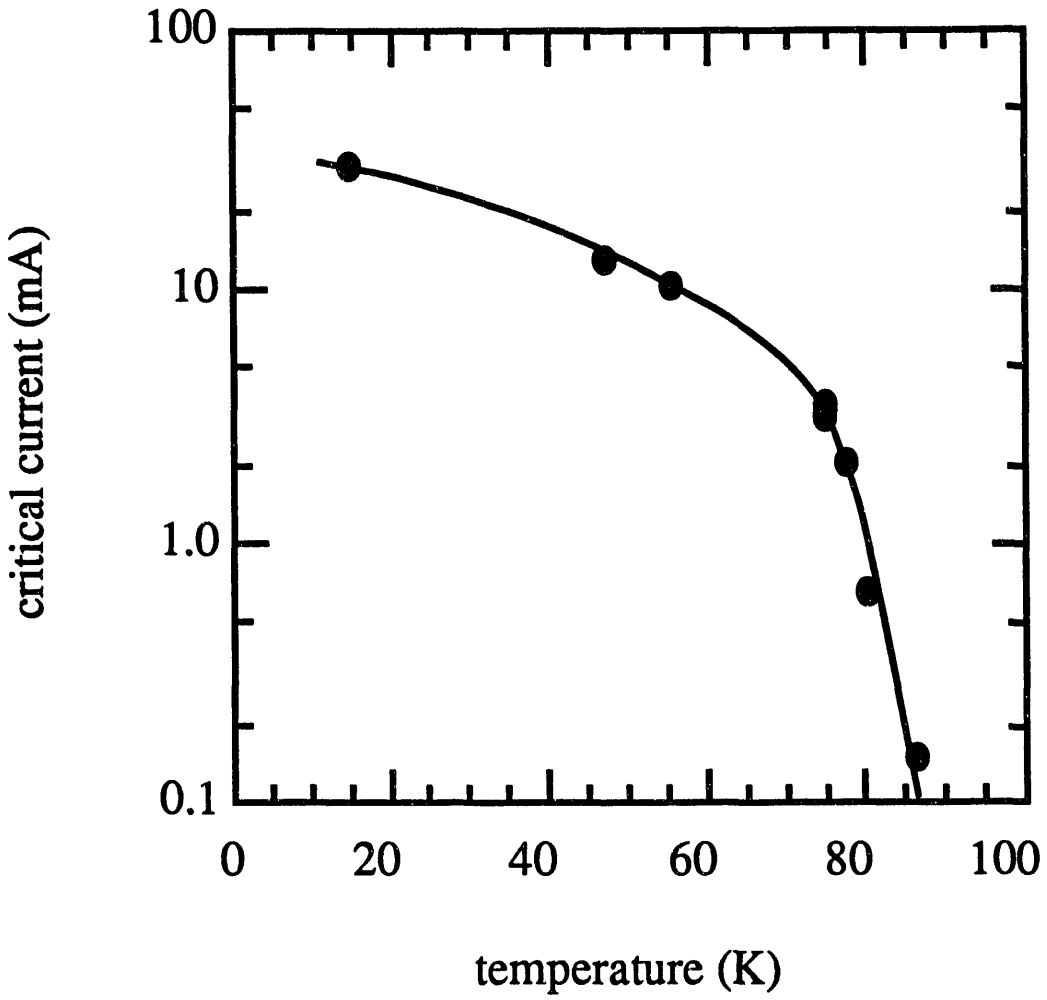

Fig. 10.2 Critical current of flux transformer vs. temperature. Line is guide to the eye.

where the mutual inductance $M_i = \alpha(LL_i)^{1/2}$, and we have neglected the area of the input coil compared to that of the pick-up coil. The measured gain, shown in Fig. 10.3, is -83±3 over the temperature range 4.2K to 80K. Taking the values $A_p = 81mm^2$, $A_s = 1.2 \times 10^{-2}mm^2$, $L_p = 20nH$ and assuming $L_i << L_p$, we find from Eq. (10.1) $M_i = 0.25 \pm 0.01nH$. If we take $L_i = 1.5nH$, this value of M_i corresponds to $\alpha \approx 0.6$.

We have measured the magnetic field sensitivity of the magnetometer by flux-modulating the SQUID at 100kHz and operating it in a flux-locked loop. The alternating voltage across the SQUID was amplified by a cooled transformer. Figure 10.4(a) shows the rms magnetic field noise, $S_B^{1/2}(f)$, vs. frequency when the magnetometer is immersed in liquid ^4He and in liquid N_2. At 4.2K, the spectral density scales approximately as 1/f from a few Hz to several kHz. AT 77K, the noise begins to flatten off above 200Hz, indicating that white noise is beginning to dominate in this frequency range. However, at lower frequencies, the rms noise has increased over that at 4.2K by only a factor of 2. The magnitude of the noise at 77K is $S_B^{1/2}(10Hz) = 0.6pT\ Hz^{-1/2}$ and $S_B^{1/2}(1kHz) = 0.09pT\ Hz^{-1/2}$. At both 4.2K and 77K, the measured flux noise $S_B^{1/2}(f)$ in the SQUID is very close to that observed in the magnetometer [right-hand axis of Fig. 10.4(a)], implying that the noise contribution of the transformer is negligible at both temperatures.

We have also measured the temperature dependence of the noise of our magnetometer cooled by ^4He gas. Figure 10.4(b) shows an example of the observed noise at 68K. The noise is about a factor of two lower than that at 77K in Fig. 10.4(a); thus, $S_B^{1/2}(10Hz) = 0.35pT\ Hz^{-1/2}$ and $S_B^{1/2}(1kHz) = 0.05pT\ Hz^{-1/2}$. We believe these are the lowest values yet reported for a high-T_c thin-film magnetometer. We note that the noise energy of the SQUID, $S_\Phi/2L$, is about $5 \times 10^{-30}JHz^{-1}$ at 3kHz.

Modest improvements in sensitivity, say by a factor of 2 to 3, can probably be achieved by increasing the number of turns on the input coil so that $L_i \approx L_p$, and by increasing the coupling coefficient α. Further improvements can be achieved by increasing the size of the pick-up loop; provided one maintains $L_i \approx L_p$, the magnetic field sensitivity

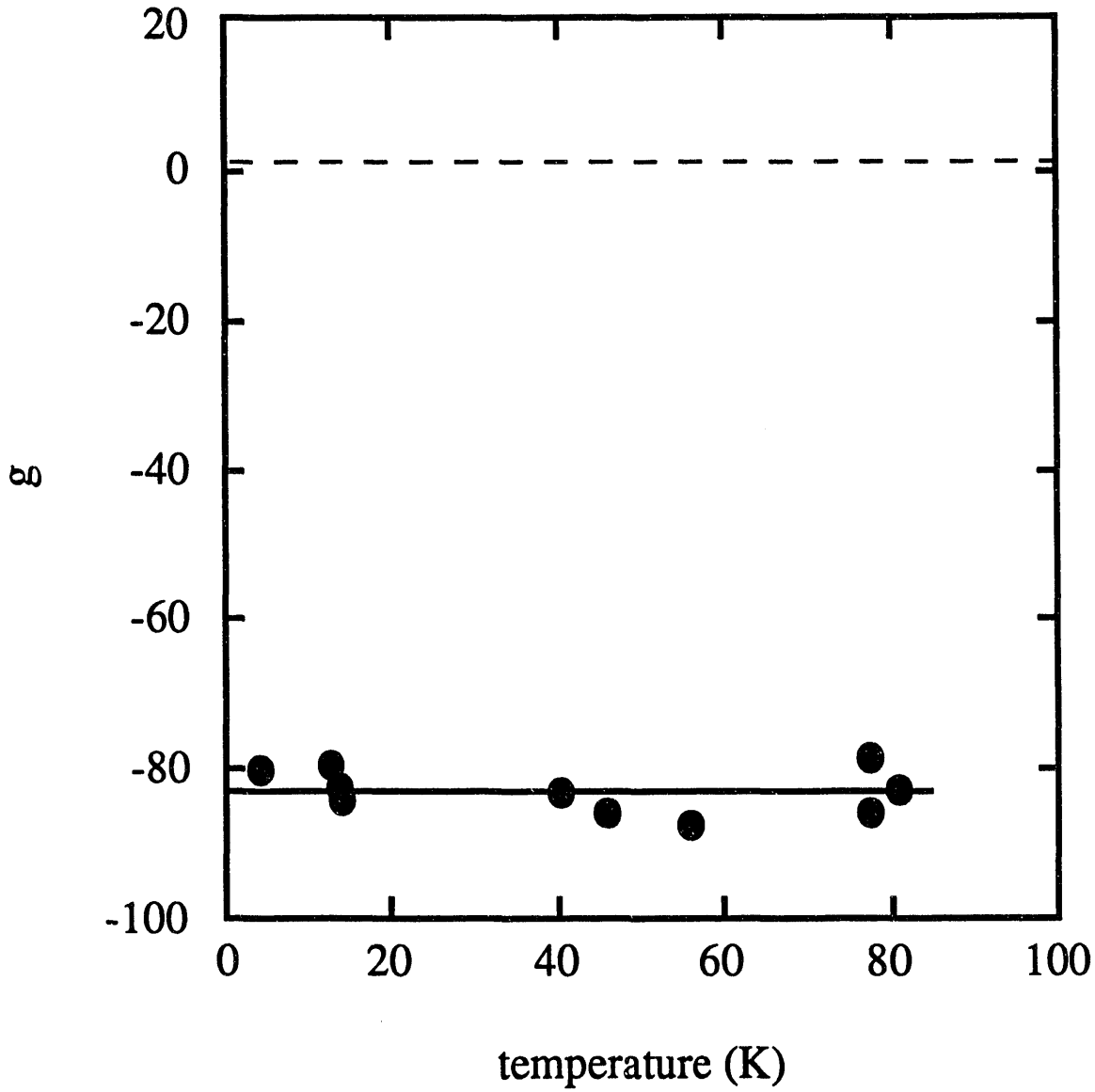

Fig. 10.3 Gain g of the magnetometer vs. temperature. The dashed line at g=+1 refers to the gain of the bare SQUID.

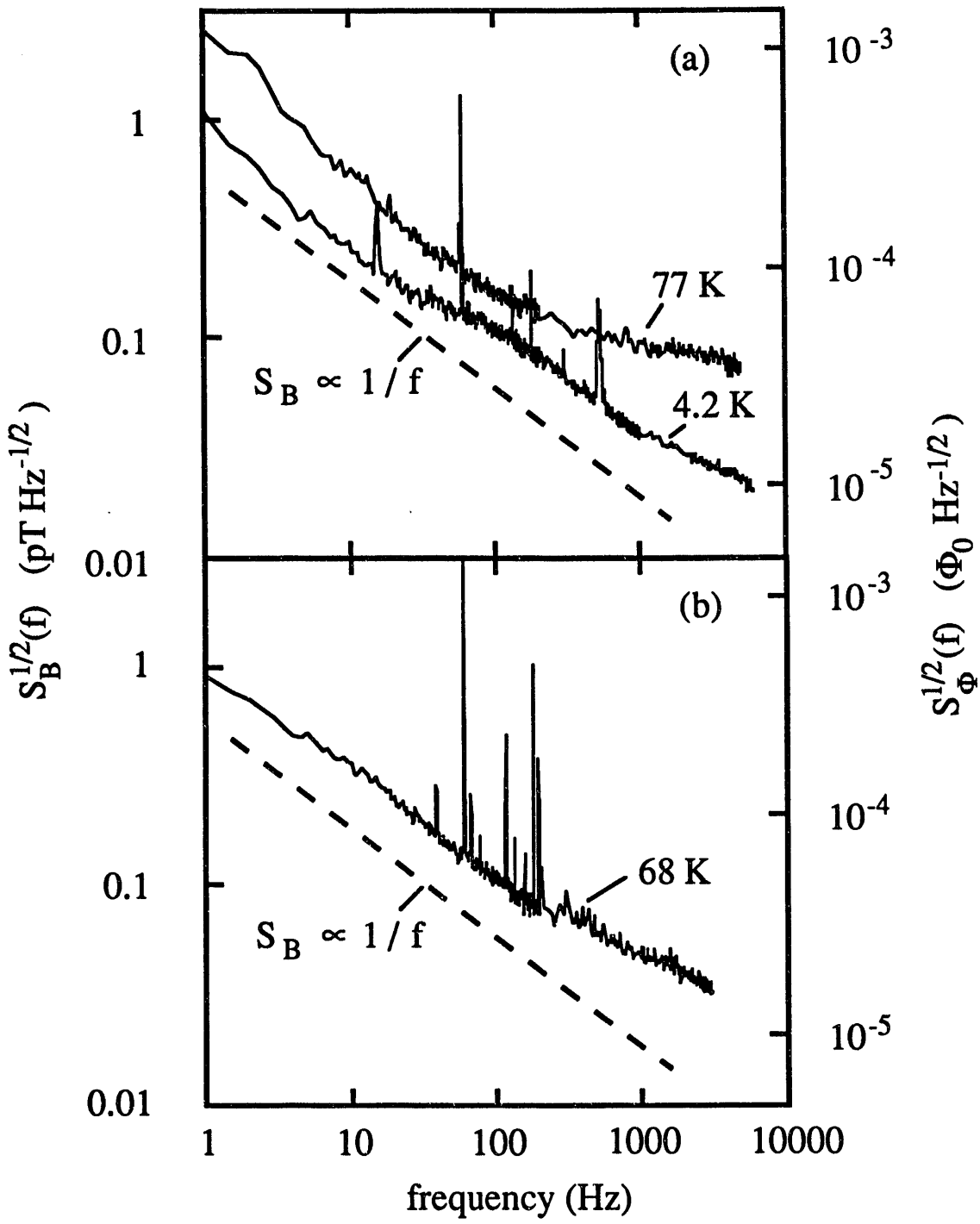

Fig. 10.4 (a) Rms magnetic field noise of magnetometer, $S_B^{1/2}(f)$, and rms flux noise of SQUID, $S_\Phi^{1/2}(f)$, vs. frequency at 4.2K and 77K. Dashed line is $S_B^{1/2}(f) \propto 1/f$. (b) $S_B(f)$ vs. frequency for magnetometer at 68K.

is expected to improve approximately as $A_p^{3/4}$. Finally, as with all high-T_c SQUIDs reported to date, the level of 1/f noise in the SQUID is quite high. At this point, we do not know the source of this noise, but if it originates in critical current fluctuations, some reduction in its magnitude may be possible by an appropriate double-modulation scheme, as has been reported recently.[7]

The magnetic field resolution demonstrated by our magnetometer is already adequate for some applications, for example, nondestructive testing and certain geophysical measurements. Furthermore, the fact that we can fabricate magnetometers using photolithographic processing on all levels indicates that the basic technology for high-T_c integrated circuits involving Josephson junctions and interconnects is now established.

References

1. K. Char, M. S. Colclough, S. M. Garrison, N. Newman, and G. Zaharchuk, *Appl. Phys. Lett.*. **59**, 733 (1991)

2. B. Oh *et al.* have recently reported a photolithographically patterned high-T_c flux transformer coupled to a high-T_c SQUID. This work and ours was reported at the 1991 March Meeting of the American Physical Society, Cincinnati, Oh, 1991 (unpublished).

3. W. C. Stewart, *Appl. Phys. Lett.* **12**, 277 (1968); D. E. McCumber, *J. Appl. Phys.* **39**, 3113 (1968).

4. M. B. Ketchen, W. J. Gallagher, A. W. Kleinsasser, S. Murphy, and J. R. Clem, in, *SQUID '85*, edited by H. D. Hahlbohm and H. Lübbig (Walter de Gruyter, Berlin, 1985), pp. 865-871.

5. J. J. Kingston, F. C. Wellstood, Du Quan, and John Clarke, *IEEE Trans. Magn.* **27**, 974 (1991).

6. A. H. Miklich, F. C. Wellstood, J. J. Kingston, J. Clarke, M. S. Colclough, A. H. Cardona, L. C. Bourne, W. L. Olson, and M. M. Eddy, *IEEE Trans. Magn.* **27**, 3219 (1991).

7. W. J. Gallagher, presented at the 1991 March Meeting of the American Physical Society, Cincinnati, OH, 1991 (unpublished).

Chapter 11

Magnetocardiology with a Thin-Film $YBa_2Cu_3O_{7-x}$ Magnetometer

In the last chapter, we described[1] a thin film $YBa_2Cu_3O_{7-x}$(YBCO) magnetometer, operating in liquid nitrogen, in which the transformer produced a magnetic field gain of approximately 80. To demonstrate the sensitivity and practical applicability of the device, we report the measurement of a human magnetocardiogram. Although a magnetocardiogram has previously been obtained with a bulk YBCO SQUID,[2] we believe the present experiment is the first to apply a thin film high-T_c magnetometer to a practical measurement.

The magnetometer used was the one described in Chapter 10 and shown in Fig. 10.1. We immersed the magnetometer in liquid nitrogen contained in a thin-walled glass dewar extracted from a household thermos flask. The flask was rigidly supported in our shielded room, so that the plane of the magnetometer was parallel to the chest of the standing subject, and within about 25mm. The dewar and subject were surrounded by two concentric high permeability cylinders (kindly loaned by Professor Eugene Commins) which attenuated the ambient magnetic fields by a factor of 300. In the absence of any subject, the SQUID exhibited low frequency noise limiting the resolution of the magnetometer to 2.3pT $Hz^{-1/2}$ at 1Hz, falling off as $1/f^{1/2}$ (f is frequency) to a white noise level of 0.35pT $Hz^{-1/2}$.

We measured magnetocardiograms from three healthy male subjects ranging in age from 27 to 32. Each subject removed metallic objects from his person, and was not in contact with the dewar. In Fig. 11.1, we show the waveforms obtained at grid locations[3] D3 and D5, over the lower right and lower left chest of one subject [see Fig. 11.1(a)]. The

bandwidth was 2Hz to 50Hz; residual 60Hz pickup is still evident in both traces. The two cardiograms differ significantly from each other, but each is similar to that previously seen by others[4] using low-T_c SQUID magnetometers placed at the same grid location.

This result demonstrates that the resolution of thin-film high-T_c magnetometers has attained the level required for practical applications. We note that in a more ideal environment[1] our magnetometer has achieved a resolution of $(1/f^{1/2})$ pT $Hz^{-1/2}$, operating at 68K. For clinical use, however, an order of magnitude improvement would be desirable. This factor should be achievable with the existing circuit process, which should also allow construction of first-derivative gradiometers that are preferable in some applications. In addition, in the near future, one might also hope for at least modest reductions in the 1/f noise of the SQUID.

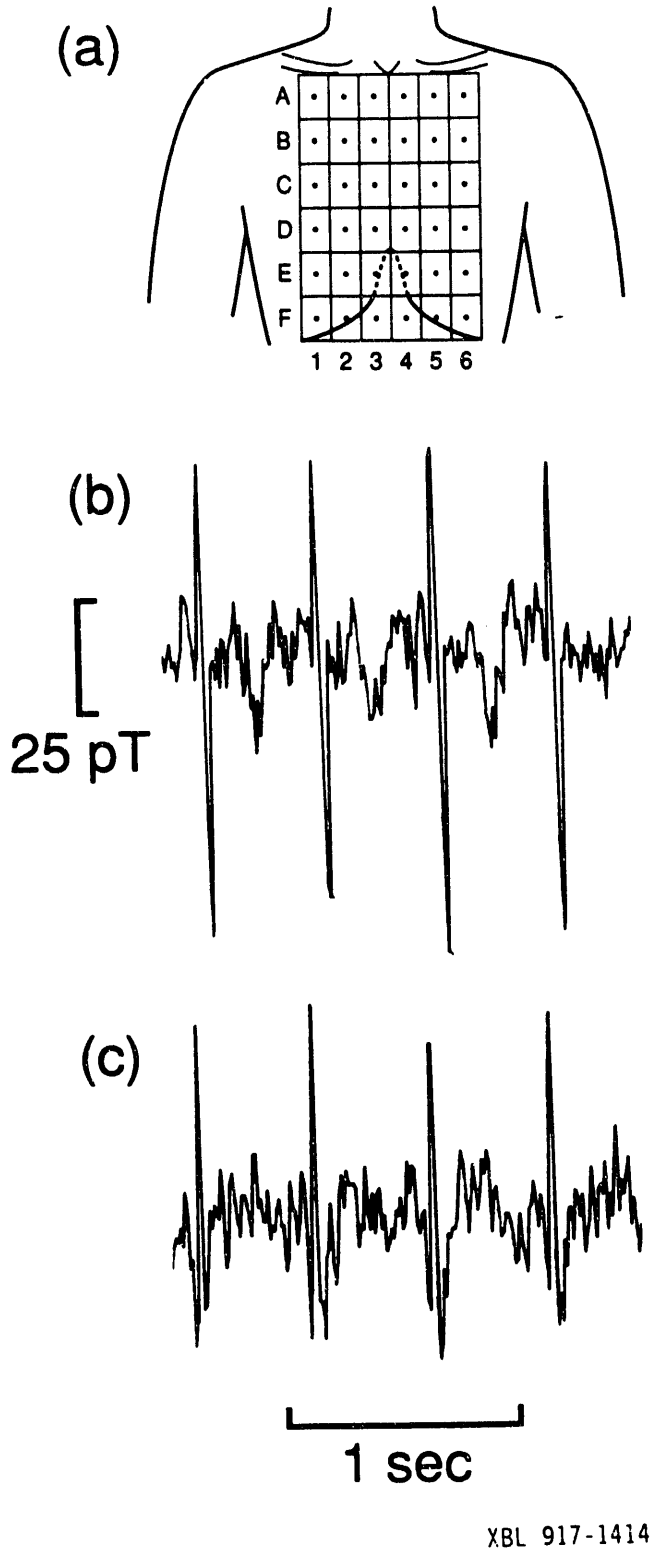

Fig. 11.1(a) Rectangular reference grid on front of chest (redrawn from ref. 5); (b) and (c) magnetocardiograms obtained from same subject at D3 and D5.

References

1. A. H. Miklich *et al.*, *Appl. Phys. Lett.* **59**, 988 (1991)

2. Likhachev, *et al.*, *Superconductor Science & Technology* **3**, 148 (1990).

3. S. J. Williamson and L. Kaufman, *J. Magnetism and Magnetic Materials* **22**, 129 (1981).

Chapter 12

Conclusions

Despite the many materials, deposition, and patterning issues that faced us, we were able to make a substantial contribution towards the development of a complete high T_c superconducting microelectronics technology. Most notably, we were the first group in the world to fabricate interconnects and then to use that capability to fabricate multiturn coils and flux transformers used to couple flux to dc SQUIDs. One magnetometers had the highest field resolution reported, and one was used to perform magnetocardiograms on human subjects.

Although much progress has been made, much remains to be done. At present, the greatest impediment to the development of a complete superconducting technology, based on the high-T_c materials, is the lack of a reproducible and extendable junction fabrication technique. In the case of YBCO, the short coherence length and anisotropic structure of the material have made it difficult to fabricate junctions. Of the many types of weak-links which have been developed to date, none is ideal for circuit applications.

There are also problems with the existing interconnect technologies. Specifically, reproducibility is lacking and the yield of devices is low. The culprit is that the edges of the photolithographically patterned films can be too steep to support the epixtaxial growth of upper layers.

The upper YBCO layer in our photolithographically patterned crossovers show a considerable reduction in the J_c, compared to that of a single layer of YBCO, whereas crossovers patterned by shadow masks do not . Films of YBCO patterned by shadow masks, have very gently sloping edges that easily support the epitaxial growth of upper layers. We suspect that the growth of the insulating film over the steep edges of the

patterned lower YBCO film is less than perfectly epitaxial. This results in degradation in the growth and electrical properties of the upper YBCO layer, where it covers the damaged part of the insulating film. When fabricating window contacts, we intentionally ion mill a gentle slope to the hole in the insulating film, to assist in the epitaxial growth of the upper YBCO film on the wall of the hole. In similar fashion, a reproducible technique needs to be developed to photolothographically pattern and etch YBCO film into wires, with gently sloping edges, that will support the epitaxial growth of upper layers.

Of course, improvements should also be made in the field resolution of high T_c SQUID magnetometers. There are two contributions to the noise that limits their overall sensitivity. The first is the noise of the junctions themselves used to form the SQUID. Fluctuations in the critical current and resistance of the junctions result in voltage outputs that limit the SQUID performance. Although modulation schemes can lower this contribution, a superior junction technology would produce inherently quieter SQUIDs.

Secondly, there is the magnetic flux noise of the YBCO films that are used to form the SQUID washer and the flux transformer. Defects in thin films are responsible for the pinning of flux lines that could otherwise move freely about and cause dissipation. However, a flux line that is insufficiently pinned can hop around creating flux noise, that in the case of magnetometers, limits their resolution. There is currently no correlation between the level of flux noise of a film and the deposition conditions used to fabricate it. For that matter, it is not known exactly what types of defects lead to strong pinning and are desirable, or those that produce weak pinning and contribute to the flux noise. Answers to these questions.could perhaps be found by performing TEM, x-ray diffraction, critical current and flux noise measurements on films fabricated under a variety of conditions.

We can only hope that the problems are overcome and that a commercially viable industry comes to life providing us with the benefits of a new technology with unique features.

DATE
FILMED
01/08/93